LOW TEMPERATURE EPITAXY OF $Hg_{1-x}Cd_xTe$

Nyles W. Cody
B.S., Colorado State University, 1985

A dissertation submitted to the faculty of the
Oregon Graduate Institute of Science & Technology
in partial fulfillment of the
requirements for the degree of
Doctor of Philosophy
in
Electrical Engineering

April, 1992

The dissertation "Low Temperature Epitaxy of $Hg_{1-x}Cd_xTe$" by Nyles W. Cody has been examined and approved by the following Examination Committee:

Raj Solanki, Dissertation Advisor
Associate Professor

Rao Gudimetla
Assistant Professor

Paul Davis
Professor

Kirk Boyer
Tektronix Incorporated

To my wife

Acknowledgments

I would like to thank my advisor, Raj Solanki, for his time and encouragement throughout the course of this work. Most of all I appreciate his patience, because I am sure that I tested it during the writing of this dissertation. Also I would like to thank the other people of my examination committee, Rao Gudimetla, Paul Davis, and Kirk Boyer.

Additionally I would like to thank John Blakemore and R.S. Tang for the use and assistance in using their variable temperature Hall system and Uppili Sudarsan for his time and expertise in operating the T.E.M.. I would also like to thank Guy Silvestri, Tyrus Monson, and Tanner Doslogu for their instructional input and useful conversations.

Finally, my family has given me continued support and encouragement throughout my schooling. I owe them very much for without that encouragement the task would have been next to impossible.

ABSTRACT

Low Temperature Epitaxy of $Hg_{1-x}Cd_xTe$

Nyles W. Cody, Ph.D

Supervising Professor : Raj Solanki

The semiconductor $Hg_{1-x}Cd_xTe$ is well established as one of the most important materials for the detection of infrared radiation. However because of high process temperatures, the material tends to form Hg vacancies and suffers from grading at heterojunction interfaces. These process related problems can be reduced by lowering the growth temperature of the alloy. Low temperature epitaxy of $Hg_{1-x}Cd_xTe$ has been achieved using photo-assisted metal organic vapor phase epitaxy. This process allows reduced processing temperatures via ultra-violet radiation. Using elemental Hg, Dimethylcadmium (DMCd), and various tellurium precursors, epitaxial growth of $Hg_{1-x}Cd_xTe$ has been investigated. The tellurium precursors used include diethyltellurium (DETe), diisopropyltellurium (DIPTe), and methylallyltellurium (MATe). These compounds show that a photo-assisted process can be used to achieve epitaxial growth at substrate temperatures in the range of 230 to 250°C while maintaining high growth rates.

Homoepitaxy and heteroepitaxy (on GaAs) of CdTe with growth rates as high as 6μm/hr and a substrate temperature of 250°C were achieved using DETe. The relationships between the deposition parameters and epilayer properties were examined using transmission electron microscopy and x-ray rocking curves. For CdTe/GaAs growth, the lattice mismatch is accommodated in the first 0.5μm of thickness yielding good quality material for subsequent growth of $Hg_{1-x}Cd_xTe$. Growths conducted using DIPTe indicate the precursor is very photo-sensitive. Attempts at growing $Hg_{1-x}Cd_xTe$ led to gas-phase nucleation resulting in poor epilayer quality.

The evaluation of MATe is done for both purely thermal as well as photo-assisted growths. The photo-assisted process allows for $Hg_{1-x}Cd_xTe$ growth at temperatures as low as 230°C and a growth rate near 4μm/hr. In addition, this method allows for a wider range of x-values and better epilayer quality. Using the photo-assisted process and a substrate temperature of 250°C, $Hg_{1-x}Cd_xTe$/CdTe/GaAs/Si structures were grown. Hall electron mobilities of the $Hg_{1-x}Cd_xTe$ ($x \approx 0.2$) were typically 4×10^4 $cm^2/V\text{-}s$ at 80°K.

Table of Contents

List of Tables

List of Figures

1. INTRODUCTION

The development of II-VI compound semiconductors has come about due to their promising applications in infra-red detectors, electroluminescence devices, solar cells, and more recently blue/green lasers. Similar to the development of III-V compound semiconductors, the growth of II-VI compound semiconductor thin films are well suited using Metalorganic Vapor Phase Epitaxy (MOVPE). Some of the more common II-VI materials grown by MOVPE include HgTe, CdTe, $Hg_{1-x}Cd_xTe$, ZnTe, $Cd_{1-x}Zn_xTe$, CdS, ZnSe, ZnS, $Se_{1-x}S_xZn$, ZnO, and CdO. Most of these materials are shown in Figure 1.1 with their corresponding direct-gap wavelength and lattice parameter. With a range of band-gaps from -0.03 eV to 3.54 eV (HgTe and ZnS, respectively) a vast array of devices can be designed for optoelectronic purposes.

An empirical trend in these materials is that as the process temperature is reduced, the materials quality improves. This is because the interdiffusion of elements is kept to a minimum, as well as thermal defects formed by high temperatures are reduced. Although molecular beam epitaxy (MBE), offers the lowest of processing temperatures, the limitations in throughput as well as low growth rates and high initial starting and maintenance costs make MOVPE more attractive for a production environment.

The processing temperature of conventional MOVPE is limited by the temperature at which the organometallics decompose. In order to reduce the processing temperature, non-thermal energy must be added to the metal organic to promote dissociation. Presented are the results of a technique developed that utilizes ultraviolet photons (generated by a microwave excited mercury lamp) to assist MOVPE. This process combines the features of conventional MOVPE and allows

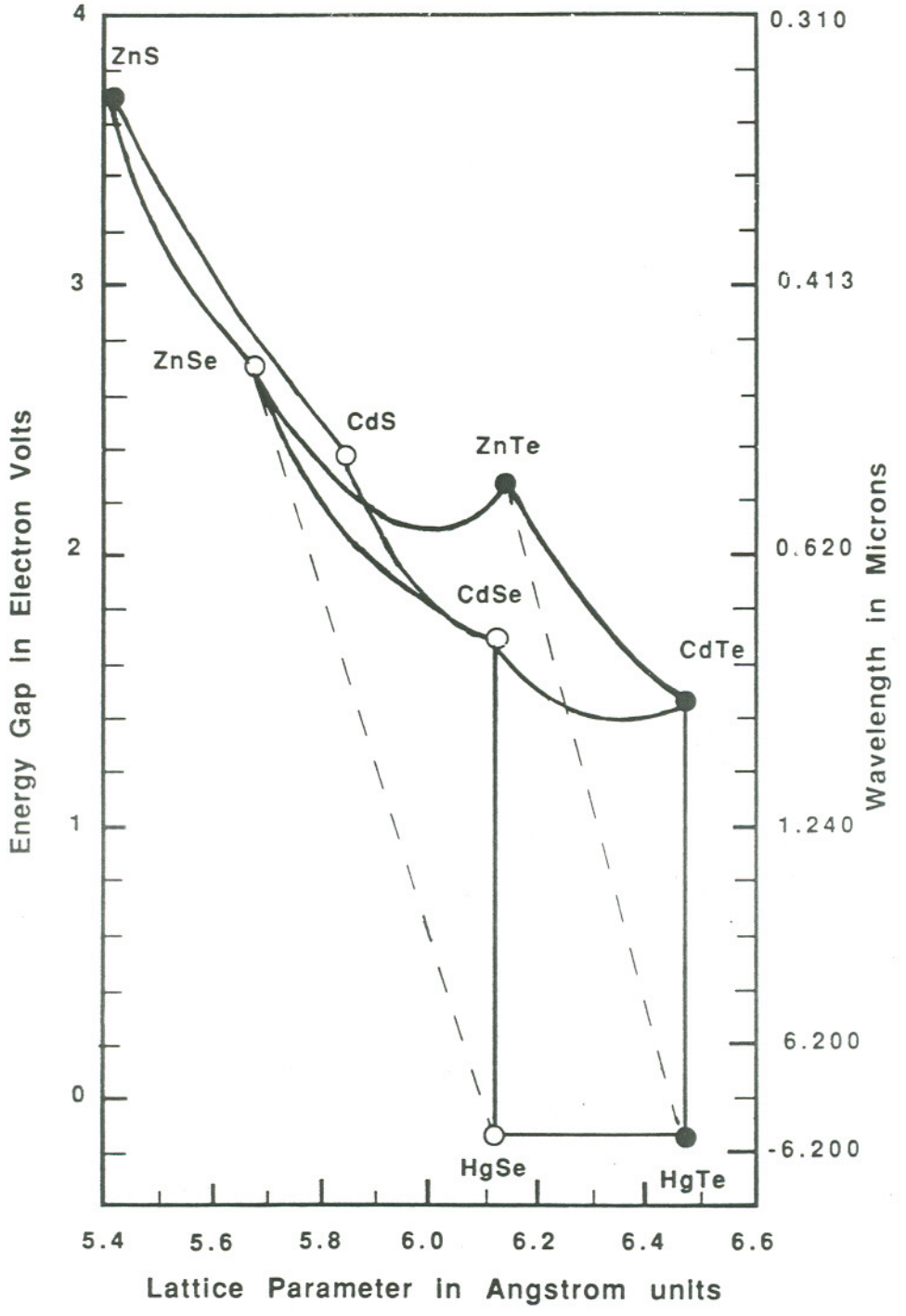

Figure 1.1 Energy gap and corresponding wavelength vs. lattice parameter for common II-VI compounds. (Dashed lines are extrapolations [1]).

epitaxial growth to occur at temperatures lower than that of a purely thermal process. This reduced growth temperature is obtainable because the effective activation energy of the precursor gases is reduced due to the additional energy supplied by UV photons. The material grown for this study was $Hg_{1-x}Cd_xTe$ with an emphasis on x-values of one (CdTe), and in the range of $0 \leq x \leq 0.4$. These values of x were chosen so that an understanding of both homoepitaxy (on CdTe) as well as heteroepitaxy could be examined and to develop a process for the growth of $Hg_{0.8}Cd_{0.2}Te$. The importance of $Hg_{0.8}Cd_{0.2}Te$ stems from its narrow bandgap that makes it an ideal material for infrared detectors in the 8 to 12μm range, the optical transmission window in the far IR in the atmosphere. The growth temperature of $Hg_{1-x}Cd_xTe$ using conventional MOVPE ranges between 350 and 450°C. At these temperatures, the Hg atoms (that have a high diffusion constant) tend to diffuse out of the films, making it impossible to fabricate sharp interfaces that are required for good devices.

CdTe is generally used as a substrate material for epitaxial growth of $Hg_{1-x}Cd_xTe$ because of thier close lattice match. In our investigation, epitaxial growth of CdTe was also studied for two main reasons. First, CdTe substrates have a high defect density that would affect the epitaxial quality of the subsequent $Hg_{1-x}Cd_xTe$ layer. Therefore, growth of a thin layer of homoepitaxial CdTe preceding $Hg_{1-x}Cd_xTe$ growth would improve the quality of the $Hg_{1-x}Cd_xTe$ film. Second, a heteroepitaxial layer would allow the use of alternate substrates. For example, although there is over a 14% lattice mismatch between GaAs and CdTe, it is possible to grow a heteroepitaxial layer of CdTe with qualities good enough to act as a substrate for $Hg_{1-x}Cd_xTe$. In addition, the mechanical strength of the starting substrate is increased and the size limitations of the CdTe substrates are removed. By using GaAs or GaAs on silicon as a starting substrate material, wafers of 1" to 4" in diameter could be feasible, compared to only 3 x 3cm CdTe substrates. Moreover, this allows for fabrication of monolithic optoelectronic devices.

This large area is of particular interest in solar cell applications. Cadmium

telluride is ideally suited as its bandgap corresponds to a maximum theoretical efficiency of 27% for a homojunction structure [2]. Although other homojunction photovoltaics are of equal significance, with theoretical values for Si and GaAs of 21% and 25% respectively, these values have not yet been achieved. The main drawback to working with the CdTe homojunction has been the inability to make low resistive ohmic contacts to p-type material. This is because the work function of p-type CdTe, 5.7 eV, is sufficiently large that no simple metal can be used to give a direct low resistance contact [3]. Thus, this material's full capabilities have not yet been examined. With the use of heteroepitaxy contact could be made to a p-type starting substrate, i.e. GaAs, where the epilayer would then be p-type CdTe followed by an n-type layer. This arrangement is also advantageous because of a factor of 24 difference in mobilities (μ_n = 1200 cm^2/volt-sec.) of the two conduction types making it easy to remove carriers from the n-type surface region.

Some other uses of CdTe include electro-optic and acousto-optic modulators, luminescent devices, lasers, and in nonlinear optics. Although these uses have had rather limited success compared to other suitable materials, the main reason is believed to be the material quality. With the advent of MOVPE this limitation may be eliminated yielding superior device performance.

As previously mentioned, the primary use of $Hg_{1-x}Cd_xTe$ is as detectors for infrared radiation. The detection of infrared radiation using $Hg_{1-x}Cd_xTe$ involves either a photo-conductive or a photo-voltaic device [4]. Simple circuits for each of these types of detectors are shown in Figure 1.2. Although the photo-voltaic device is slightly more difficult to fabricate due to the need for a p-n junction, it offers the ability of forming large focal plane arrays. These arrays when coupled to charge coupled devices (CCD's), charge injection devices (CID's), or MOSFET X-Y addresses, allow for a more efficient detector system compared to the photo-conductive detectors because of the lower power and decreased background dependency [5].

To form an efficient detector of the photo-voltaic type, it is desirable to tailor

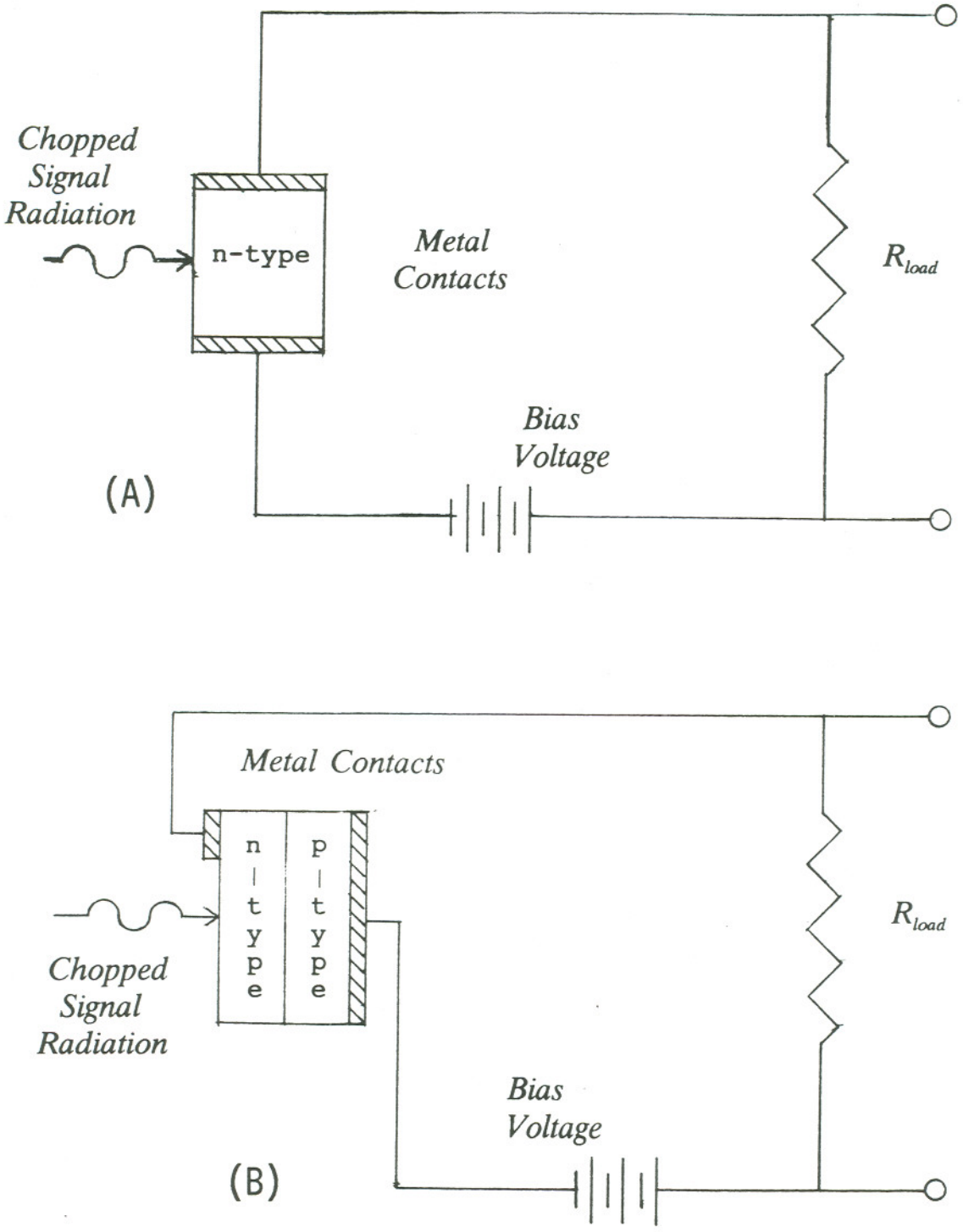

Figure 1.2 Simple detector circuits showing a.) photo-conductive type b.) photovoltaic type.

the band-gap of the detector such that the absorption takes place at the junction. Shown in Figure 1.3 are various schemes used to maximize the absorption. Although simple in design, the standard photo-voltaic device has a poor quantum efficiency due to the recombination of carriers at the surface. Figure 1.3b is an improved design because the radiation is transmitted to the junction and simultaneously filters out the unwanted radiation which is greater than E_w. However, if the unwanted radiation is intense in nature then the generation of carriers due to a photo-conductive effect near the p-n junction may create a high noise level. By increasing the thickness of the n-type layer and using backside illumination, this layer will act as a filter. The configuration shown in Figure 1.3c combines both advantages of a backside illuminated device as well as having a tailored spectral filter by using a multilayered heterostructure. Although this structure is by far the most difficult to fabricate, the efficiency of such a device is maximized.

For the photo-conductive device, n-type $Hg_{1-x}Cd_xTe$ is used because the electron-hole mobility ratio is more than 20. The detector is also operated with a chopped signal so that the background radiation can be eliminated from the actual a.c. source signal. To reduce the thermal effects, which give rise to a "dark current", both types of detectors are often cooled to 77°K.

In order to realize the full capability of such devices, it is essential to grow *device quality* $Hg_{1-x}Cd_xTe$. This investigation was undertaken to evaluate a low temperature MOVPE technique that utilized UV photons.

The next chapter describes the properties of $Hg_{1-x}Cd_xTe$ and CdTe with an emphasis on the optical properties of the materials. Also included is a summary of the growth of these materials using various techniques together with the advantages and disadvantages which have led to the development of the photo-assisted MOVPE growth process. The system used for this study is described in Chapter 3 with the results obtained discussed in Chapters 4 and 5. Electrical characterization of the $Hg_{1-x}Cd_xTe$ layers is described in Chapter 6 followed by conclusions in Chapter 7.

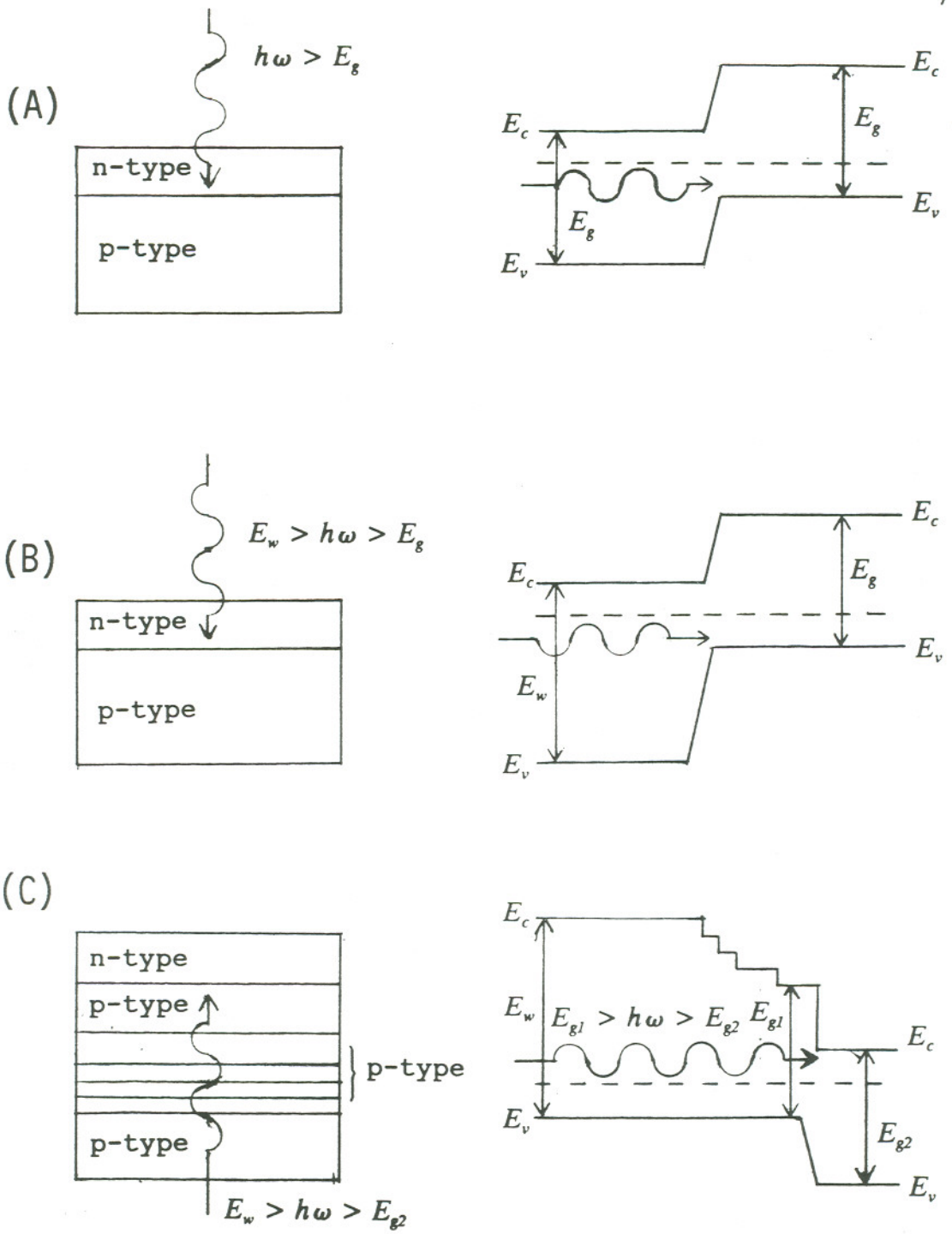

Figure 1.3 Photo-voltaic detectors showing a.) basic detector b.) frontside illuminated detector with spectral filtering c.) backside illuminated detector with spectral filtering using a multilayered heterostructure [6].

2. BACKGROUND

2.1 Material Properties

The development of $Hg_{1-x}Cd_xTe$ came about from the need to have a semiconducting material which had a direct, narrow bandgap suitable for the detection of photons in the 1-12 μm wavelength range. In 1959 Lawson et.al reported that the ternary compound made from HgTe and CdTe met this need and was "tunable" to the incident photon energies by changing the molar ratio of the two compounds [7]. This tunability comes about because HgTe is a semimetal with a room temperature energy gap of E_g = -0.15 eV, and CdTe is a semiconductor with E_g = 1.45 eV. The materials fundamental gap $E_o = E(\Gamma_6) - E(\Gamma_8)$ increases linearly from negative to positive as x increases with the transition from semimetal to semiconducting occurring at x = 0.146 at 77°K [8]. Because of this property, $Hg_{1-x}Cd_xTe$ has become one of the most important semiconducting materials for infrared detection [9,10].

Some of the properties of CdTe, HgTe, and $Hg_{0.8}Cd_{0.2}Te$ are shown in Table 2.1. Most values for intermediate compositions can be extracted using a linear fit between CdTe and HgTe. However, one variation from a linear fit is in the lattice constant which is expressed in Equation 2.1.

$$Lattice\ Constant = 6.461 + 0.011x + 0.009x^2 \qquad \textbf{Eq. 2.1}$$

Because of the close lattice match between CdTe and $Hg_{1-x}Cd_xTe$, CdTe is a natural choice for epitaxy of $Hg_{1-x}Cd_xTe$. For an exact lattice matched substrate to

Table 2.1 Room Temperature Properties of $Hg_{1-x}Cd_xTe$ [4,9,11]

Property		**CdTe**	**HgTe**	**$Hg_{0.8}Cd_{0.2}Te$**
Lattice Constant (Å)		6.481	6.461	6.475
Energy Gap (eV)		1.44	-0.15	0.16
Electron Mobility ($cm^2/V-s$)		1200	25000	15,000
Hole Mobility ($cm^2/V-s$)		50	350	$500 - 10^3$
Melting Point (°K)		1365	943	1040
Lineal Thermal Expansion Coefficient ($X\ 10^{-6}\ °K^{-1}$)		5.5	4.0	4.3
Elastic Constants ($X\ 10^{11}$ dyne/cm^2)	C_{11}	5.35	5.4	5.39
	C_{12}	3.681	3.8	3.98
	C_{44}	1.994	2.05	2.04

$Hg_{1-x}Cd_xTe$ the ternary $Cd_{1-x}Zn_xTe$ is used. With $Cd_{0.95}Zn_{0.05}Te$ being lattice matched to HgTe a linear relationship can be assumed for the amount of ZnTe in the ternary. Thus, for $Hg_{0.8}Cd_{0.2}Te$, the latticed matched substrate is $Cd_{0.98}Zn_{0.02}Te$.

Although the change in lattice constant as a function of x-composition for $Hg_{1-x}Cd_xTe$ is not linear, the change in density is linear and is expressed in Equation 2.2.

$$\rho = 8.196 - 2.226x \qquad \textbf{Eq. 2.2}$$

The density is often used in determining the composition and or film thickness indirectly by measuring the increase in weight of a substrate after an epitaxial film has been deposited. Both Equation 2.1 and Equation 2.2 were obtained from graphical data shown in Figure 2.1 and have correlation coefficients of 0.999.

In order to fabricate reliable devices it is necessary to know the cutoff energy, E_{co}, accurately. With $Hg_{1-x}Cd_xTe$ having a direct band-gap structure ,E_{co} is equal to the energy gap, E_g, and is thus obtainable directly from optical absorption techniques. The most commonly used method for this measurement is Fourier Transformed Infrared Spectroscopy (FTIR). When a FTIR spectrum is obtained, the absorption or transmission is plotted versus wavelength. The determination of the energy gap is obtained from the cutoff wavelength λ_{co} (in microns) by the following expression.

$$E_g = hc/\lambda_{co} = 1.24/\lambda_{co}(\mu m) \qquad \textbf{Eq.2.3}$$

Hansen, et al. have compiled data from various workers and derived an empirical expression relating the energy gap to the alloy composition against temperature [13]. This expression is given in Equation 2.4 in terms of eV where, x is the alloy

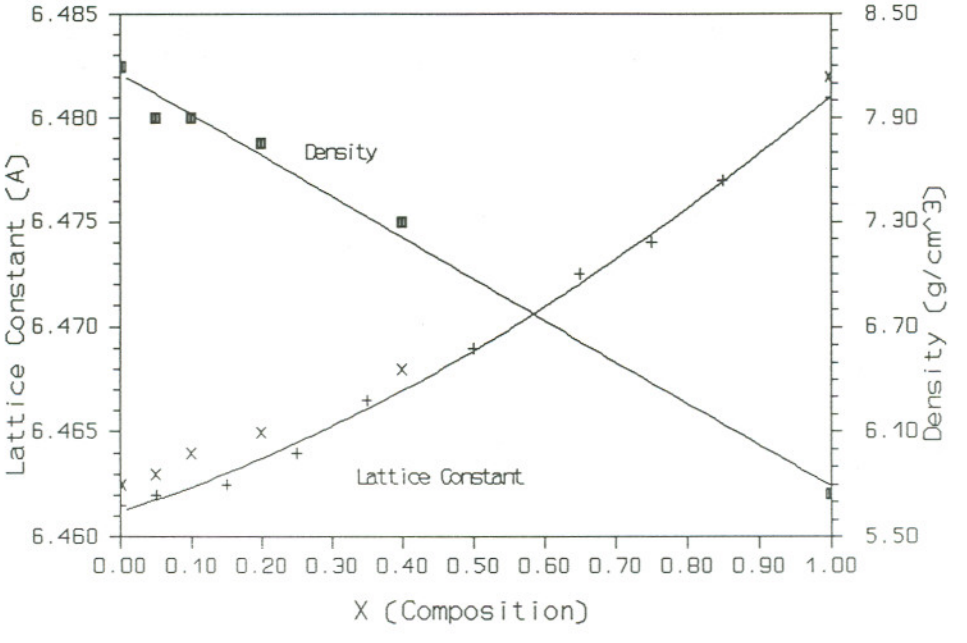

Figure 2.1 Lattice constant and density of $Hg_{1-x}Cd_xTe$ as a function of composition [11].

composition and the temperature T is in degrees kelvin.

$$E_g(x,T) = -0.302 + 1.93x + T(1-2x)5.35E-4 - 0.810x^2 + 0.832x^3 \quad \textbf{Eq. 2.4}$$

This equation was obtained using compositions of $x \leq 0.6$ and $x = 1.0$ and has a standard estimate of error equal to 0.0013 eV. A second expression developed by Chu et al. has an estimated standard of error to be 0.0008 eV and is applicable to the range of $0 \leq x \leq 0.37$ and $x = 1.0$ [14]. This equation (given in Equation 2.5) as well as Equation 2.4 are valid over the entire temperature range from 4.2 to 300°K.

$$E_g(x,T) = -0.295 + 1.87x - 0.28x^2 + T(6 - 14x + 3x^2)E-4 + 0.35x^4 \quad \textbf{Eq. 2.5}$$

The thickness of either bulk samples or heteroepitaxial layers of $Hg_{1-x}Cd_xTe$ can also be obtained from the FTIR spectrum. In such a spectrum interference fringes are created due to the interfaces of the sample with air or the substrate interface. These fringes can be related to Equation 2.6 where n is the index of refraction of the $Hg_{1-x}Cd_xTe$, d is the thickness, and $\delta\nu$ is the spacing between successive maximum fringes in units of wave-numbers [15].

$$d = \frac{1}{2n\delta\nu} \qquad \textbf{Eq. 2.6}$$

Given in Table 2.2 are some values for the refractive indices of $Hg_{1-x}Cd_xTe$ at room temperature.

The early work on the electrical characterization of $Hg_{1-x}Cd_XTe$ did not agree

Table 2.2. Refractive index of $Hg_{1-x}Cd_xTe$ for various alloy compositions [12].

Wavelength (μm)	Index of Refraction @ 300°K			
	x=0.17	x=0.21	x=0.27	x=0.36
4	---	---	---	3.50
5	---	---	3.60	3.40
6.7	4.50	3.72	3.47	3.32
10	4.15	3.55	3.37	3.25
12.5	4.05	3.52	---	---

well with the values obtained by theoretical calculations. This is due mainly to anomalous behaviors which are believed to be caused by nonstoichiometric materials [16,17]. However, the dependencies on composition did agree and as improved materials are grown the absolute values agree with theoretical calculations.

The most commonly used method of characterizing $Hg_{1-x}Cd_xTe$ is by Hall measurements. Because properties vary dramatically over temperature and composition, simple closed expressions are difficult to obtain for all ranges. For compositions between x=0.18 and 0.25, there has been extensive data collected on bulk crystals obtained by the melt growth process. Using room temperature values, relationships for electron mobility and resistivity versus x-value are given in Equation 2.7a and 2.7b respectively [18].

$$\mu_e(300°K) = (8.754E\text{-}4x - 1.044E\text{-}4)^{-1} \qquad \textbf{Eq. 2.7a}$$

$$\log(\rho) = x\ 15.2201 - 4.9042 \qquad \textbf{Eq. 2.7b}$$

In 1972, Scott reported the temperature dependence of the Hall mobility as a function of composition and is shown in Figure 2.2. This figure shows the trends in the material but, as it is rather dated, it may need to be updated as better quality reference samples become available throughout the industry.

Another parameter of interest is the carrier concentration. Using a two-variable simultaneous least squares fit to the calculated nonparabolic n_i, Hansen et.al. have developed an expression for the intrinsic carrier concentration [20]. This equation gives results which are within 1% of the calculated n_i and is valid for the range of $E_g > 0$, $50 < T < 300°K$, and $x < 0.7$.

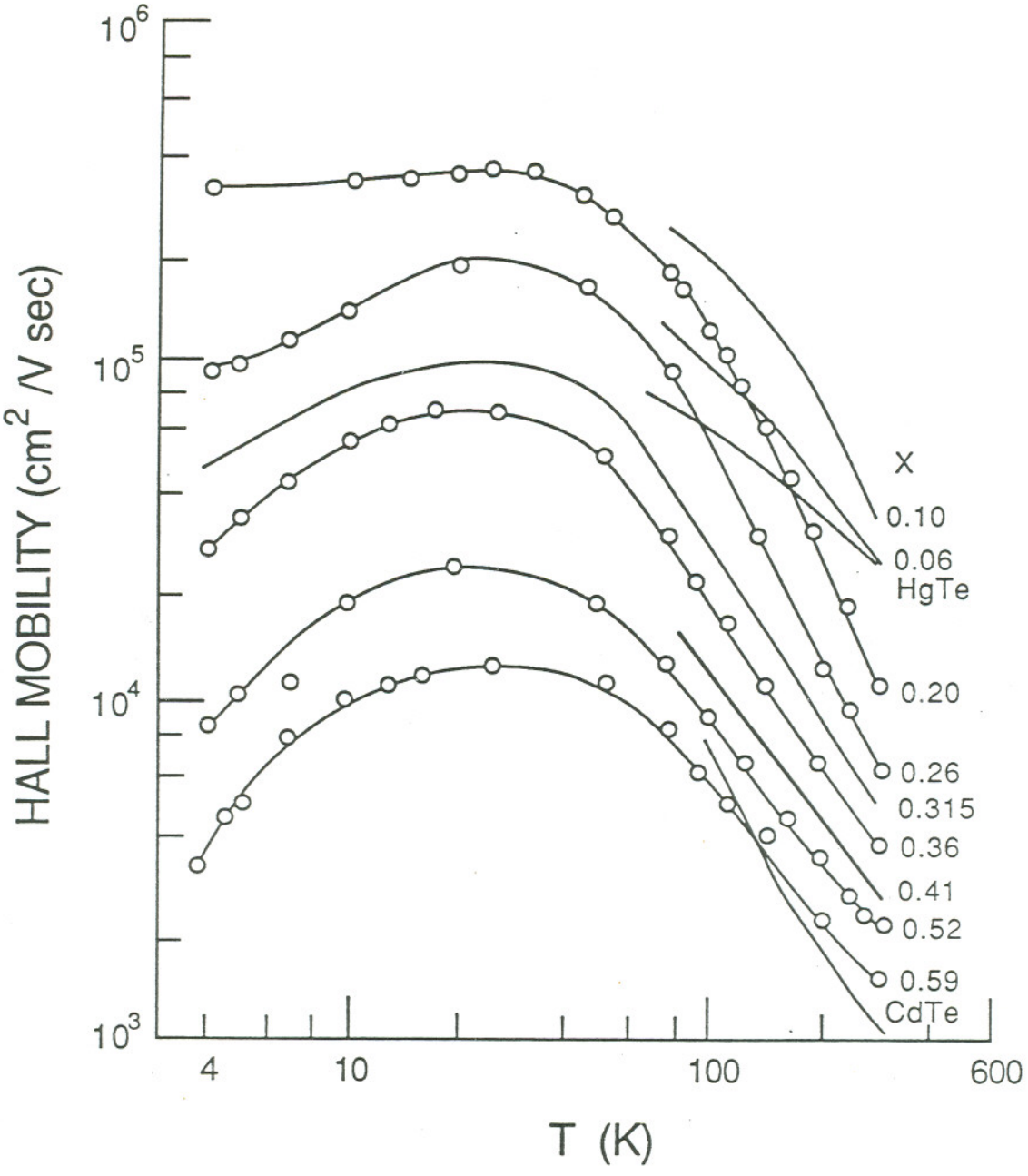

Figure 2.2 Temperature dependence of the Hall mobility in $Hg_{1-x}Cd_xTe$ as a function of composition. (From Scott [19]).

$$n_i = [5.585 - 3.820x + (1.753 - 1.364x)\,T\,E{-}3] * [E14 E_g^{3/2} T^{3/2} \exp(-E_g/2Tk_b)] \quad \textbf{Eq. 2.8}$$

As more data is collected it should be possible to obtain standard equations which will relate the properties of $Hg_{1-x}Cd_xTe$ over a wider range of compositions and temperatures. However if further information is needed on $Hg_{1-x}Cd_xTe$, the reader is referred to the book "Properties of Mercury Cadmium Telluride"[12]. Given are additional data as well as special case studies.

2.2 Growth of $Hg_{1-x}Cd_xTe$

2.2.1 Bulk Growth

The initial growth of $Hg_{1-x}Cd_xTe$ was achieved using the Bridgeman technique [7]. As with other bulk growth methods the elements, called a charge, are mixed to give the desired stoichiometry. However, since Hg is a liquid at room temperature it has a much higher vapor pressure than does Cd or Te at the liquidous temperature. This overpressure of Hg, typically about 80 Atm. at 750°C, limits the size of the ampoule which can withstand such pressures. As a result the cross-sectional diameter of ingots produced are only on the order of 1-3 cm. In addition to the size limitation, there tends to be large compositional gradients both in the radial as well as the longitudinal direction. Portions of the ingots can be made relatively constant in composition with careful attention to recrystallization speeds and homogenization anneals. Further annealing is also typically done on portions of ingots and individual slices to obtain a desired carrier type and concentration [4].

Although there has been much progress made in the growth of $Hg_{1-x}Cd_xTe$ since its beginnings, the size limitation of the material has increased the trend in

growing heteroepitaxial layers. With CdTe being so well suited as a substrate material, much work has been done in growing heteroepitaxial layers of various compositions by a variety of growth techniques. These include liquid-phase epitaxy (LPE) [21-23], molecular beam epitaxy (MBE) [24,25], and metal organic vapor phase epitaxy (MOVPE) [26-29]. Although other growth techniques have achieved good results, these three are predominantly used.

2.2.2 Liquid Phase Epitaxy

Conventional LPE involves the growth of an epitaxial layer by passing a cooled substrate through the meniscus of a melt. The composition of the layer is controlled by the mix of the melt and the layer thickness by the speed the substrate is passed through the liquid, together with the cool down time and temperature of the substrate. In addition to the conventional LPE method, dipping, and tipping the melt over a substrate has been used. Bowers et. al. give a good comparison of Te, Hg, and HgTe rich melts using these three types of LPE techniques.[30].

All of these methods give a good layer quality however, traditionally LPE is one of the most used methods of growth for detector fabrication. However, because the substrate is in contact with the liquid $Hg_{1-x}Cd_xTe$, the interface is highly graded. This grading is attributed in part by the interdiffusion of the CdTe substrate and the liquid melt, but Hg diffusion during the cool down also has an effect on the compositional profile [4]. By cooling the substrate quickly, the diffusion of Hg can be kept to a minimum but the interdiffusion of the melt and substrate give rise to a grading on the order of a few microns in thickness.

2.2.3 Molecular Beam Epitaxy

The growth of $Hg_{1-x}Cd_xTe$ by molecular beam epitaxy (MBE) involves the evaporation of the elements onto a substrate in a high vacuum chamber. Each of the

elements as well as dopant sources are contained in an effusion cell which is in turn heated to control the evaporation rate. The substrate, usually CdTe or $Cd_{1-x}Zn_xTe$, is held at a temperature that is less than 200°C and thus allows for very good control over the interdiffusion of Cd and Hg. This controllability allows for the fabrication of superlattice structures, which are classified as type III heterostructures because of the semimetallic wells (HgTe), and semiconducting barriers (CdTe) [31]. One of the major interests in this type of a structure arises because the mobilities can be over two orders of magnitude higher than in the $Hg_{1-x}Cd_xTe$ alloys [32].

Although these properties seem ideal, the growth of the ternary is difficult to control. There is an exponential change in the Hg condensation coefficient with temperature which results in a narrow range of temperatures available for growth and strict control of the surface temperature. Twinning defects are also a severe problem for the (100) and (111) growth orientations. By using a photo-assisted MBE process Harris et. al. reduced the number of hillocks on the (100) orientation but could not obtain a specular surface [33]. For the (111)B orientation, twin free growth was obtained by holding the substrate temperature (T_s) at 180°C ± 1°C and Hg flux variation to less than ± 2%. Similarly, Lange et.al. report that a T_s less than 190°C, results in excess Hg being desorbed giving rise to twinning [34]. When T_s is above 195°C, excess Te is reevaporated resulting in an increase in x-value of 1.5-2% for each 1°C as well as a change in growth rate. However, if parameters are maintained within the narrow operating range, uniformities of 1.4% in x-value are obtained over a two inch area using a rotating susceptor.

Although the uniformity is very good for the (111)B orientation there is a tendency for in-plane twins to form during nucleation [35-37]. To avoid this problem, the (211)B substrate orientation is used. With this orientation the propagation of the planar twins is not stable and produces a smooth surface [38]. However, the range of Hg flux that can be used is only about a factor of two, compared to a factor of 15 for the (001) orientation.

Therefore, the requirements on Hg flux and substrate temperature are

stringent. MBE is a viable growth technique for $Hg_{1-x}Cd_xTe$ heteroepitaxial layers. However, the limitation in throughput makes this growth technique less desirable for thick structures, > 10μm, because of the typical slow growth rates of 1-2 μm/hr.

2.2.4 Metal Organic Vapor Phase Epitaxy

Perhaps one of the most promising methods of growth for $Hg_{1-x}Cd_xTe$ is by metal organic vapor phase epitaxy (MOVPE). This growth technique allows for large areas as well as reduced substrate temperatures compared to LPE. The growth of $Hg_{1-x}Cd_xTe$ by MOVPE is usually done using elemental Hg and metalorganics for the tellurium and cadmium sources. Some of the first MOVPE $Hg_{1-x}Cd_xTe$ growths were made by Irvine and Mullin using a horizontal reactor at atmospheric pressure [39]. In this work diethyltellurium (DETe) and dimethylcadmium (DMCd) were used with a hydrogen carrier gas and passed over a Hg reservoir. Films varying in composition of x= 0.0 - 0.3 were obtained at a substrate temperature of 410°C. At this growth temperature and composition of x=0.2, the interface examined by SIMS depth profiling, showed an interdiffusion depth of 0.4μm for a 30 minute growth. This value is nearly five times lower than that of comparable films grown by LPE at a temperature of 500°C and a growth time of only ten minutes [40].

The lower temperature limit of growth using MOVPE is governed by the decomposition of the precursor metalorganics. For the case of DMCd and DETe these temperatures are 360°C and 460°C respectively for total pyrolysis [41]. Using these precursors HgTe growths can be achieved at a temperature of 410°C while a substrate temperature of only 350°C is needed for the growth of CdTe. Although the decomposition of DETe is autocatalytic in the presence of Te [42], this mechanism is eliminated as a reason for the reduced growth temperature because there is less than 1.0 % of elemental Te pyrolized below 400°C [41]. In addition the substrate surface can also be neglected as there would be the same amount of Te atoms present for both types of films. As a result it was initially proposed that an adduct

was formed between the DMCd and DETe which in turn had a lower pyrolysis temperature [41,42]. However for DMCd, the activation energy for the removal of one methyl radical is 201.6 kJ/mole which is nearly twice that of the 100 kJ/mole activation energy for the growth of CdTe [43]. A good explanation is given by Bhat et. al. who found that CdTe could be deposited at 230°C using Cd vapors and DETe [44]. From this work they propose a heterogeneous decomposition of the metalorganics with the rate limiting step in the process being determined by the decomposition of DMCd. This is in good agreement with their results as the activation energies for the deposition of Cd and CdTe were 87 kJ/mole and 92 kJ/mole respectively for temperatures less than 350°C. Further evidence for this catalytic reaction is given by Liu et. al. where data from Mullin [43] and Bhat [44] have been modeled [45]. This model shows that the rate limiting step at low temperatures is the decomposition of the adsorbed organometallic compounds, whereas at high temperatures it is the adsorption of the organometallic compounds. As a result this catalytic decomposition effect makes the control of the x-value for $Hg_{1-x}Cd_xTe$ difficult to predetermine and usually leads to large variations across the substrate surface.

Another parameter which leads to a variation in x-value is the substrate temperature. As the substrate temperature is reduced from 410 to 380°C an increase in x-value from 0.2-1.0 occurs [46]. This 3% change in x-value for every 1°C is more than that observed in MBE and as a result leads to a large variation in x-value (5%),over a $1cm^2$ sample. In order to overcome this temperature sensitivity Mullin et. al. have developed an interdiffused multilayer process (IMP) [47]. With this process alternating layers of HgTe and CdTe are grown under optimized conditions for each material which are then allowed to interdiffuse. The final composition of the film is controlled by the thickness of the alternating layers and determined by Equation 2.9 where T_1 and T_2 are the thicknesses of the HgTe and CdTe respectively.

$$x\text{-}value = T_2/(T_1 + T_2) \qquad \textbf{Eq. 2.9}$$

As the growth progresses the first layers interdiffuse. When the final thickness of the film is obtained an additional 10 minutes of annealing is usually needed to allow the final layers to interdiffuse. This type of process yields very uniform films both laterally as well as in depth when the total thickness of T_1 and T_2 is maintained around 0.2μm. Although epitaxial films of $Hg_{1-x}Cd_xTe$ can be grown using the IMP method, the drawback is an increase in the interface region compared to the standard growth method. This increase is because of the higher concentration of Hg in the initial HgTe layer.

The optimum substrate temperatures for the growth of Te based compounds are high, e.g. for HgTe is 410°C using DETe, as the Te source. To lower the growth temperature, many new tellurium compounds have been synthesized which pyrolize at lower temperatures. Hoke et. al. have demonstrated a number of these new tellurium precursors in the growth of HgTe and $Hg_{1-x}Cd_xTe$ where reduced substrate temperatures have been used compared to those used with DETe [48-51]. These precursors include di-N-propyltellurium (DNPTe), diisopropyltellurium (DIPTe), ditertiarybutyltellurium (DTBTe), and diallyltelluruim (DATe) with DATe yielding a growth rate of 1μm/hr at a substrate temperature of 180°C. This type of temperature reduction, achieved by attaching a Te atom to long chained organic molecules, is seen in other organometallic compounds and is consistent with the increase in instability of these compounds [52]. The uniformities of the $Hg_{1-x}Cd_xTe$ films was not reported nor was there any mention of a possible temperature reduction going from HgTe growth to $Hg_{1-x}Cd_xTe$ with the addition of DMCd, indicating a catalytic effect. However, Kisker et.al. using dimethylditelluride (DMDTe) and DMCd, have observed that CdTe could be grown at a substrate temperature of 50°C lower than the decomposition temperature of DMDTe [53]. Also a dependance on growth rate as a function of DMCd decomposition is observed in the growth of CdTe using dimethyltellurium [44]. These two examples show that the difficulties observed with DETe and DMCd may also be present in these newer tellurium metalorganic compounds. Even if these new tellurium compounds do

exhibit a catalytic type of behavior, their reduced pyrolysis temperatures will benefit the IMP growth method for $Hg_{1-x}Cd_xTe$.

2.2.5 Photo-Assisted MOVPE

The development of the photo-assisted process came about from the need to reduce the substrate temperature from the conventional temperature range of 350 - 420°C used in MOVPE. The reduction in substrate temperature is obtained by adding energy to the organometallics via UV photons. In this process the organometallics are photolytically dissociated while the substrate temperature is maintained such that the adatoms have sufficient surface mobility to promote epitaxial film growth. The first photo-assisted MOVPE growths of $Hg_{1-x}Cd_xTe$ were done by Irvine et. al. using DETe, DMCd, and elemental Hg at a substrate temperature of 250°C [54-56]. The requirement for such a process to work is that the absorption spectra of the organometallics must overlap the output spectra of the light source being used. Shown in Figure 2.3 is the absorption spectra for DMCd and DETe [57]. The spectrum of DMCd shows a discrete absorption band between 200 and 300nm, whereas DETe shows a series of discrete absorption bands. The UV photolysis of DMCd has been shown to be a single photon process where the removal of the second methyl radical is removed immediately after the loss of the first [58-61]. This process is shown below for 193nm but has also been proven to have the same dissociation mechanism for 248nm.

$$Cd(CH_3)_2 + h\nu(193nm) \rightarrow Cd(CH_3)\cdot^* + CH_3\cdot \qquad \text{(Step 1)}$$

followed by

$$Cd(CH_3)\cdot^* \rightarrow Cd + CH_3\cdot \qquad \text{(Step 2)}$$

(a)

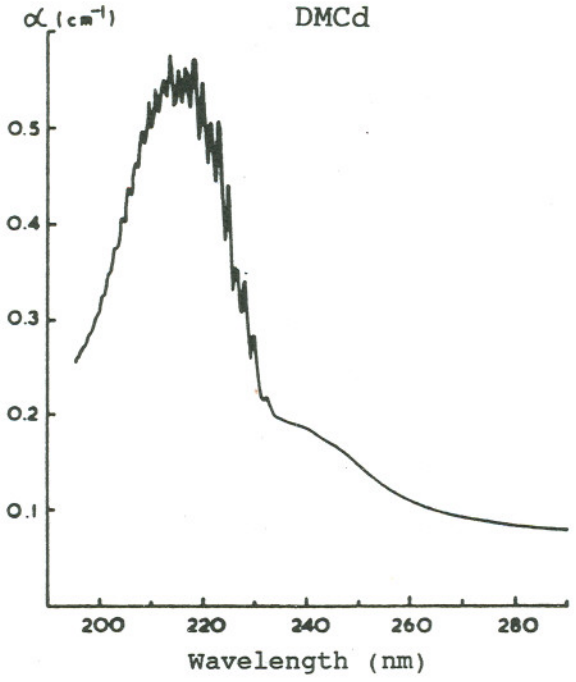

(b)

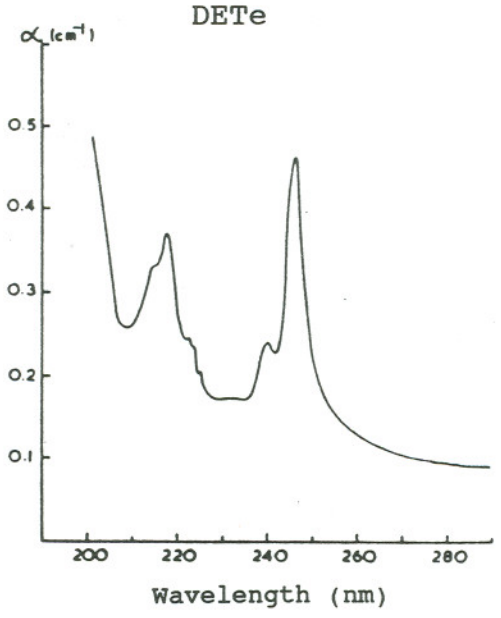

Figure 2.3 Absorption coefficient versus wavelength for a.) DMCd b.) DETe

Initial studies on the UV photolysis of DETe using a high pressure Hg lamp, gave no deposition of Te in the region of high intensity but instead had uneven deposits down stream of the radiation [57]. This type of a behavior would indicate a more complex type of dissociation other than just a single photon. However Jensen et.al. have shown that ground state Te atoms are produced from a single photon dissociation process using a 248nm excimer laser [62]. The output spectrum from a Hg lamp is made up of many wavelengths including 248nm. The cause for no deposition in the high intensity region of the lamp may be more a function of sticking coefficient for Te on silica than a result of photolysis. Using X-ray photoelectron spectroscopy (XPS), Stinespring et.al. found that no adspecies of dimethyltellurium ,DMTe, were present on SiO_2 but both DMTe and Te were present on gold and GaAs surfaces [63]. Although this study was done at room temperature using DMTe, it suggests that a similar result may occur with DETe especially at elevated temperatures created by a high intensity Hg lamp.

Because Hg is present in the growth of $Hg_{1-x}Cd_xTe$ another possible dissociation route for the organometallics is a Hg photosensitization process. This involves exciting a Hg atom to a metastable or resonance level via the UV absorption of photons ($\lambda \leq 253.7$nm) which in turn will collide with another atom. When a collision between the a metastable Hg atom and an organometallic molecule occurs, the Hg atom transfers its energy, $\approx$ 4.9eV, to the molecule which can in turn dissociate. For the case of DMCd and DETe the average metal - carbon bond energies are 1.5 eV and 2.44 eV respectively [64]. It is therefore possible that both DMCd and DETe could be dissociated via the Hg sensitization process. In addition, H_2 can also be dissociated which can in turn combine with the methyl and ethyl radicals forming methane and ethane. These byproducts are volatile, leaving Cd and Te available for epitaxial film growth to occur.

When the photo-assisted process is controlled such that the dissociation of reactants occurs on the surface of a substrate, high quality epitaxial layers are formed [65-67]. However if this process is not controlled, gas phase nucleation can occur

which will result in polycrystalline films being deposited [56]. This condition will be discussed further in Chapter 4 with the experimental results obtained from the current work presented.

3. EXPERIMENTAL EQUIPMENT and PROCEDURE

3.1 The Deposition System

There is no commercial deposition system available that would allow study of photo-assisted MOVPE of II-VI compounds, therefore an all stainless steel reactor was constructed. A schematic of this system is shown in Figure 3.1. Using stainless steel rather than quartz was mainly an issue of safety but also offered the advantage of easily making vacuum connections to a diffusion pump system for removal of atmospheric impurities. The UV photon source was a 2Kw microwave excited medium pressure Hg lamp (Fusion Systems). A sapphire viewport on the reactor admitted the UV radiation to the growth area and was kept free of deposits using a window purge and a baffle assembly. Partial pressures of the reactants were maintained using constant temperature baths or heaters and appropriate carrier gas flows. The partial pressure of elemental Hg was maintained by heating the stainless steel reservoir which was monitored with a thermocouple controller. In order to prevent the condensation of Hg from the vapor, five additional heaters were used to heat the Hg line as well as the deposition chamber. All flows, including the window purge, were maintained using mass flow controllers. The chamber pressure was controlled using a feedback system and a throttling valve.

Shown in Figure 3.2 is a typical output spectrum from the lamp source. Also shown are the absorption spectra for DMCd and DETe. As can be seen, there is a good overlap of the two precursors and the output of the lamp in the 200-250nm range. Since this is the only useful output of the spectrum, a bandpass filter was designed (Fusion Systems) to measure the available power at the substrate for these wavelengths. When measured at the substrate (inside of the chamber) the total power was measured to be 100mW/cm^2 in the 200 - 250nm range. Although a filter

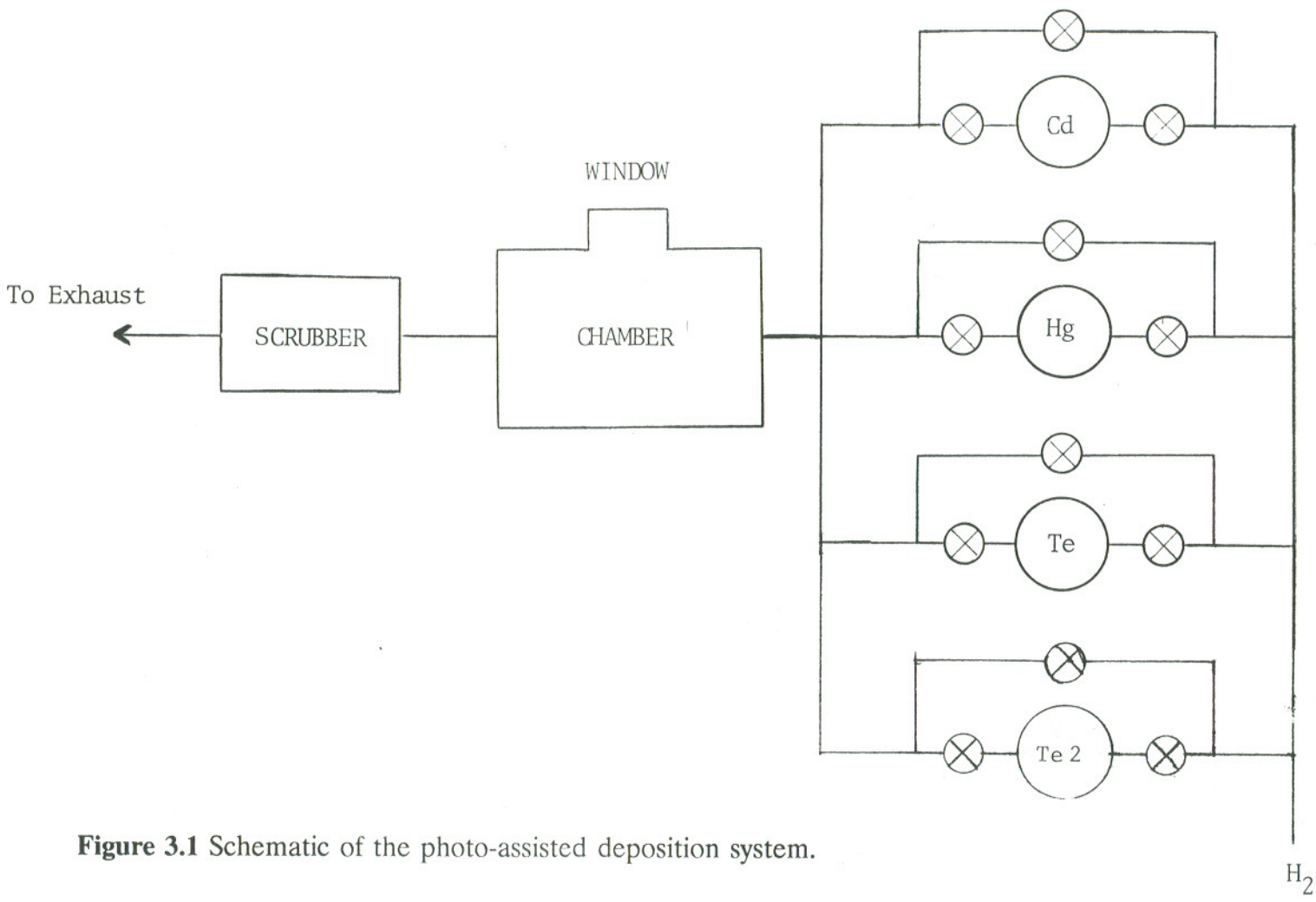

Figure 3.1 Schematic of the photo-assisted deposition system.

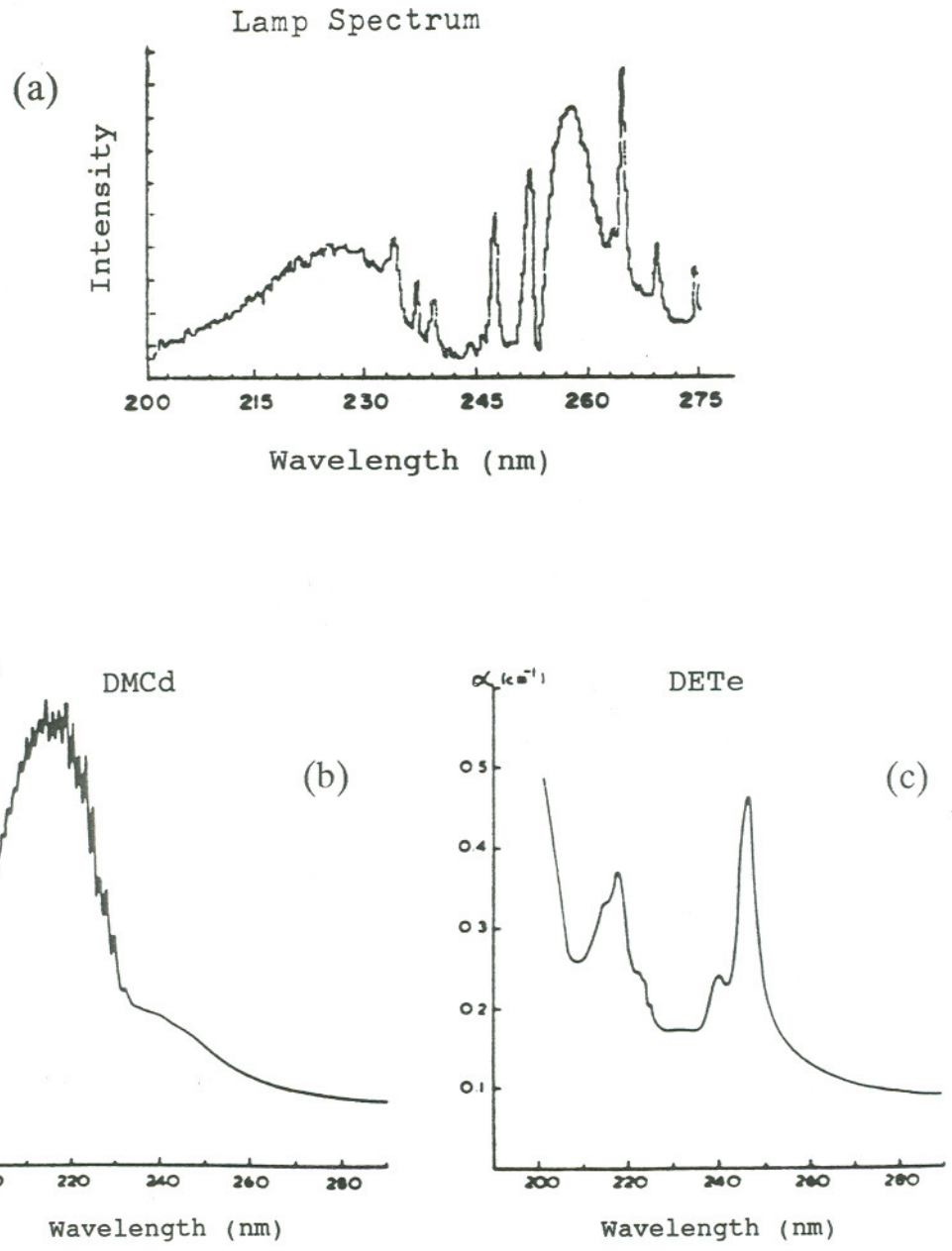

Figure 3.2 a.) Output spectrum of lamp source b.) Absorption spectra for DMCd c.) Absorption spectra for DETe.

was never placed above the window to eliminate the additional spectra, the effects of thermal irradiation were taken into account . This was accomplished by placing a thermocouple on the surface of the substrate holder next to the sample (where there was no illumination from the lamp) as shown in Figure 3.3. With the lamp on and at atmospheric pressures, the measured difference between this thermocouple and a thermocouple mounted on a CdTe substrate (with illumination) was a constant 4°C over the temperature range of 20-250°C.

3.2 Procedure and Analysis

Substrates used for this investigation included CdTe (100) 2° toward (110), (110),(100), GaAs (100), (100) 2° toward (110), and (111) orientations. Because of the limited availability of CdTe substrates, samples were repolished after growth and analysis for reuse. This procedure consisted of mounting the substrates on a glass rod using Crystal Bond and polishing the samples using 0.1μm aluminum oxide in a mixture of ethyleneglycol (40%) and water to remove about 5μm of material. After this first step, samples were then polished using a mixture of ethyleneglycol and 5% bromine in methanol (1:1) on a latex pad to remove another 5-10μm of material. The samples were then removed from the rod by dissolving the Crystal Bond in acetone. Prior to deposition, the substrates were degreased in organic solvents and then etched. The final etching procedure for the CdTe substrates included a 2% bromine in methanol etch followed by a methanol rinse and a nitrogen blow dry. GaAs substrates were etched using a H_2SO_4:H_2O_2:H_2O (5:1:1) solution followed by a deionized water rinse and a nitrogen dry. After loading the substrates, the chamber was first pumped down with the diffusion pump (base pressure 2-5 X 10^{-5} Torr), then brought up to growth temperature and pressure. The depositions were obtained over periods of four minutes to three hours (which are extrapolated to μm/hr).

After deposition the physical and electrical properties of the films were examined. The morphology of the epilayer was examined using Nomarski contrast

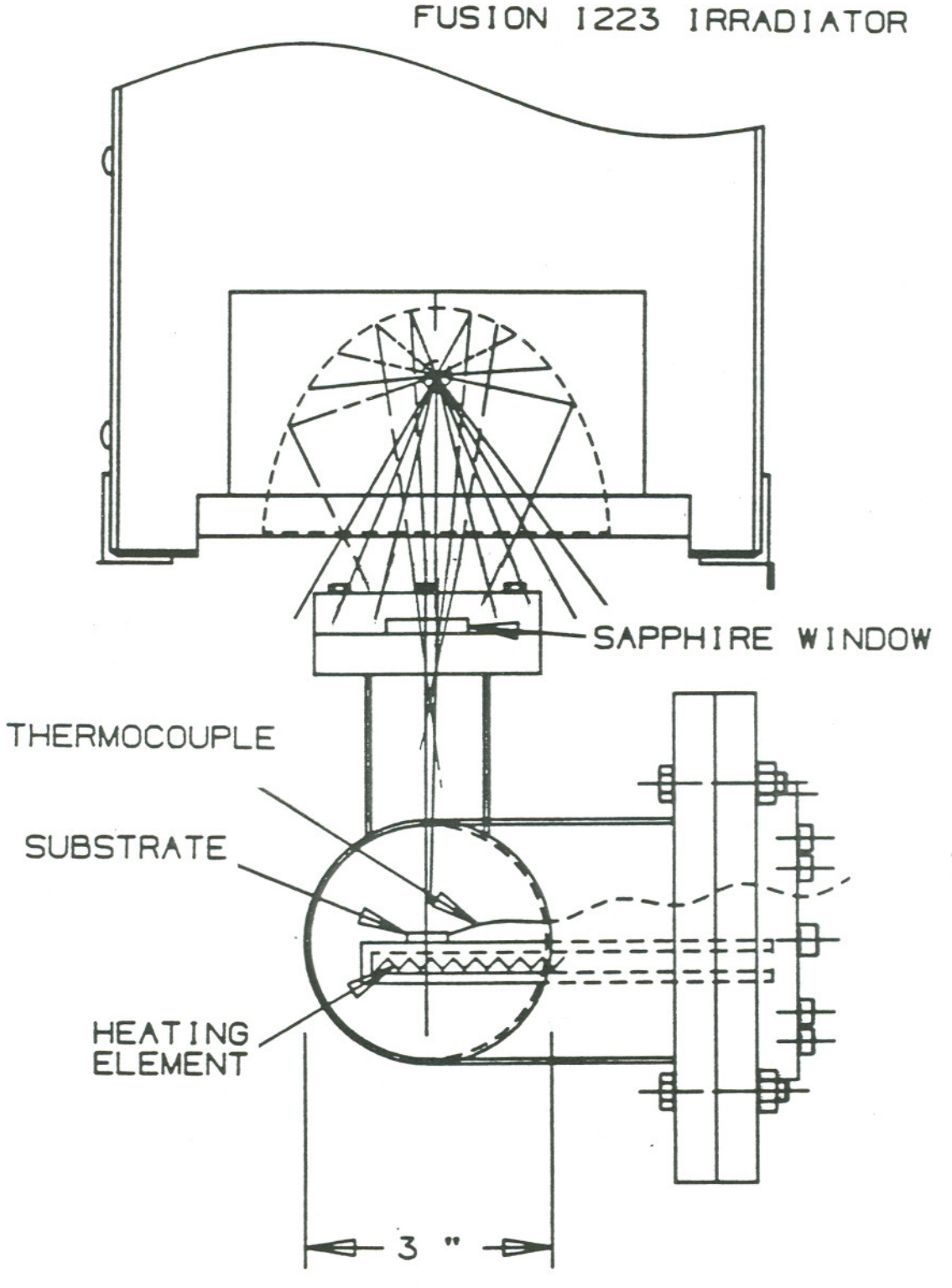

Figure 3.3 Cross section of the deposition system.

and scanning electron microscopy (SEM). Thickness measurements were made from cleaved cross sections using these microscopy techniques. The film surface roughness was characterized using a Dektak profilometer. The stoichiometry of the films was checked using energy dispersive x-ray analysis (EDX) and the crystalline properties using double crystal x-ray diffraction (DCXRD). The EDX results were calibrated with a series of substrates of known composition. Defects of the films were studied using transmission electron microscopy (TEM). The TEM samples were prepared using standard procedures which included mechanical grinding followed by Ar ion milling using a liquid nitrogen cooled stage. Also during analysis of these cross sectional profiles, the samples were kept cool with a liquid nitrogen cold finger to prevent the propagation of defects.

4. Low Temperature CdTe Growth

4.1 UV Assisted Homoepitaxy

4.1.1 Introduction

The results presented below are from an investigation of homoepitaxy of CdTe using UV photon-assisted MOVPE. The goal for this investigation was to achieve high growth rates (> 4μm/hr) using the standard DMCd and DETe precursors and to reduce the growth temperature employing UV photons. The results reported here utilized this approach to grow epitaxial films of CdTe at 250°C. At this temperature, there was no film growth using a purely thermal process.

4.1.2 Results and Discussion

One of the first deposition parameters examined was the ratio of DETe to DMCd by holding the pressure of one constant and varying the other so the ratio between the two ranged from 1 to 4. In one case the partial pressure of DETe was held constant at 1.62×10^{-3} atmosphere and in the second case DMCd was held constant at 5.41×10^{-4} atmosphere. Under both of these conditions, when the ratios were between 2 and 3.5, the CdTe films deposited were found to be stoichiometric. For all subsequent depositions, the DETe:DMCd ratio of 3 was used.

The deposition rate could be varied by several parameters, including the partial pressure of the precursors. By increasing the partial pressures, it was noticed that the surface roughness of the films increased with the growth rate. The average surface roughness was determined with a profiler and are plotted in Figure 4.1. Best fit to the data yields a curve given by $Y = 2.21 \times 10^{-2} \exp(0.218\ X)$, where Y denotes

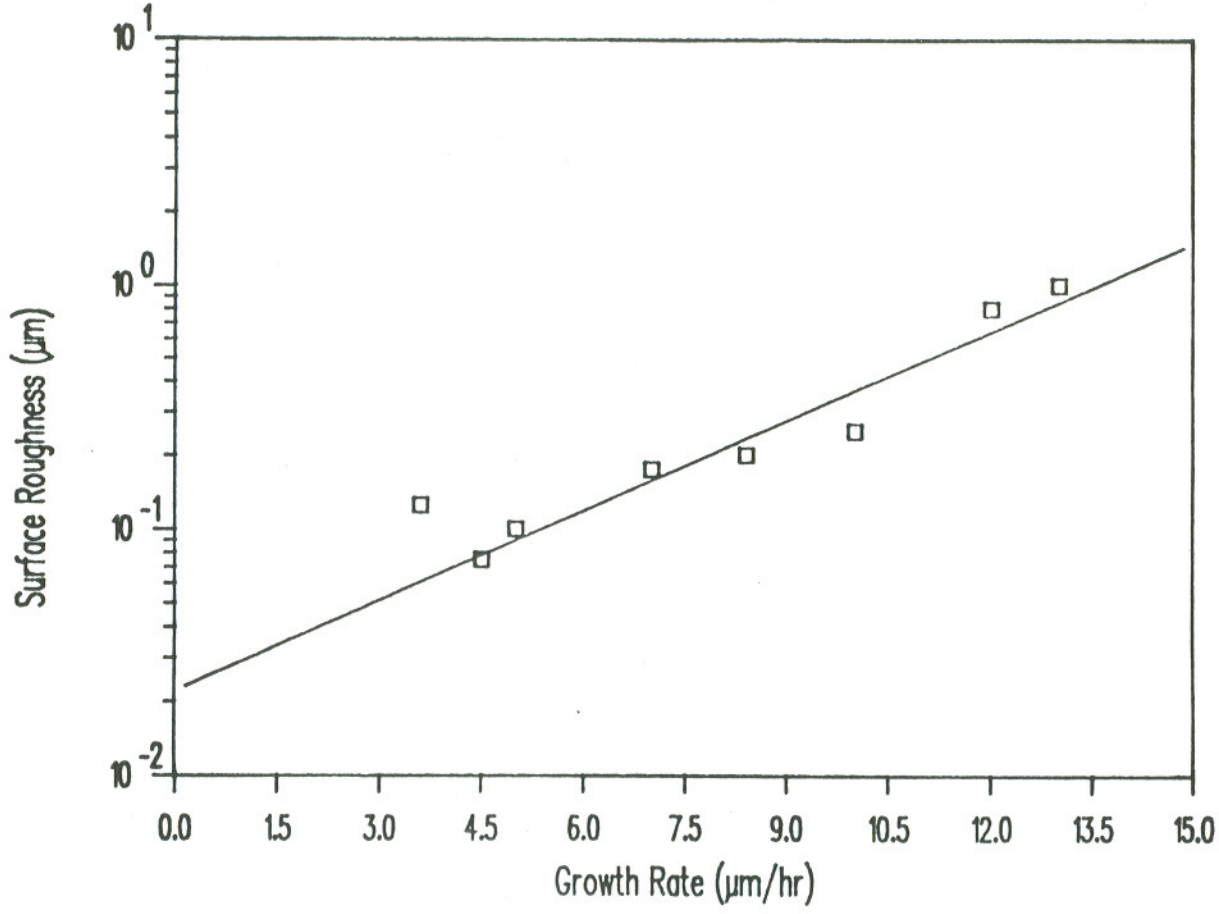

Figure 4.1 Surface roughness versus the growth rate for homoepitaxial growth of CdTe.

the surface roughness and X the growth rate. When the growth rate is zero, the roughness is 0.022μm, which is consistent with the 0.02μm surface roughness of bare substrates. From the plot it can be seen that an exponential relation exists between these two parameters. The reason for this behavior is not understood, however the severe roughness at higher growth rates is probably due to gas phase nucleation. It has been reported that by using He as the carrier gas, gas phase reactions can be decreased, hence allowing growth of films with smooth surfaces [53]. However, when He was used as a carrier gas in our system, a slight drop in growth was observed which resulted in a corresponding decrease of surface roughness, consistent with Figure 4.1.

The surface roughness was also examined as a function of the film thickness. Epilayers were grown over periods ranging from ten minutes to one hour with DETe and DMCd partial pressures of 1.62×10^{-3} and 5.41×10^{-4} atmospheres, respectively, and the UV lamp intensity of 100 mW/cm^2. These results are plotted in Figure 4.2. In the range examined, the relationship between the surface roughness and the film thickness was found to be $Y = 2.46 \times 10^{-2} X^{1.15}$, where X is the film thickness and Y the roughness. The film growth rate was 12 μm/hr.

The dependence of the growth rate on the lamp intensity was examined at the same partial pressures of DETe and DMCd as above. Stainless steel screens of different sizes were placed over the sapphire window to vary the intensity without changing the emission spectrum of the lamp. The results, as plotted in Figure 4.3, show a linear relationship over the range of values examined.

The dependence of growth rate on the substrate orientation was investigated by growing CdTe on (100), (110), and (100) with 2° offset towards (110) oriented CdTe substrate. These results are presented in Table 4.1, where the growth rate on (110) substrates is nearly twice that of (100) and the 2° offset substrates having the lowest growth rate of the three. Similar dependence on substrate orientation has also been reported with photon-assisted epitaxy of HgTe [43]. At high growth rates (> 8μm/hr), the surface morphologies of the CdTe films on (110) and (100) oriented

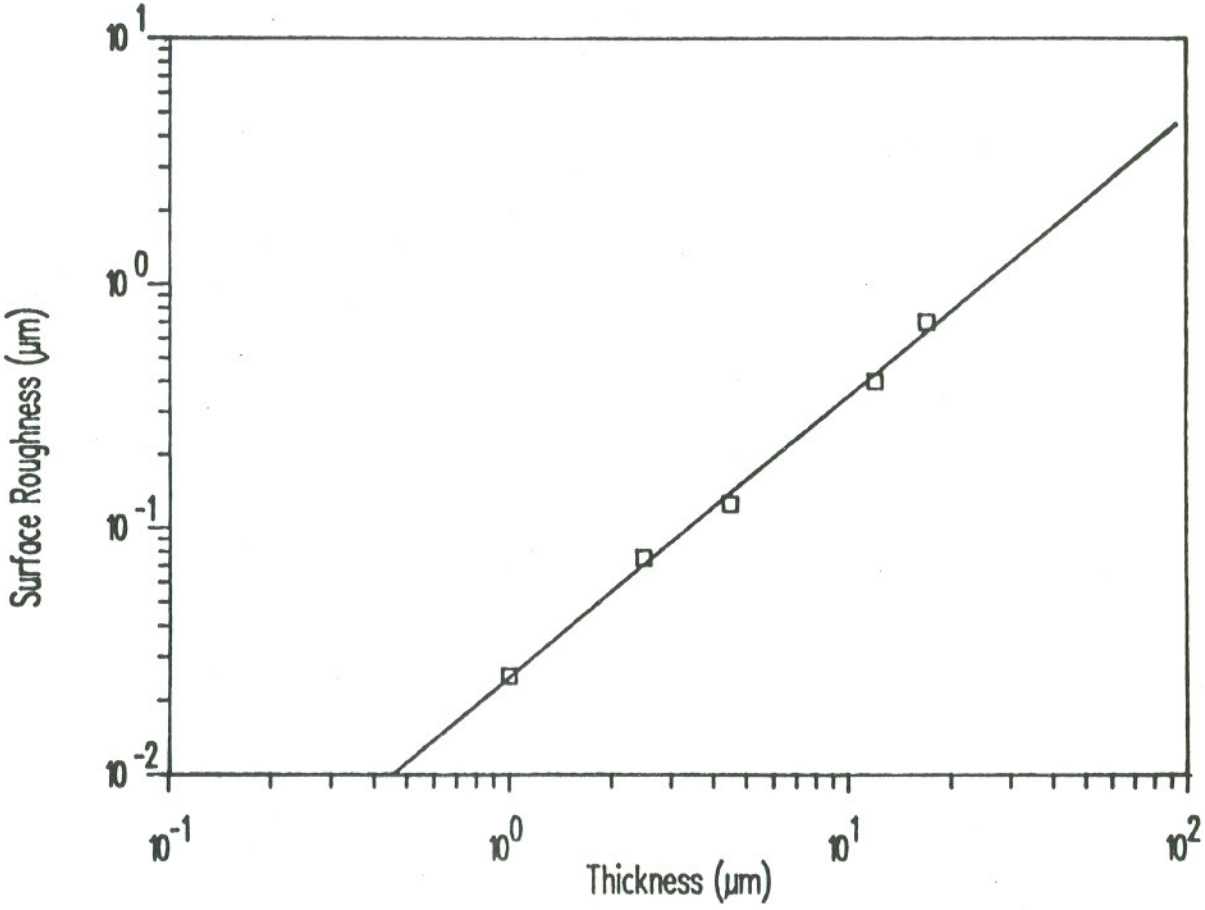

Figure 4.2 Dependence of the surface roughness on the thickness of the CdTe epilayers.

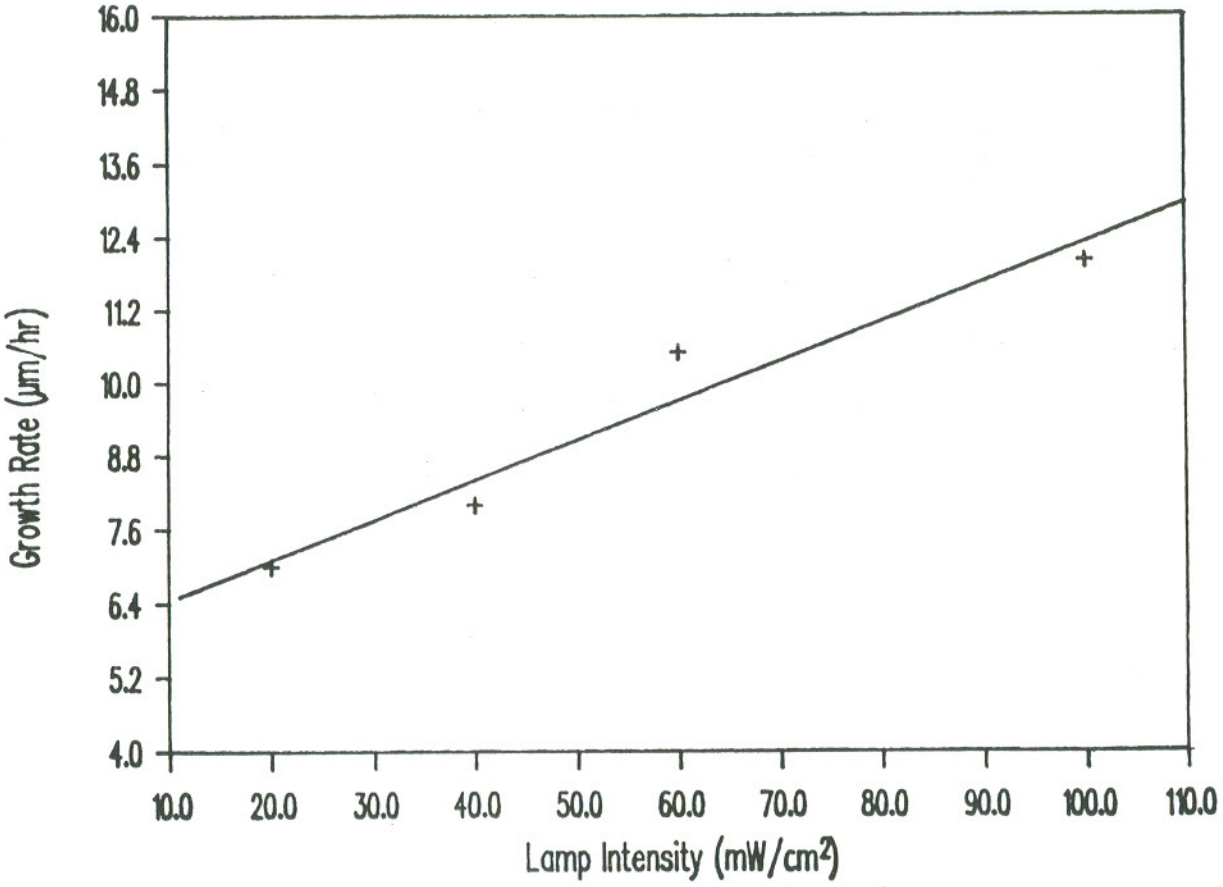

Figure 4.3 Plot of growth rate of the epilayer versus the UV light intensity.

Table 4.1 Growth rate of epitaxial CdTe versus the substrate orientation at three different DMCd and DETe partial pressures.

Substrate Orientaion	Growth Rates (μm/hr)
(100) --> 2° (110)	0.2 2.8 7.6
(100)	0.4 3.2 8.4
(110)	1.0 9.4 13.8

substrates appeared distinctly different, as shown in Figures 4.4a and 4.4b, which are SEM micrographs. While the film on (110) appears grainy, the (100) oriented substrates have 'weaved' surfaces. The film on the 2° misoriented substrates appeared similar to that on (100), except the width of the stringy structures was about half. One should note that films grown at low growth rates (< 2 μm/hr) had smooth nearly featureless surfaces.

All the films grown on the different substrates were also analyzed using x-ray diffraction. The results showed that the films had the same orientation as the substrates. An example of the x-ray diffraction pattern of a 7μm thick film grown at 10 μm/hr on (100) substrate is shown in Figure 4.5. The bulk defects in these films were then examined using cross-sectional TEM. A TEM micrograph of the same sample shown in Figure 4.5 is presented in Figure 4.6. It shows band structures which propagate obliquely through the film thickness. We believe it is these structures which give rise to the weaved texture of the film surface.

Double crystal x-ray (Cu $k_{\alpha 1}$) rocking curves of the CdTe epilayers ((004) reflection) were obtained using a Si four crystal monochrometer. Typical values of full width half maximum (FWHM) of the CdTe films (> 6 μm thick) were in the 48 to 200 arc sec range, where the films grown at slow rates exhibited narrower values. One should note that the FWHM of the substrates prior to deposition were typically in the 28 to 80 arc sec range, therefore, the growth of the films almost doubled this value.

Electrical properties examined included resistivity and room temperature Hall measurements using the van der Pauw technique. Ohmic contacts were made to the epilayers using evaporated AgIn (10% Ag) followed by a 20 second anneal in N_2 at 200°C. All samples exhibited an n-type behavior and a general trend of decreasing mobilities (121 to 88 cm^2/V-sec) and carrier concentrations (10^{18} to 3.6 x 10^{17} cm^{-3}) with an increase in growth rate. At the same time, the resistivity increased from 0.05 to 0.2 ohm-cm, probably due to incorporation of more defects in the films at the higher growth rates.

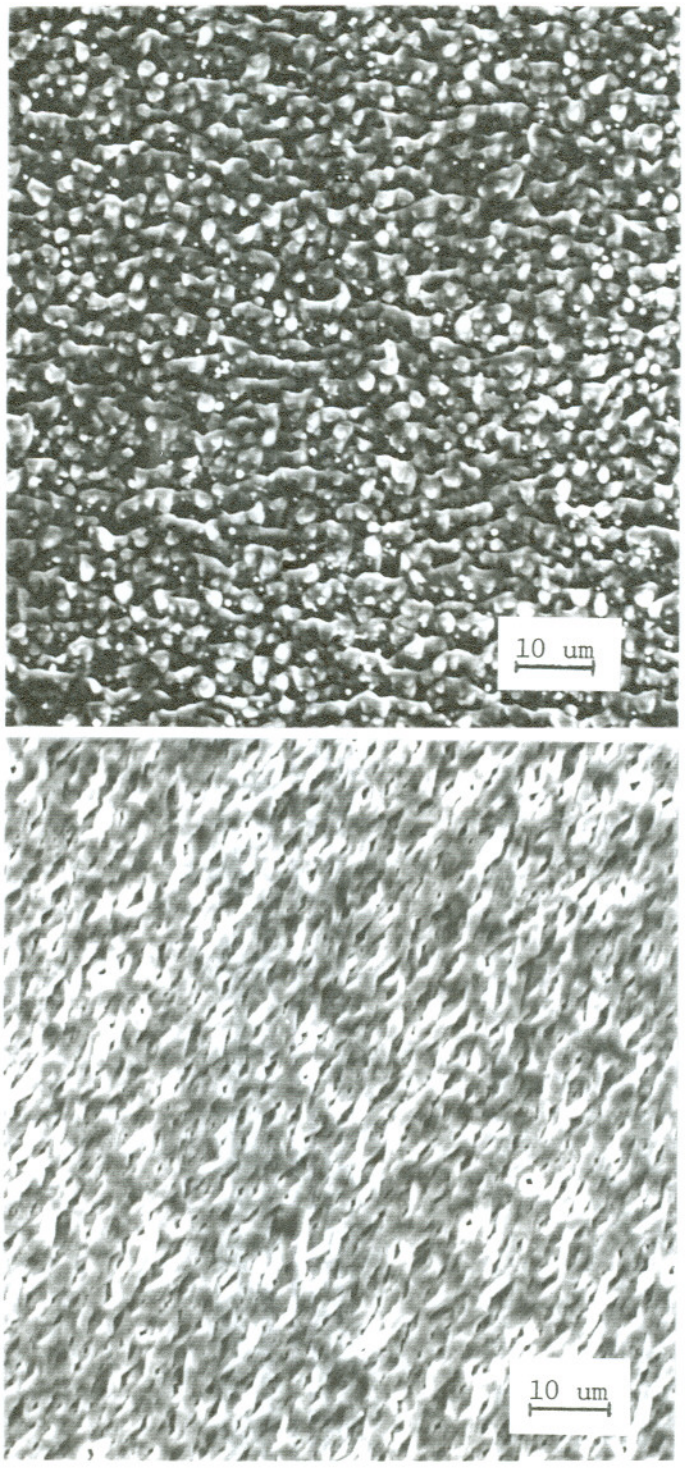

Figure 4.4 SEM micrographs of the CdTe epilayers grown on (a) (110) and (b) (100) oriented substrates.

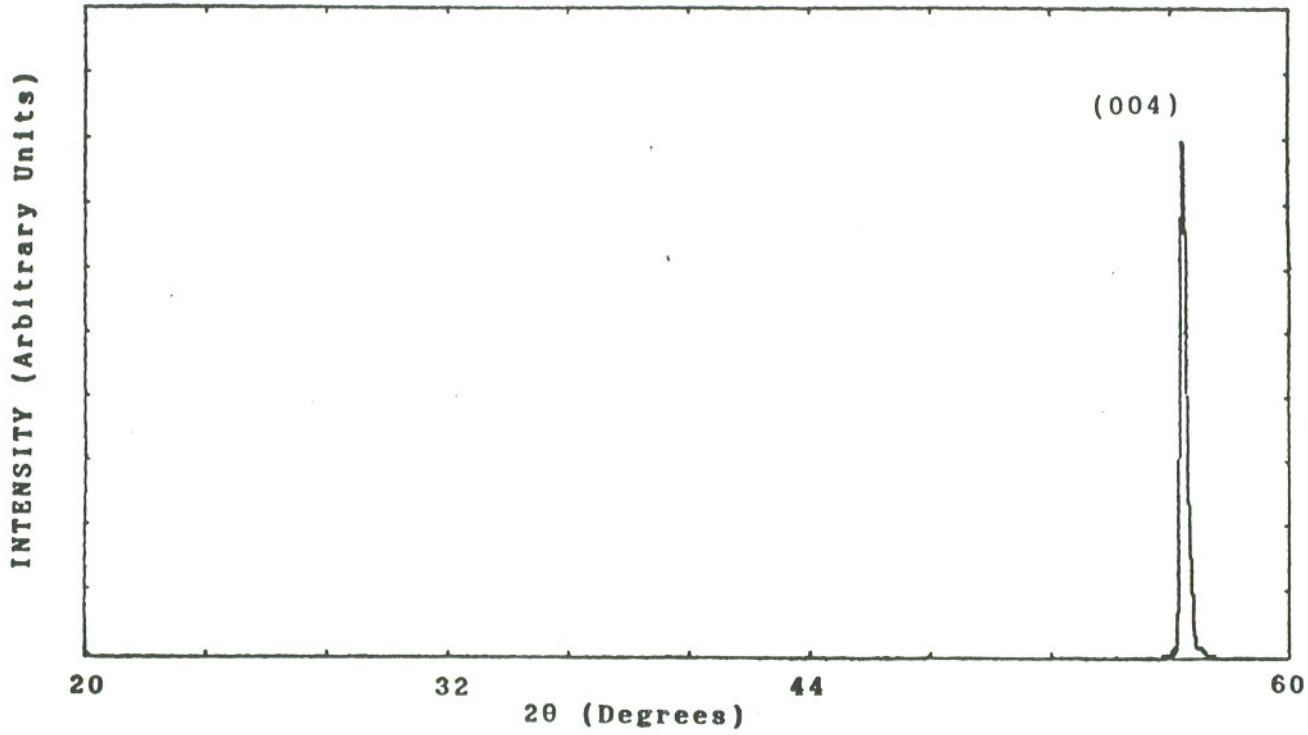

Figure 4.5 X-ray diffraction pattern of a 7μm thick CdTe film grown at 10 μm/hr on (100) substrate.

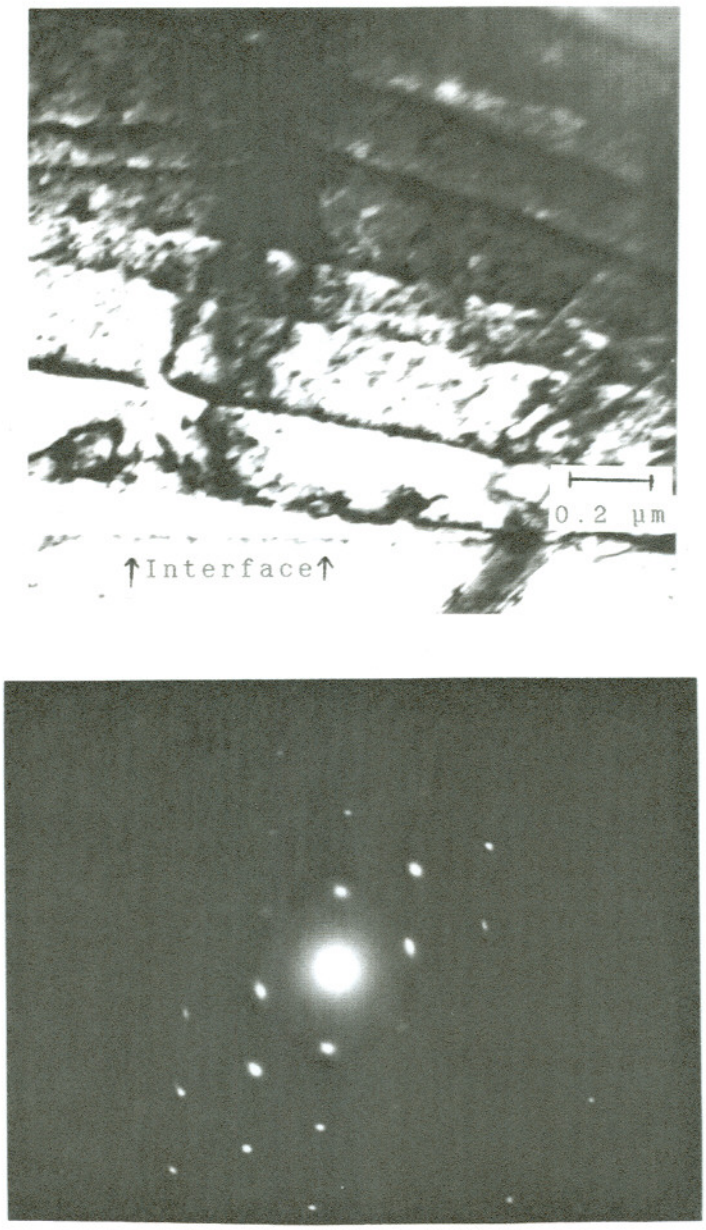

Figure 4.6 TEM micrograph of a CdTe film grown at 10 μm/hr.

In summary UV photon-assisted MOVPE has been utilized to achieve homoepitaxy of CdTe at high growth rates. Empirical relationships between the growth parameters and the growth rates have been obtained. It is found that the surface roughness of the epilayers increased with the growth rate. In order to maintain smooth surfaces the growth rate must be reduced to less than 2 μm/hr which will be necessary for subsequent growth of $Hg_{1-x}Cd_xTe$ epitaxial layers.

4.2 UV Assisted Heteroepitaxy

4.2.1 Introduction

Ultraviolet assisted MOVPE of CdTe on GaAs was investigated using DETe and DMCd. As discussed previously, alternate substrates such as GaAs offer the advantage of increased substrate size as well as the fabrication of monolithic optoelectronic devices. Heteroepitaxy of CdTe has been investigated using InSb [68], sapphire [69], and GaAs [26,27,70]. Of these materials GaAs is preferred because signal processing electronics can be built into the substrate as well as high quality wafers are available at a modest price. Although epitaxial growth of CdTe on GaAs has been achieved using several techniques including photodeposition [64,66,67], detailed investigation of defects (arising from the 14.6% lattice mismatch at room temperature) have been limited to films grown via MBE [71,72], and MOVPE [35,73,74]. Because the photo-assisted process allows for film growth to occur at temperatures as low as 220°C, the thermal stress between the two materials at the interface should be less compared to conventional MOVPE. The films described below were grown at a substrate temperature of 250°C using photo-MOVPE. At this temperature there was no growth using purely thermal MOVPE.

4.2.2 Results and Discussion

The CdTe film growth rates as high as 13 and 9 μm/hr were obtained on CdTe and (100) GaAs substrates, respectively. However, at these high growth rates the surface morphology appeared rough on both GaAs and CdTe substrates. Since similar surface texture was present on both CdTe and GaAs substrates, the cause is believed to be substrate independent and related to the high growth rate of photo-MOVPE, as discussed in the previous section.

In an attempt to determine the cause of the surface roughness and its relationship to the defects present in photo-MOVPE grown films a series of depositions were obtained under various conditions. Energy dispersive x-ray (EDX) analysis was used to check the stoichiometry of the films.

Similar to the homoepitaxial work, the ratios of DETe:DMCd were investigated by holding the partial pressure of one precursor gas constant and varying the other, i.e., keeping DETe constant (DETe = 1.62×10^{-3} atm) and varying DMCd and then holding DMCd constant (DMCd = 7.42×10^{-4} atm). This is illustrated in Figure 4.7 where an increase in DETe results in an increased deposition rate whereas an increase of DMCd leads to a drop at these partial pressures. This decrease in growth rate is believed to be a result of the increased production of methyl radicals from DMCd which in turn reduces the amount of UV photons reaching the substrate due to absorption.

At a ratio of about 3, the surface roughness reached a minimum. Using this ratio the total flow rate was varied to eliminate the effects of window purge and maximize the growth rate. Operating at these growth conditions, depositions were made with various lamp powers. Similar to homoepitaxy the resulting growth rate gives a linear relationship versus lamp intensity.

Nomarski and scanning electron micrographs showed that the films grown at high growth rates exhibited rougher surfaces whereas at low growth rates near featureless surfaces were obtained on both CdTe and GaAs substrates. The average

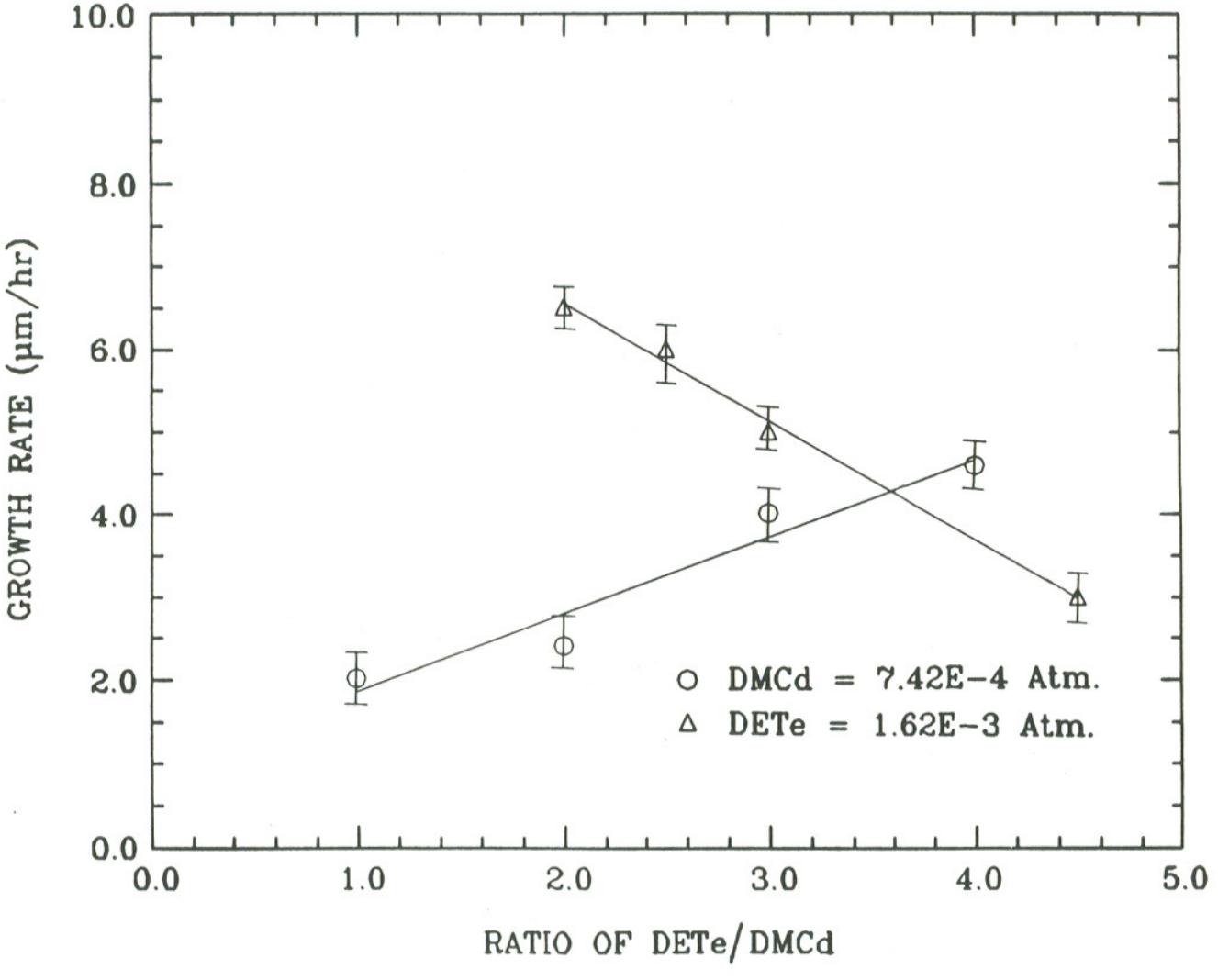

Figure 4.7 Growth rate versus DETe:DMCd ratio.

surface roughness was measured with a profilometer and is plotted in Figure 4.8 against the growth rate. It can be seen that there appears to be a threshold, independent of substrate, beyond which the surface roughness increases significantly. For these growth parameters the surface roughness increases linearly with the growth rate beyond a threshold value of ≈ 7 μm/hr. One should note that for most of these growth conditions examined, both CdTe and GaAs substrates were used together so that identical conditions for epigrowth occurred. However, the growth rate of homoepitaxial films was higher (1.5-2 times) than for heteroepitaxy. This could be due to the same lattice constant and lower activation energies for homoepitaxy.

The structure of the CdTe films grown on GaAs substrates at both below and above the threshold growth rate was examined using transmission electron microscopy (TEM). The epitaxial growth of a 4.5μm thick CdTe film grown on (100) GaAs substrate at 9 μm/hr is shown in Figure 4.9a. The cross-sectional transmission electron diffraction pattern of the interface region observed along a [110] direction shows an epitaxial growth and an accurate alignment of the two lattices. The diffraction pattern is composed of pairs of spots, where the inside spot corresponds to CdTe and the outer to GaAs. The separation between the two spots represents the lattice mismatch.

Transmission electron micrograph of the CdTe/GaAs interface region of the above sample is shown in Figure 4.9b. Moire fringes can be observed at the well-defined interface and a periodic array of misfit dislocation 31Å apart were measured along [100] direction. The spacing of the dislocations obtained via photo-MOVPE is the same as that observed with MBE [71,72] and MOVPE [74]. Dislocations that originated at the interface and traversed along [111] planes into the epilayer were also observed. In addition, single dislocations and dislocation pairs were found to be present throughout the thickness of the film, which could be responsible for the surface roughness.

In isolated areas of the epilayer, thin lamella twins were also observed lying parallel to the interface, as shown in Figure 4.10. Such twins have been reported

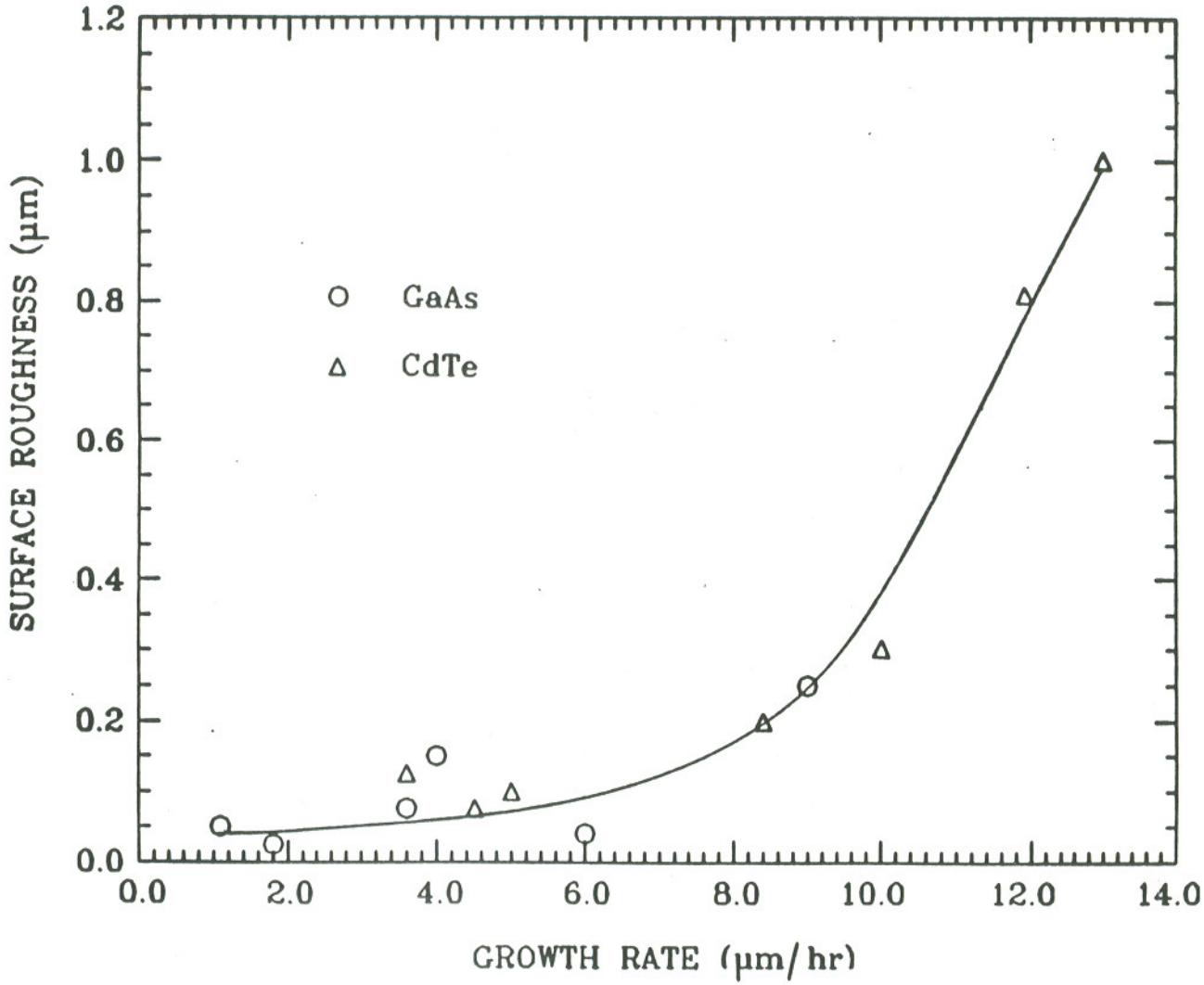

Figure 4.8 Surface roughness versus growth rate with DETe:DMCd ratio of three.

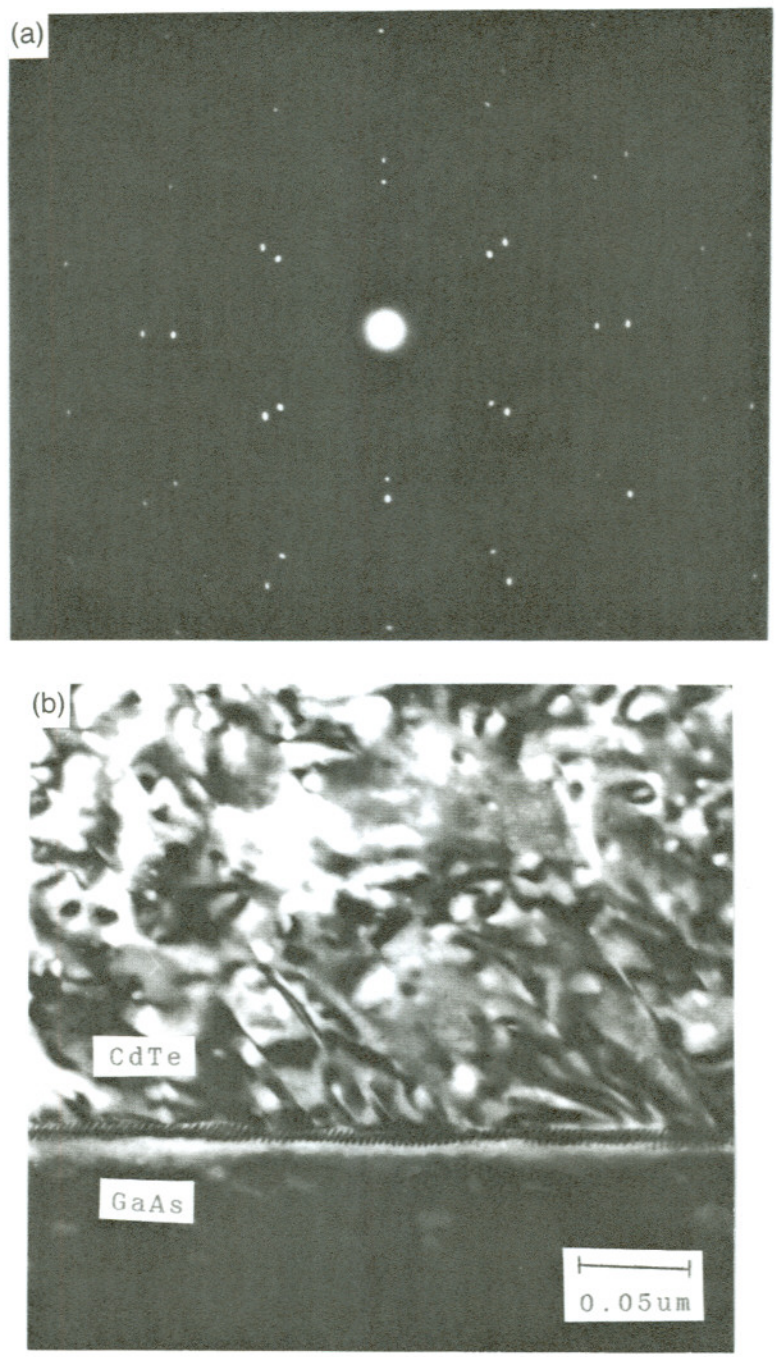

Figure 4.9 (a) TEM [110] diffraction pattern of CdTe grown at 9μm/hr on (100) GaAs. (b) TEM micrograph showing interface of CdTe on (100) GaAs and Moire fringes.

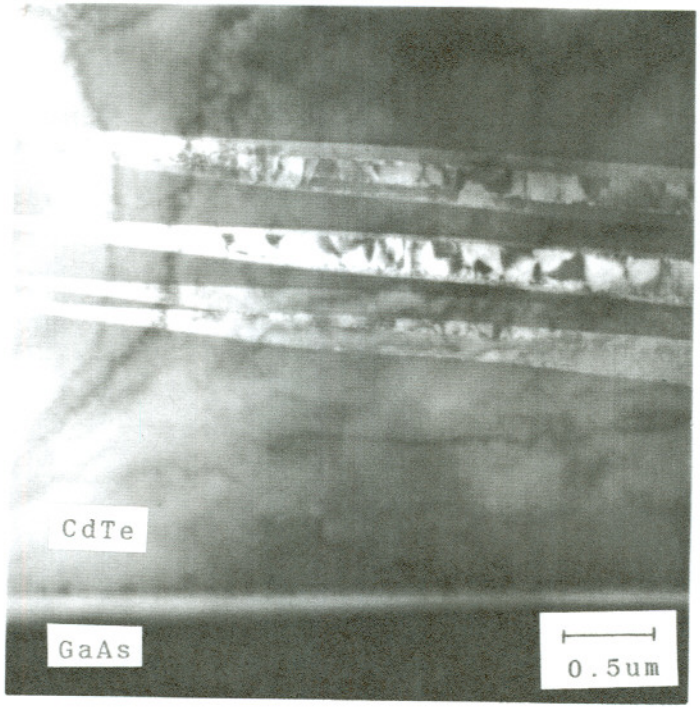

Figure 4.10 TEM micrograph showing the presence of lamella twins in the bulk of CdTe epilayer parallel to the interface.

previously only when (111) CdTe has been grown on both (111) and (100) GaAs substrates and the oxide desorption step was included prior to film growth [73]. The identity of the twins observed in our study was confirmed to be twin lamella by the presence of extra spots in 1/3 *a* (where *a* is the lattice constant) [111] positions in [110] selected area diffraction patterns. The reason for creation of these twins is not understood; however, it could be related to gas-phase nucleation at high photodeposition rates.

The CdTe epilayers grown on GaAs below the threshold growth rate were also examined in a similar manner. A cross-sectional transmission micrograph of CdTe epilayer grown on (100) GaAs at 2.5 μm/hr is shown in Figure 4.11. Transmission electron diffraction pattern of this sample was similar to that shown in Figure 4.9a, indicating growth of epitaxial (100) CdTe film. A high density of dislocations extending $\approx 0.2\mu$m from the interface in the [111] plane was observed in the epilayer and dropped significantly beyond $\approx 0.9\mu$m from the interface. There is a noticeable absence of the twins which were observed at the higher growth rates.

Photo-MOVPE of CdTe on (111) GaAs was briefly examined. Transmission electron diffraction pattern (Figure 4.12a) showed the growth of the (111)-oriented epitaxial CdTe film. Transmission electron micrograph of the interface region shows the presence of Moire fringes (Figure 4.12b) and dislocations; however, there were no twins observed lying parallel to the interface in the epilayer as have been reported in MOVPE of CdTe on (111) GaAs [35,73]. The growth rate for photo-MOVPE of CdTe on (111) GaAs was about an order of magnitude lower than on (100) GaAs.

The growth of CdTe on GaAs as a function of time is shown in Figure 4.13 together with their corresponding surface roughness. From the slope of the thickness versus time curve, a growth rate of 6 μm/hr is obtained as well as a nucleation time of about six minutes at partial pressures of 1.62×10^{-3} atm. of DETe and 5.41×10^{-4} atm. of DMCd. For growth periods of greater than 30 minutes the surface roughness of the epilayers remains constant. This roughness is probably due to the process of photo-deposition alone since the growth is occurring far enough from the interface

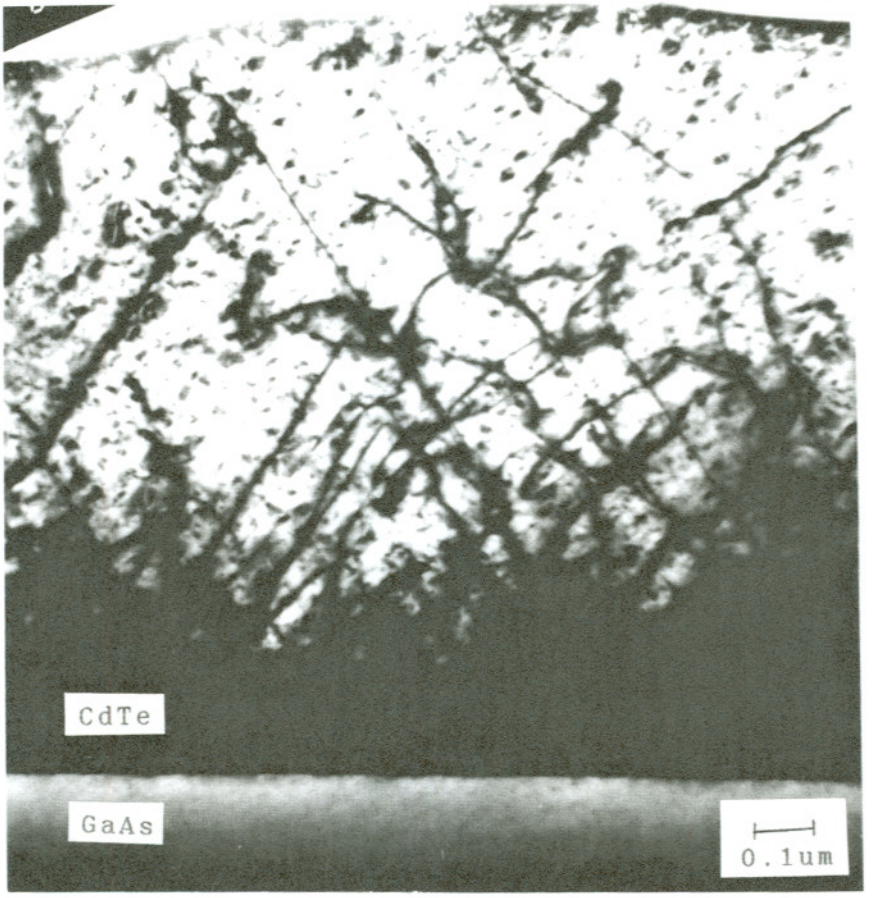

Figure 4.11 TEM micrograph of CdTe epilayer grown at a slow growth rate (2.5 μm/hr) on (100) GaAs.

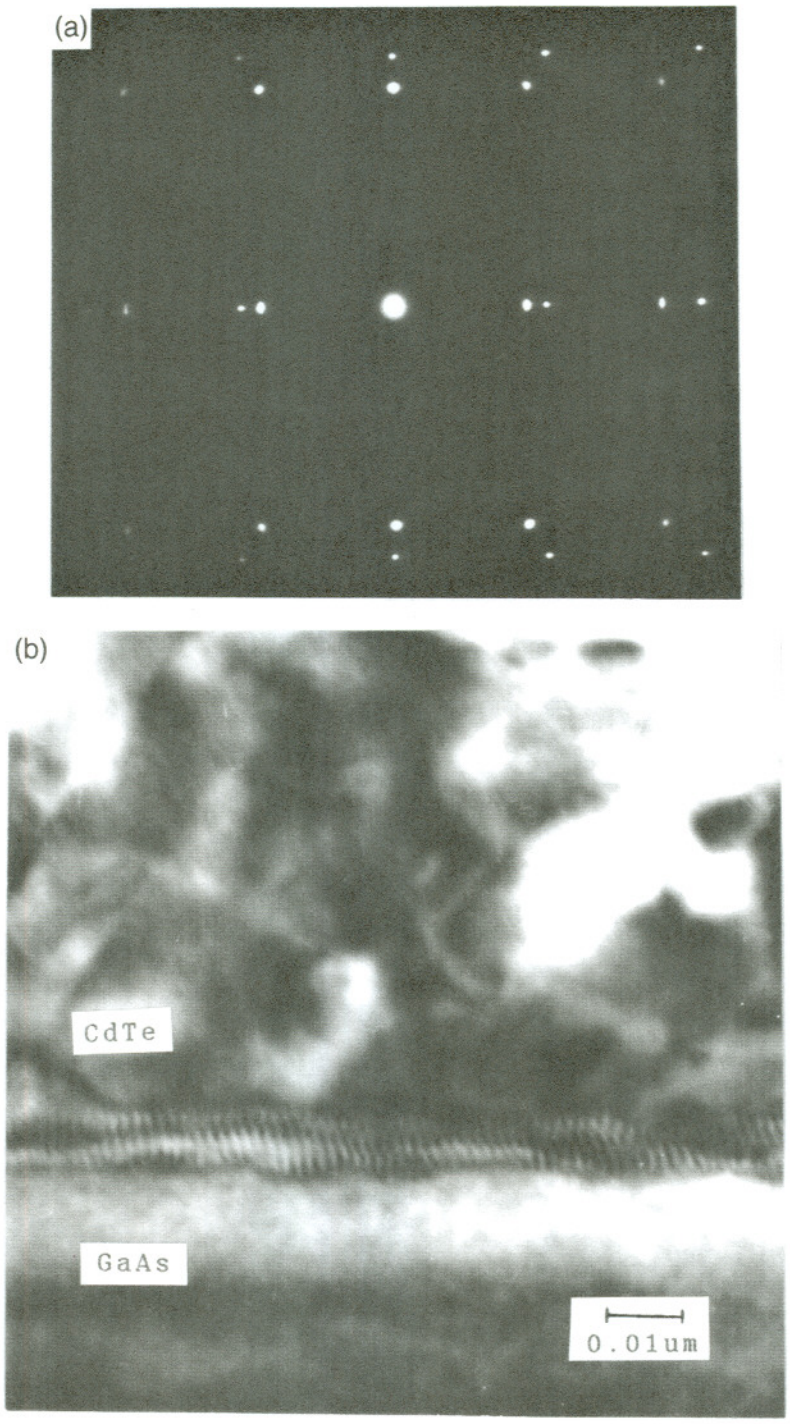

Figure 4.12 (a) TEM [211] diffraction pattern of CdTe grown on GaAs (b) TEM micrograph of the CdTe/GaAs (111) interface and resulting Moire fringes.

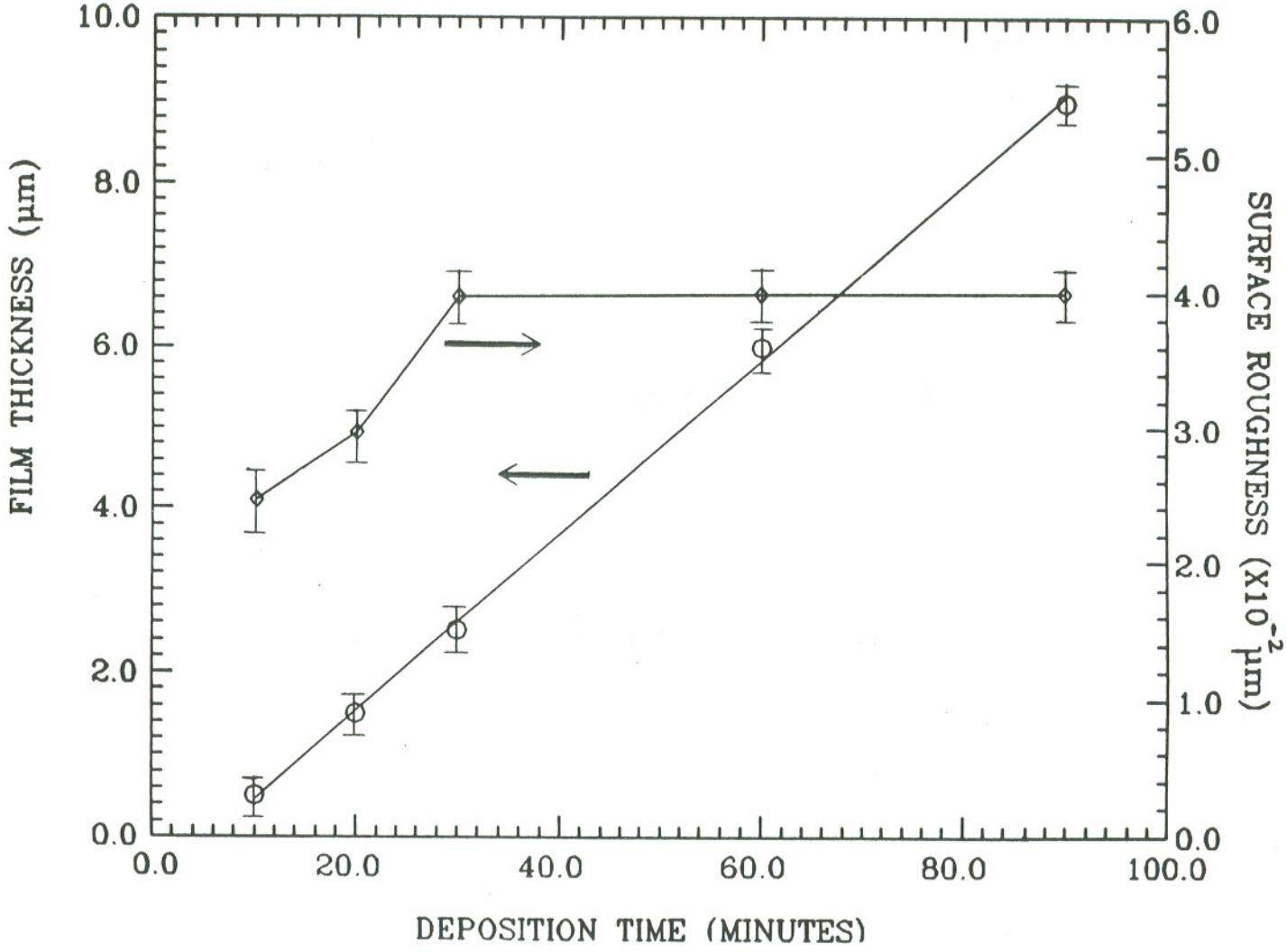

Figure 4.13 Growth rate and surface roughness versus deposition time with DETe:DMCd ratio of three.

region. The surface of a 6μm thick CdTe epilayer is shown in the Nomarski micrograph of Figure 4.14.

X-ray (Cu $K_{\alpha 1}$) double-crystal rocking curves (DCRC) of the CdTe epilayers were obtained using Si four-crystal monochrometer where the spot size at the sample was 1 X 2 mm. A FWHM of 750 arc seconds was obtained for the (004) reflection of a 2.5μm thick CdTe film grown at a deposition rate of 6μm/hr as shown in Figure 4.15. As the film thickness was increased to 9 μm, the FWHM value was reduced to 250 arc seconds. This reduction in FWHM values was consistent with the TEM analysis that showed a reduction in defect density with the thickness of the film (x-ray penetration $\approx$ 10μm). Films with a surface roughness greater than 0.1μm generally exhibited FWHM values in excess of 700 arc seconds, independent of film thickness.

4.2.2 Summary

Epitaxial CdTe films were grown on GaAs using DETe and DMCd via photo-MOVPE. It was found that a threshold exists for the growth rate beyond which the surface roughness increased rapidly. Below this threshold, near featureless surfaces were obtained. The TEM analysis showed that dislocations were confined near the interface for films deposited at low growth rates. At high growth rates, dislocations were observed throughout the thickness of the epilayers. DCRC FWHM values of 250 arc seconds were obtained for 9μm thick CdTe films with smooth surfaces. Epilayers on the order of 1 - 2μm produced at low growth rates should provide a good starting substrate material for the growth of $Hg_{1-x}Cd_xTe$.

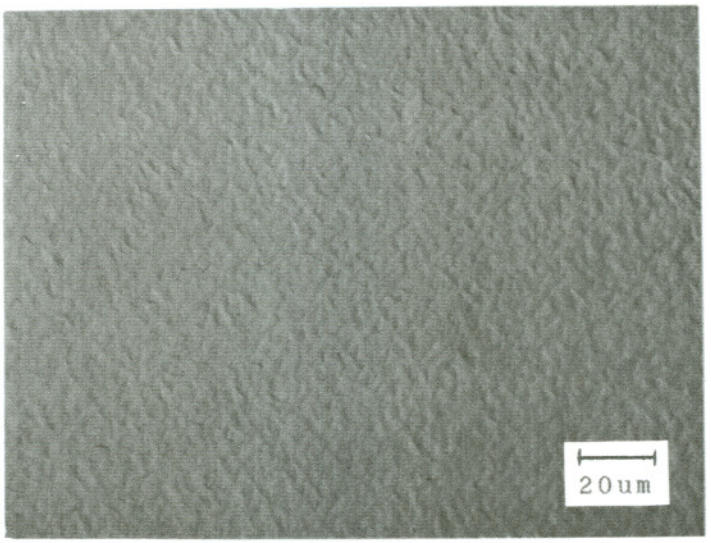

Figure 4.14 Nomarski contrast micrograph of 6μm thick CdTe epitaxial layer showing surface morphology.

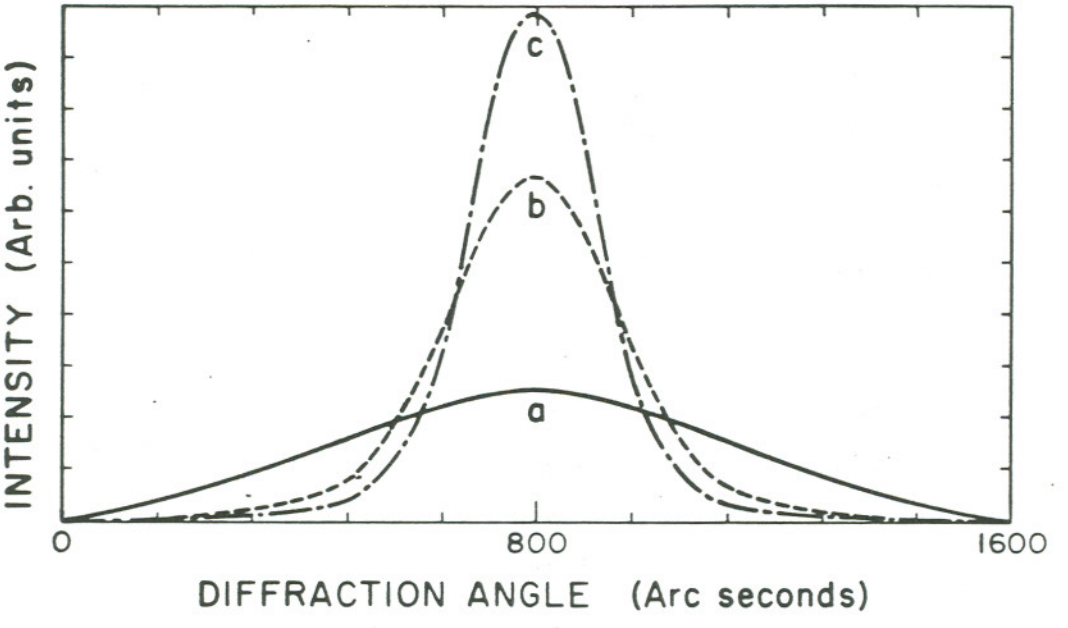

Figure 4.15 X-ray rocking curves for CdTe epilayers grown at a growth rate of 6 μm/hr where (a) 2.5μm thick film FWHM = 750 arc-second. (b) 6μm film FWHM =350 arc-second. (c) 9μm film FWHM = 250 arc-sec.

5. Low Temperature Growth of $Hg_{1-x}Cd_xTe$

5.1 Introduction

The main objective was to grow $Hg_{0.8}Cd_{0.2}Te$ at a reduced substrate temperature (≈ 250°C). However a secondary goal was to achieve a growth rate in excess of 3 μm/hr. This value was deemed necessary in order to facilitate production capabilities in an industrial process, which would allow 1½ growths per eight hour shift for a 10 μm thick structure. Growth studies made using DETe, DMCd, and elemental Hg resulted in $Hg_{1-x}Cd_xTe$ films of good quality but, with a maximum achieved growth rate of only 2 μm/hr. As a result different tellurium compounds were investigated using the photo-assisted process. These results are described below where diisopropyltellurium (DIPTe) and methylallyltellurium (MATe) were used as the tellurium precursor.

5.2 $Hg_{1-x}Cd_xTe$ Growth Using DIPTe

The growth of $Hg_{1-x}Cd_xTe$ was conducted using both CdTe and GaAs substrates. All growths using DIPTe had a substrate temperature of 250°C and a lamp power of 100 mW/cm^2 in the 200 to 250nm spectral range. The lamp power was not varied because of results obtained from CdTe depositions. These results indicated that the growth of CdTe occurred only in the center of the illumination spot (≈ 1.5 cm diameter) with no growth upstream or downstream. Although $Hg_{1-x}Cd_xTe$ has been grown at 350°C [48], no thermal growth was present at 250°C.

Because of the high degree of photo-sensitivity, HgTe growth was first investigated. Unlike the CdTe depositions, HgTe film growth occurred uniformly inside as well as outside of the illumination spot. This is believed to be a result of

Hg photo-sensitization. Growth rates in the range of 4 to 5 μm/hr were obtained on both CdTe and GaAs with both substrates having identical rates. Using a total flow rate of 0.5 lt/min, the partial pressures of DIPTe and Hg were varied while holding the other constant. Shown in Figure 5.1 are the results of various Hg partial pressures with a DIPTe partial pressure of 2×10^{-3} atm. At a Hg partial pressure of 0.025 atm. both the hillock density and X-ray double crystal rocking curve FWHM values were at an apparent minimum. For values of Hg partials $\geq$ 0.03 atm. polycrystalline films resulted while below 0.02 atm the growth rate dropped to 2 μm/hr without any improvement in surface quality. Holding the Hg partial at 0.025 atm and varying the DIPTe partial pressure resulted in an increase in hillock and FWHM values for both higher and lower partial pressures of DIPTe.

Using the values of 0.025 atm and 2×10^{-3} atm, for Hg and DIPTe respectively, DMCd was added to the reactant stream. The partial pressures of DMCd used ranged from 5×10^{-5} to 5×10^{-4} atm. The resulting $Hg_{1-x}Cd_xTe$ film quality quickly degraded with hillocks of various sizes covering the entire sample. Shown in Figure 5.2 are Nomarski contrast micrograph showing the surface of HgTe and $Hg_{1-x}Cd_xTe$ films where 1×10^{-4} atm of DMCd was used. The HgTe surface shows hillocks of approximately the same size indicating that they are probably substrate related with a textured background. However, the $Hg_{1-x}Cd_xTe$ film had hillocks of varying size and shape indicating they were being formed during the growth of the film. The hillock formation in the $Hg_{1-x}Cd_xTe$ films were believed to be caused by gas phase nucleation where particulates were generated in the gas phase. Similar results were obtained for DMCd partial pressure values of 5×10^{-5} atm which resulted in film composition of $Hg_{0.95}Cd_{0.5}Te$.

5.2.1 DIPTe Summary

The results of this study indicated that DIPTe was not a good tellurium precursor for use in a photo-assisted process for the growth of $Hg_{1-x}Cd_xTe$. However,

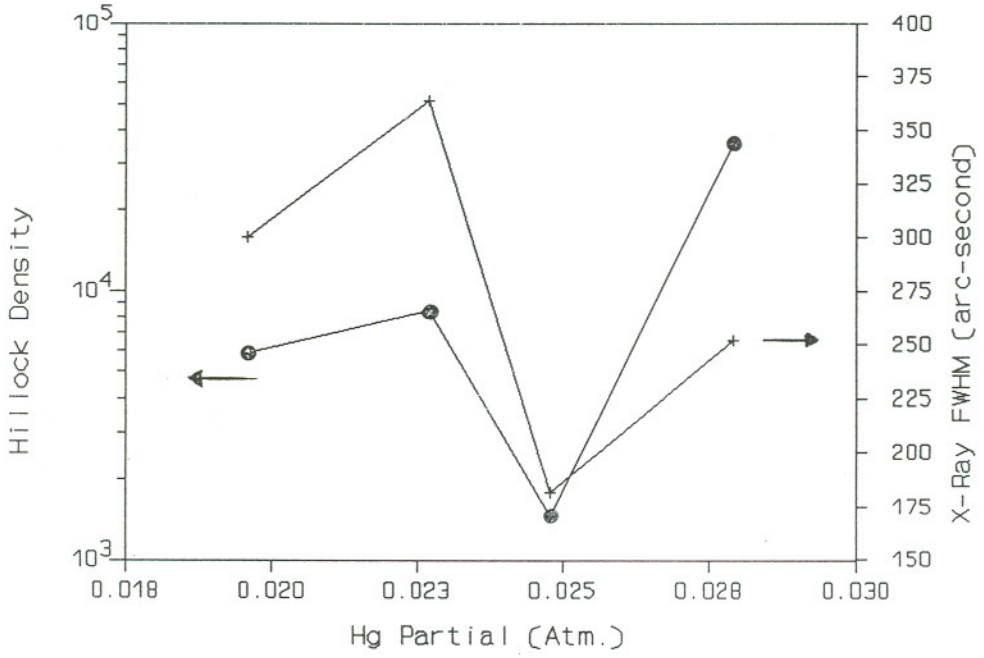

Figure 5.1 Hillock density and FWHM values versus Hg partial pressure for HgTe films.

(a)

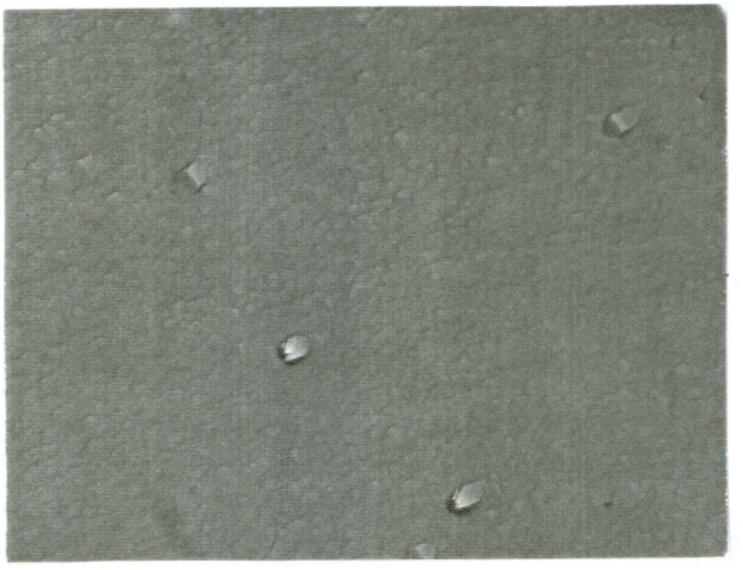

(b)

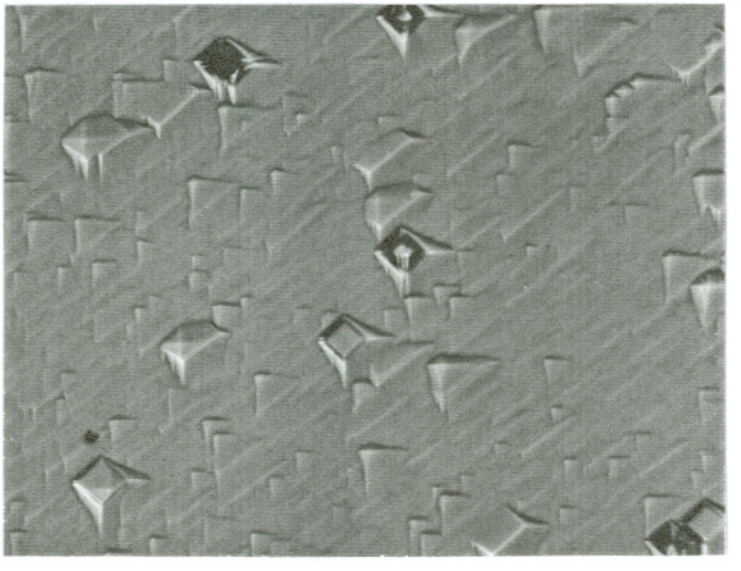

Figure 5.2 Nomarski micrographs showing hillocks for a.) HgTe and b.) $Hg_{1-x}Cd_xTe$ films grown with DIPTe.

for the growth of CdTe using a pattern projection technique, with a mask outside the reactor, DIPTe may be a good precursor.

5.3 $Hg_{1-x}Cd_xTe$ growth using MATe

5.3.1 Introduction

The first reported growth of $Hg_{1-x}Cd_xTe$ using MATe was done by Parsons et.al. using DMCd and dimethylmercury (DMHg) [75]. In their work HgTe was grown at 320°C which was the lower limit of growth due to DMHg. More recently Ghandi et. al. have produced $Hg_{1-x}Cd_xTe$ at a substrate temperature of 320°C with improved surface morphology compared to other tellurium precursors requiring a higher growth temperature [76]. In addition HgTe growth was obtained at a substrate temperature of 240°C with a growth rate of 1 μm/hr. The investigation described below was undertaken to compare the properties of epitaxially grown $Hg_{1-x}Cd_xTe$ films by purely thermal and photon-assisted process using MATe to determine if there were any advantages for using the latter technique.

The parameters investigated included variations of all reactant partial pressures as well as a temperature study for a fixed reactant condition. This study showed that there was some prereaction occurring up-stream of the substrate which resulted in HgTe deposition. This prereaction was significantly reduced by using an internal extension of the MATe line. This extension reduced the amount of time the MATe was in contact with the Hg vapor (250°C source temp.) and resulted in doubling the growth rates achieved.

5.3.2 Results and Discussion

In order to characterize the MATe as a tellurium source for OMVPE, all reactant partial pressures were varied while holding two constant. Shown in Figure 5.3 is a plot of the growth rate against Hg partial pressures. The growth was

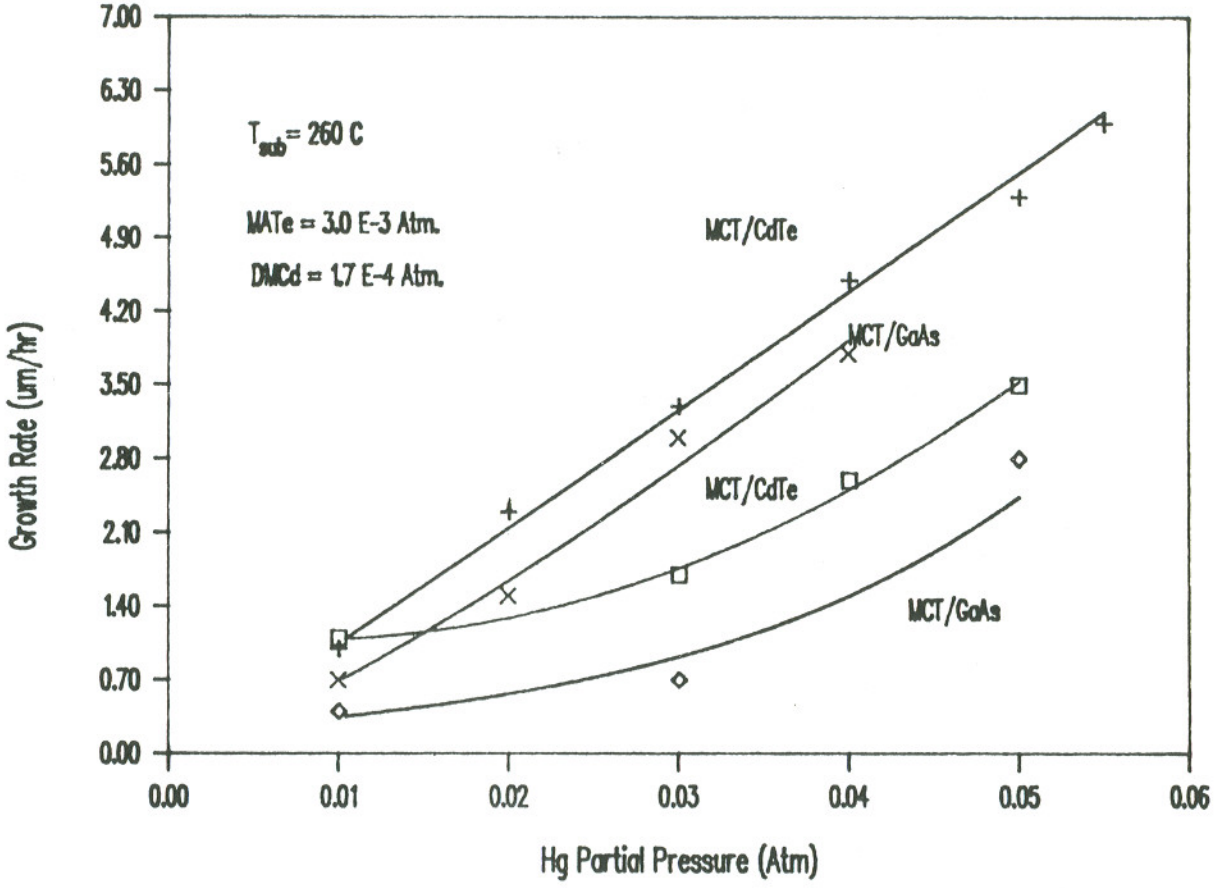

Figure 5.3 Growth rate of $Hg_{1-x}Cd_xTe$ vs. Hg partial pressure for photon-assisted and thermally grown $Hg_{1-x}Cd_xTe$ epilayers on CdTe and GaAs substrates.

investigated using both CdTe and GaAs substrates and resulted in a linear relationship for the photon-assisted case and an exponential relationship for the purely thermal growth conditions for both substrates. At Hg partials of 0.01 atm. films were Hg deficient resulting in films of nearly CdTe being deposited and thus near equal growth rates. At high Hg partial pressure (≥ 0.04 atm), Hg condensation was observed which formed many ring patterns on the films surface due to etching. Over the range investigated the growth rate for the photon-assisted growth rate was nearly twice that of the thermal and is linear. The thermal growth has a second order dependance which fits the form of a Langmuir-Hinshelwood adsorption isotherm of the form shown in Equation 5.1 where k is the adsorption/ desorption rate constant [77]. Another difference between the two processes is the growth on

$$Growth\ Rate = CdTe\ Growth\ Rate + kP_{Hg}/(1+kP_{Hg}) \qquad \textbf{Eq. 5.1}$$

CdTe and GaAs differs by a constant of ≈ 0.4μm for the photon-assisted process and ≈ 0.8μm for the thermal. This constant difference is believed to be a result of the nucleation time required for growth to start on the two substrates. However the photon-assisted process does reduce this thickness approximately a factor of two indicating that the process is surface related.

The dependance of growth rate for MATe partial pressure was investigated for CdTe and GaAs substrates which is shown in Figure 5.4. Using only the photon-assisted process the resulting growth rate varied linearly from 2.4-2.8 μm/hr for CdTe and 2.0-2.4 μm/hr for GaAs. A doubling of the partial pressure of MATe resulted in an increase in growth rate of approximately 20%. For the conditions examined the growth rate was not dependant on MATe concentration so much but rather was more dependant on the Hg partial pressures as a doubling of Hg resulted in a doubling of the growth rate for the photo-assisted process.

Using CdTe substrates and holding Hg = 0.03 atm. and MATe = 1.9 x 10^{-3}

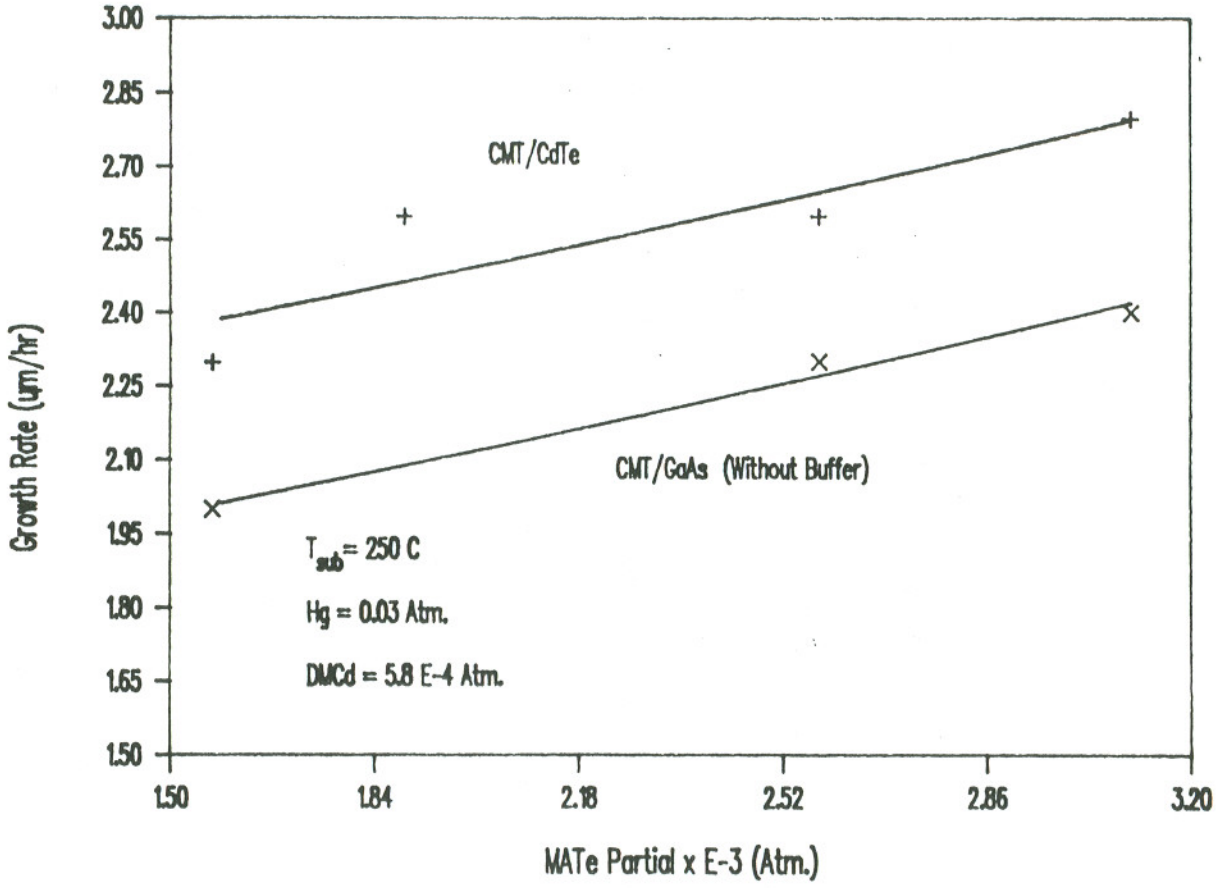

Figure 5.4 Growth rate of $Hg_{1-x}Cd_xTe$ versus MATe partial pressure.

atm. constant and varying the DMCd partial pressure from 3.2-8.5 x 10^{-4} atm, a linear change in x-value as well as growth rate resulted for both photo and thermal growths (Figure 5.5). For the photon-assisted case the growth rate decreased from 4.3 -2.0 μm/hr with a corresponding change in x-value from 0.01 - 0.4 whereas for the thermal case the change was only 0.3 - 0.35 with a corresponding growth rate decrease from 2.2 - 0.8 μm/hr. This difference was attributed to a more efficient dissociation of both MATe and DMCd for the photon-assisted case giving rise to a higher growth rate as well as a wider range in x.

With the incorporation of Cd into the films the defect density increaseed linearly as shown in Figure 5.6. For the photon-assisted case this density was lower than that of the thermal process for DMCd partial pressures less than 7 x 10^{-4} atm. This indicated that the defect density was not being increased by the photo-assisted process and the film's growth rate was being enhanced without any detrimental consequences. However the curves do intersect at an x-value of about 0.3 indicating that the defect density is a function of x-value and not process dependent.

A plot of growth rate against substrate temperature is shown in Figure 5.7. As can be seen the photo-assisted process gives a nearly constant growth rate of 2.5 - 3 μm/hr over the temperature range investigated. This process allows for good growth rates at temperatures of 230°C which is one of the lowest values for epitaxial $Hg_{1-x}Cd_xTe$ growth at such a high growth rate. However at a temperature of 210°C the films were polycrystalline and appeared to be the lower limit to film growth at this particular condition. The thermal growth rate reached a maximum at a substrate temperature of 280°C and then droped off rapidly. This sharp drop was also present for higher partial pressures of both Hg and MATe which indicated a temperature related process where an intermediate product is possibly being formed.

To better understand the formation of hillocks, various substrates were used including CdTe (100) 2° --> (110),CdTe 3.5° --> (110), CdTe (110), GaAs (100) and GaAs/Si (100) 3° --> (110). Although there was no observed difference in the growth rate for the CdTe substrates, a variation in the surface morphology was

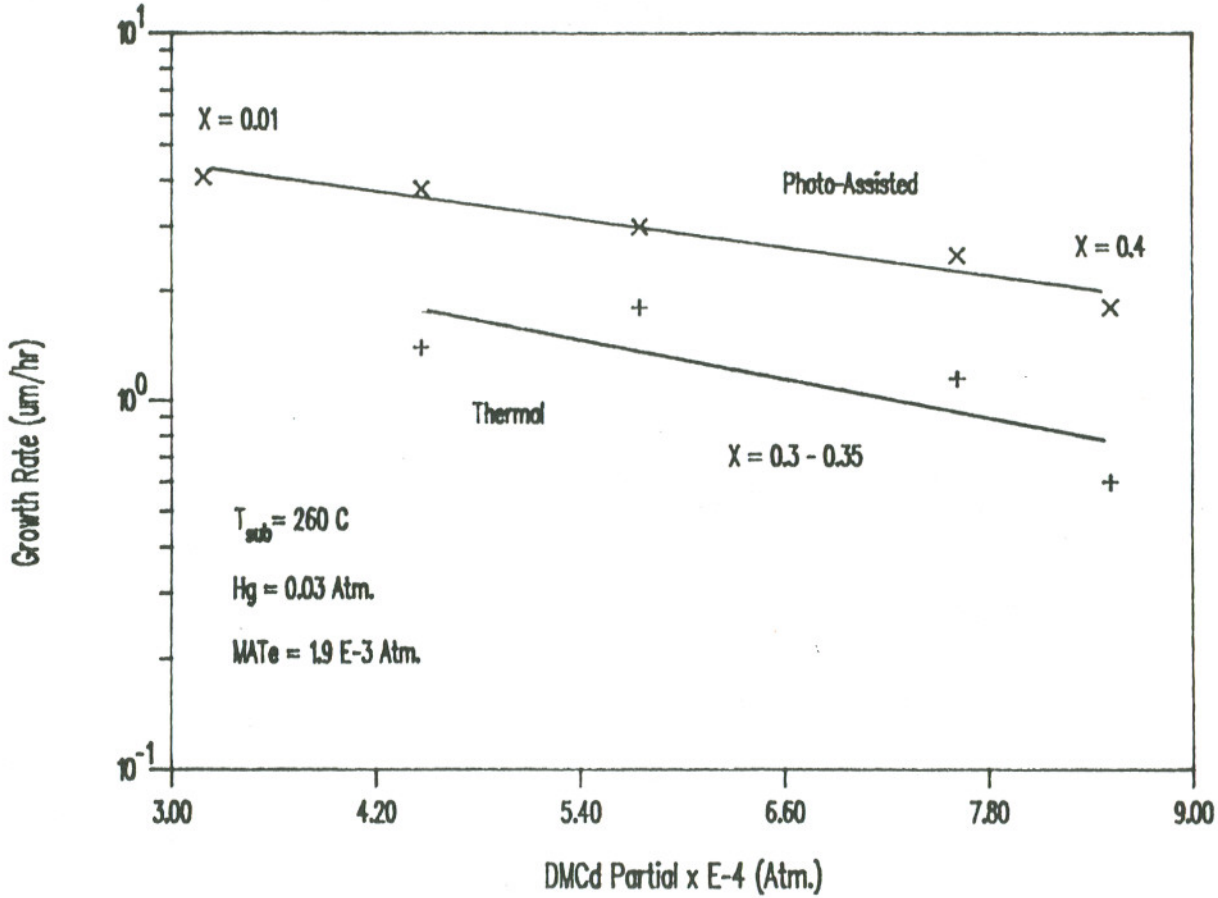

Figure 5.5 Photo-assisted and thermal growth versus DMCd partial pressure.

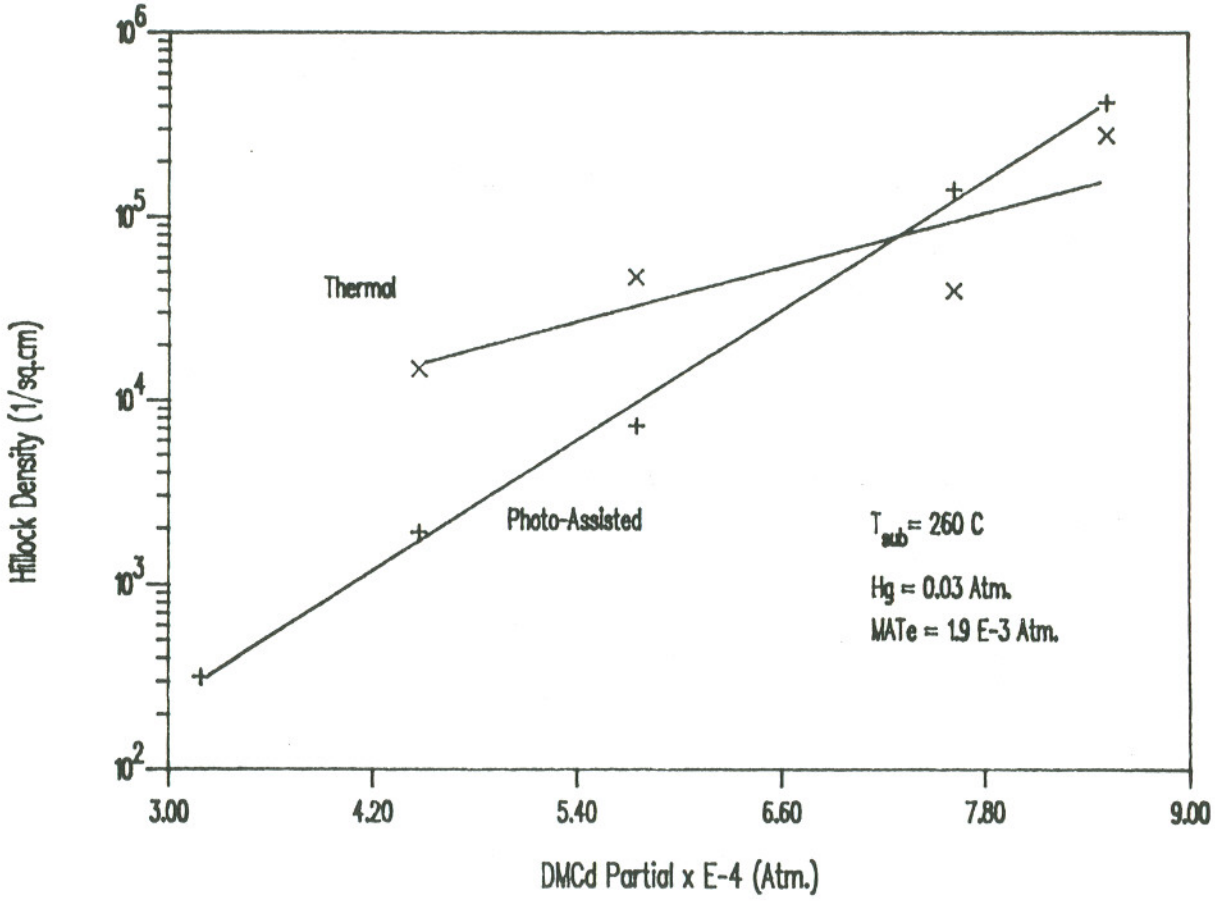

Figure 5.6 Defect density of $Hg_{1-x}Cd_xTe$ films versus DMCd partial pressure.

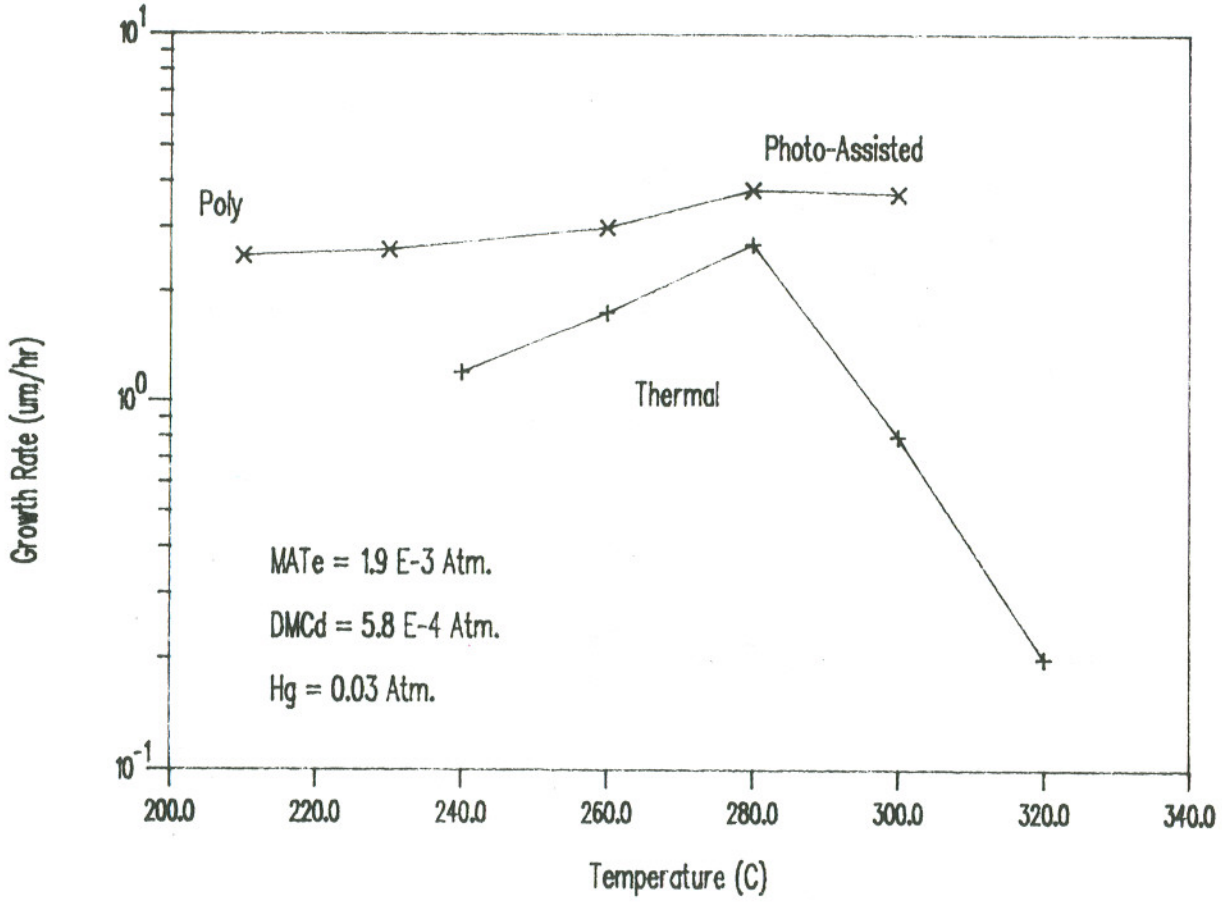

Figure 5.7 Thermal and photo-assisted growth rates versus substrate temperature.

present. Shown in Figure 5.8 and 5.9 are representative Nomarski contrast micrographs of the surfaces grown under various conditions. Comparing the two offset (100) CdTe orientations (Figure 5.8), the main difference is in the vertical height of the hillocks because their growth proceeds at the same offset as the substrate resulting in a *tipped* pyramidal growth. For the (110) orientation (Figure 5.9 a), the surface is completely covered with hillocks all of which were square in nature. The (100) GaAs surface (Figure 5.9 b) had hillocks similar to the (110) CdTe, but are of varying sizes. The cause of the hillocks is believed to be due to the formation of Te clusters that cause dislocations and stacking faults in the epilayer [78,79]. Capper et.al. also have observed that there is an increase in x-value as shown by EDAX when scanned across the pyramidal shaped hillock [80]. This analysis is consistent with the results observed for increased Cd content leading to an increase in the hillock density. It can be speculated that for the growth of HgTe films the Te clusters are kept to a minimum and or are reduced by interactions with Hg to an extent that hillock formation is supressed. However when Cd is combined with the Te cluster this mechanism is not allowed due to the formation of CdTe around the cluster which would give a higher x-value. Snyder et. al. has eliminated the pyramidal hillocks by using (100) 3° --> the nearest (111) Te plane [81]. The explanation given is that on a Te terminated surface, the steps would be delineated by a row of Cd-centered tetrahedra which could prevent the formation of Te clusters.

The growth $Hg_{1-x}Cd_xTe$ on GaAs and CdTe substrates was investigated using transmission electron microscopy (TEM) Cross-sections of films deposited under identical conditions are shown in Figure 5.10. As would be expected, the $Hg_{1-x}Cd_xTe$ layer on CdTe films is of better quality indicated by the relatively clean interface region with only a few dislocations present (Figure 5.10 a). These dislocations do not propagate from the interface to the surface but rather terminate in the epilayer with other dislocations appearing at random directions for short lengths throughout the films thickness. This behavior seems to be characteristic of $Hg_{1-x}Cd_xTe$ epilayers and has been reported by other workers. Growth on the GaAs substrates similar but with

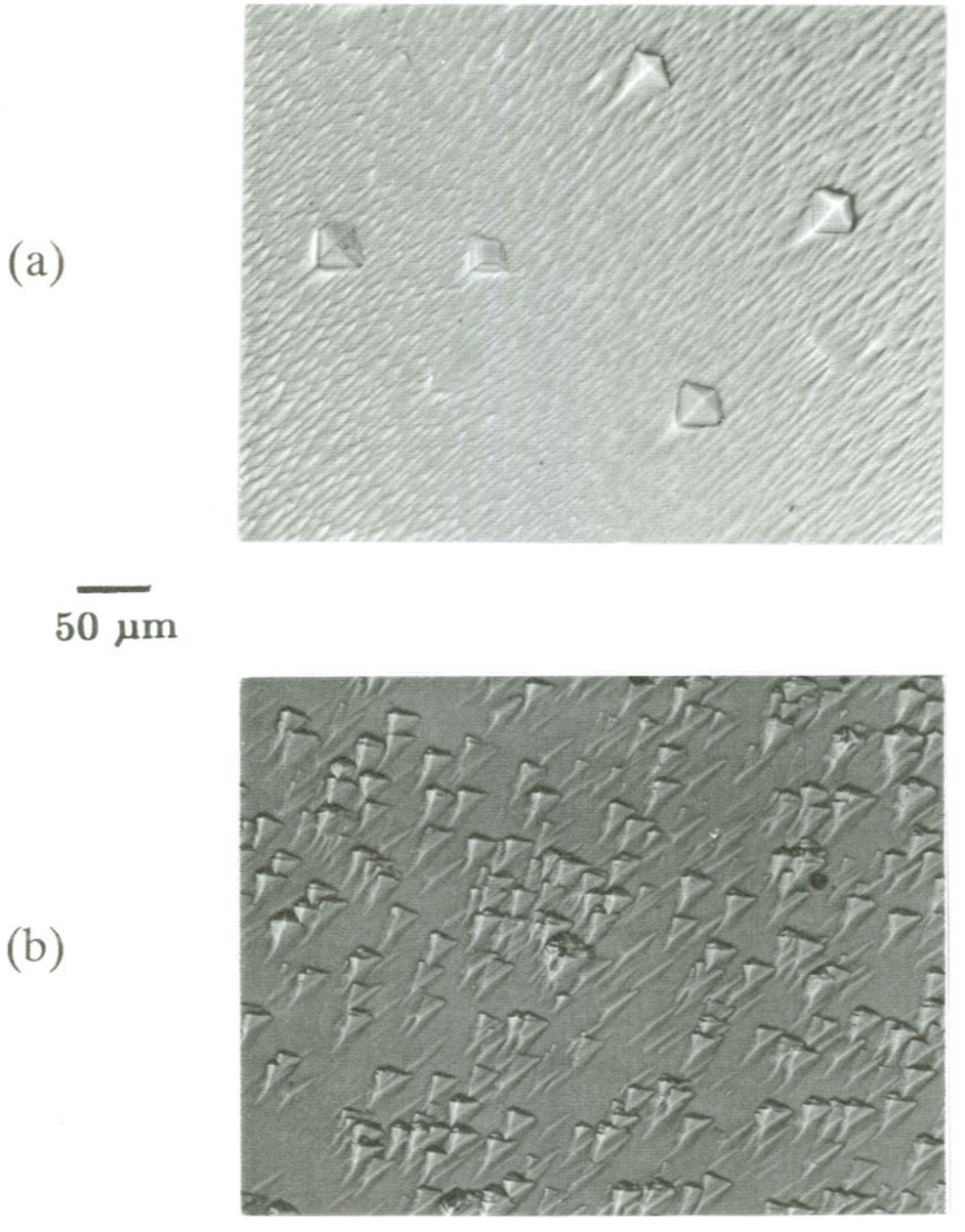

Figure 5.8 Nomarski contrast micrographs of $Hg_{1-x}Cd_xTe$ films where a.) (100) 2° toward (110) CdTe substrate b.) (100) 3.5° toward (110) CdTe substrate.

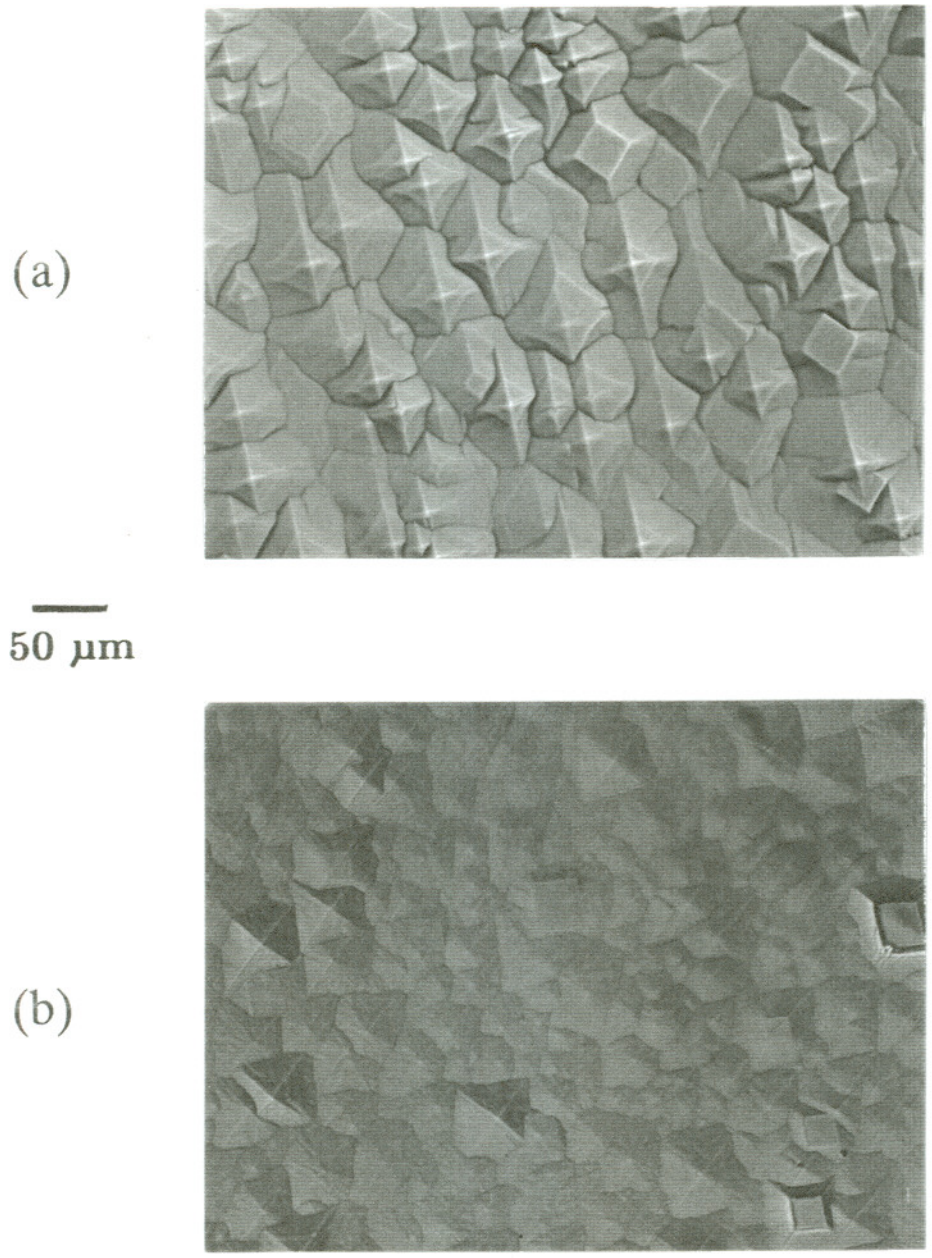

Figure 5.9 Nomarski contrast micrographs showing $Hg_{1-x}Cd_xTe$ films grown on a.) (110) CdTe and b.) (100) GaAs substrates.

(a)

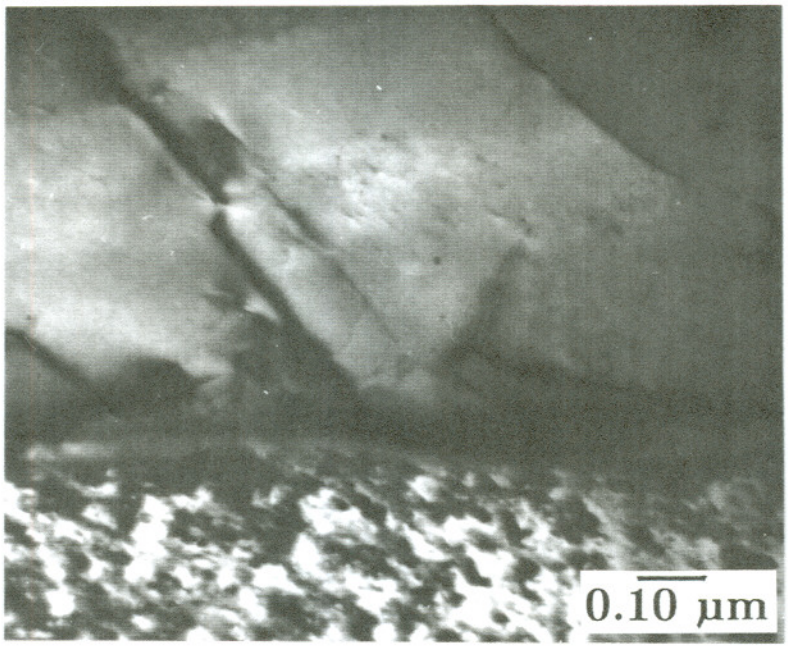

(b)

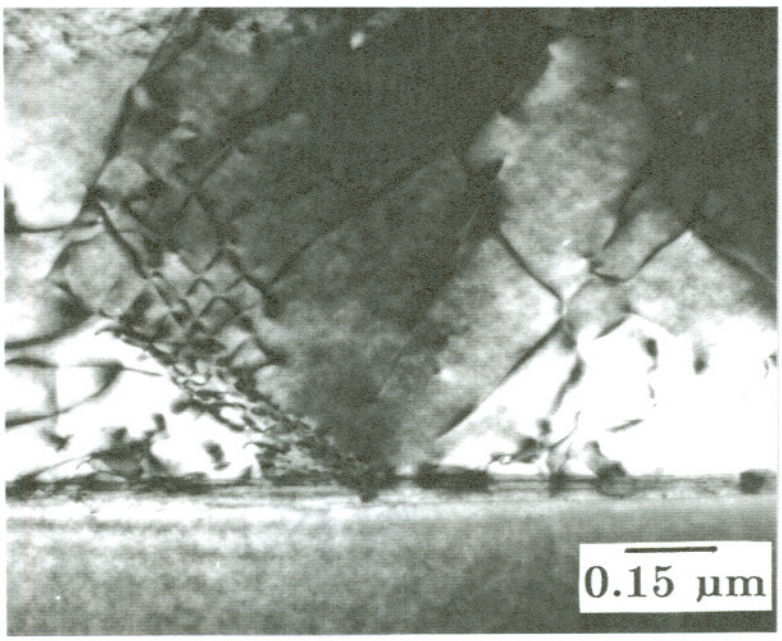

Figure 5.10 Cross-sectional TEM of a.)Photo-assisted $Hg_{1-x}Cd_xTe$ on CdTe b.)Thermal growth of $Hg_{1-x}Cd_xTe$ on GaAs.

a higher density of dislocations indicative of the lattice mismatch (Figure 5.10 b). Attempts at using the photo-assisted process did not seem to improve the quality of the $Hg_{1-x}Cd_xTe$ films, however an increase in the growth rate was observed as indicated before. Thus the accommodation of the lattice mismatch apparently can be made directly by thick $Hg_{1-x}Cd_xTe$ films such that dislocation free (or as good as that on CdTe) epilayers are grown.

In order to achieve better quality $Hg_{1-x}Cd_xTe$ films on GaAs a buffer layer of CdTe was employed. To optimize the conditions for CdTe growth a small set of runs were made. However under the conditions used (similar to those of DETe and DMCd) a good quality epitaxial layer using MATe was not achieved. Examples of these growths for both thermal and photo-assisted are shown in the TEM micrographs of Figure 5.11. The thermal growth (Figure 5.11 a) is very defective with extensive twinning giving rise to what appears to be large crystalline structures. For the photo-assisted growth (Figure 5.11 b) there are a large number of dislocations which propagate from the GaAs substrate to the surface of the CdTe epilayer. This photo-assisted growth could have been optimized further but instead was abandoned to conserve the limited supply of MATe. The buffer layers were then grown, as before using DETe and DMCd at partial pressures of 1.6×10^{-3} atm and 5.4×10^{-4} atm respectively. These films are relatively free of dislocations about $0.5\mu m$ from the interface and basically clean $1\mu m$ away. Using this approach buffer layers of $2\text{-}4\mu m$ were grown followed by the growth of $Hg_{1-x}Cd_xTe$. This allowed for a very clean CdTe surface which yielded a much improved interface region and resulting film as is shown in the TEM micrograph and corresponding diffraction pattern of Figure 5.12.

The growth of $Hg_{1-x}Cd_xTe$ on GaAs was carried out using GaAs on Si substrates. The objective here was to combine the optical properties of $Hg_{1-x}Cd_xTe$ with the enormous signal processing capabilities of silicon devices into a monolithic structure. The three inch diameter GaAs/Si wafers were acquired from Kopin corporation which consisted of $3\mu m$ of GaAs grown on (100) 3° towards the (110) Si,

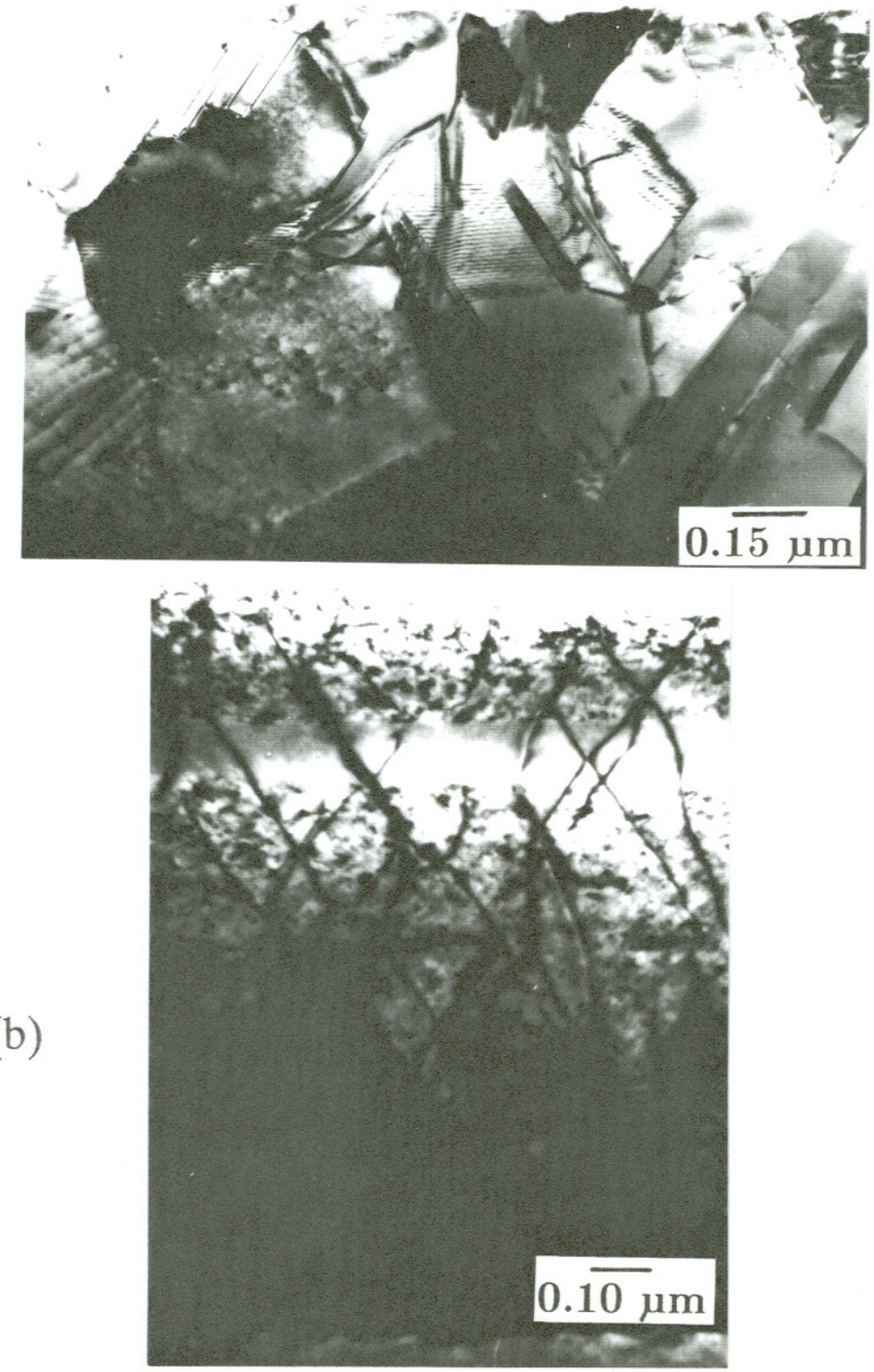

Figure 5.11 Cross-sectional TEM of CdTe/GaAs interface showing a.) Thermally grown CdTe using MATe b.)CdTe grown Photo- assisted using MATe

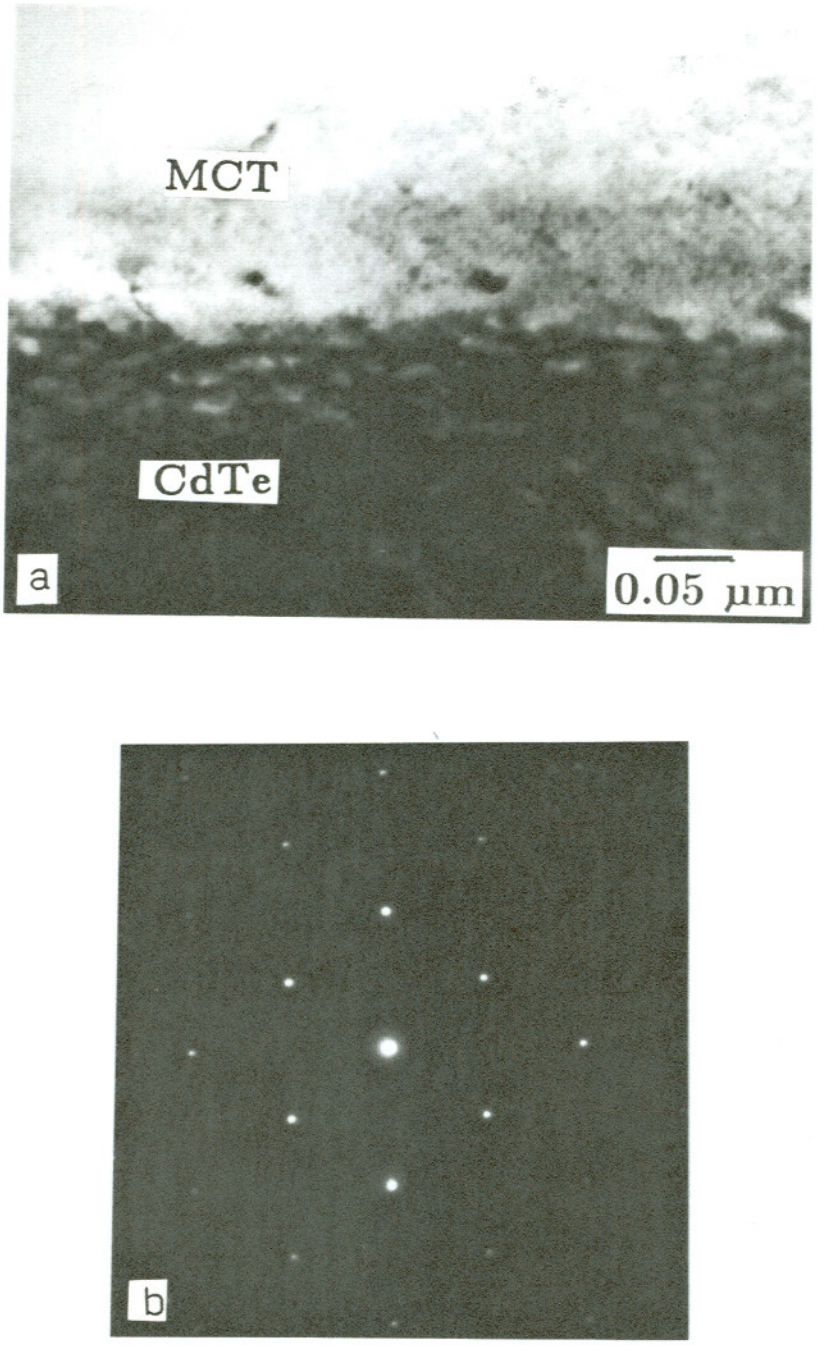

Figure 5.12 Cross-sectional TEM of $Hg_{1-x}Cd_xTe$/CdTe buffer a.) interface b.) TEM diffraction pattern.

which was scribed into 15 x15 mm^2 squares. These samples were cleaned with an etch of H_2SO_4:H_2O_2:H_2O (80:1:1) solution, rinsed in deionized water and dried with nitrogen. Following the growth of a CdTe buffer layer (1.5 - 3μm using DETe) the subsequent growth of $Hg_{0.8}Cd_{0.2}Te$ was achieved using DMCd, MATe, and Hg with partial pressures of $5.4X10^{-4}$, $1.9X10^{-3}$, and 0.03 atm respectively. As a reference, $Hg_{0.8}Cd_{0.2}Te$ was also grown on (100) 3.5° towards the (110) oriented CdTe substrates under identical conditions.

The surfaces of $Hg_{0.8}Cd_{0.2}Te$ on the multilayered structure on Si had a near specular surface whereas the CdTe substrate had hillocks similar to those described previously. Shown in Figure 5.13 is a $Hg_{0.8}Cd_{0.2}Te$ surface grown on a GaAs/Si substrate.

The crystal quality of the epilayers was checked using X-ray double crystal rocking curves (DCRC). Typical rocking curves are shown in Figure 5.14 for a $Hg_{1-x}Cd_xTe$/CdTe as well as a thick $Hg_{1-x}Cd_xTe$/CdTe/GaAs film. For the $Hg_{1-x}Cd_xTe$/CdTe films the smallest FWHM values occured for films which were of a low x-value. As the x-value increased the resulting FWHM values also increased in the range extending from 100 - 200 arc seconds for films of thickness from 3 - 9μm. This broadening is probably a result of the increased hillock density giving rise to a poorer crystalline quality. For films grown on GaAs without a buffer layer the FWHM range was from 200-250 arc seconds with film thicknesses from 4 - 7μm. With a buffer layer the FWHM values tended to be about 250 -300 arc seconds with a $Hg_{1-x}Cd_xTe$ film thickness of 3 - 4μm and a 2 - 3μm buffer. For example, a value of 290 arc seconds was obtained for a CdTe and $Hg_{1-x}Cd_xTe$ film thickness of 2.0 and 3.0μm, respectively grown on GaAs/Si. For the films with buffer layers, the FWHM values become narrower for thicker buffer layers which is consistent with the trend observed for CdTe/GaAs epilayers.

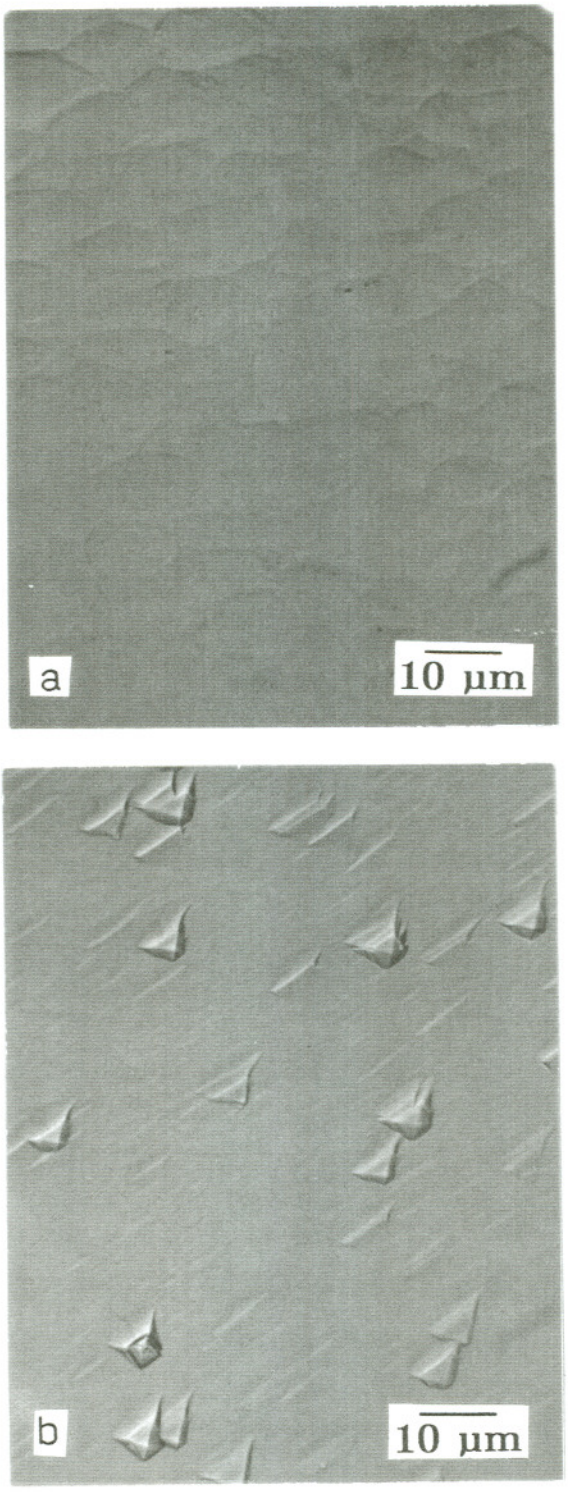

Figure 5.13 Nomarski contrast micrograph of the $Hg_{1-x}Cd_xTe$ surface grown on a.) CdTe/GaAs/Si and b.) CdTe substrate.

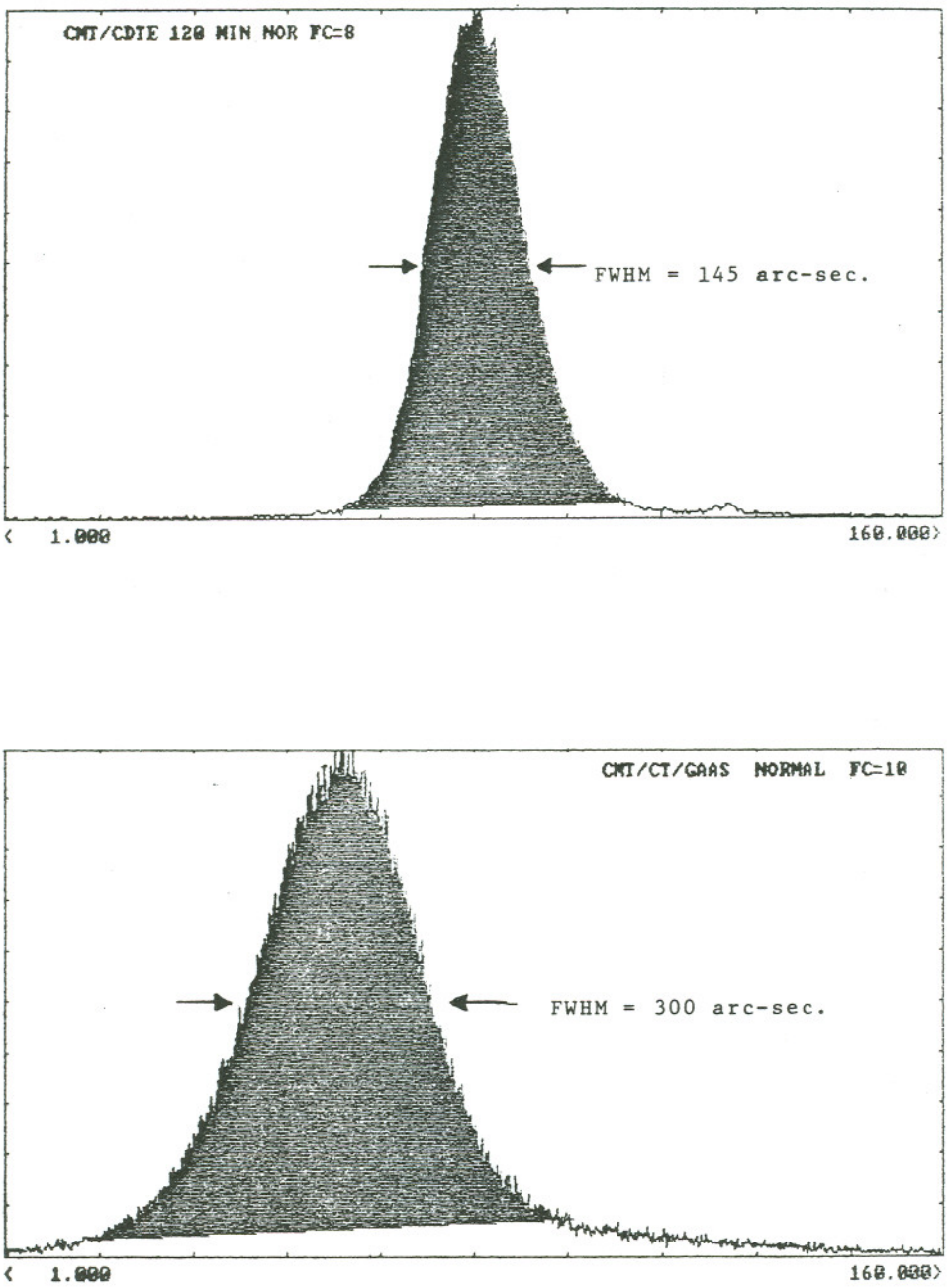

Figure 5.14 Double crystal rocking curves of a.) $Hg_{1-x}Cd_xTe$/CdTe and b.) $Hg_{1-x}Cd_xTe$/CdTe/GaAs films.

6. Electrical Characterization of $Hg_{1-x}Cd_xTe$

In order to compare the electrical properties of films grown thermally and photo-assisted, films of same thickness and x-values were grown. This was accomplished using a substrate temperature of 250°C for the photo-assisted growth and a temperature of 280°C for the thermal growth. Using the same reactant partial pressures films of nearly equal thickness and an x-value of 0.32 were produced. Variable temperature Hall measurements were made using the standard van der Pauw technique where In was used to make ohmic contacts. The results of these measurements are shown in Figure 6.1 where both films were n-type. The carrier concentration (N_A-N_D) for the two films at 80°K differed by an order of magnitude giving rise to a higher resistance for the photo-assisted growth. The thermally grown $Hg_{0.68}Cd_{0.32}Te$ film showed scattering at lower temperatures whereas the photo-assisted film gave a continuous rise in the mobility. This is believed to be due to impurities in the source reactants which would not be completely thermally dissociated at 280°C but could be by the photon-assisted deposition allowing for the incorporation into the film as acceptor sites. Comparisons are also made for films grown on CdTe and GaAs/Si substrates as shown in Figure 6.2. Both of these films were grown under identical conditions except the GaAs/Si substrate had a buffer layer deposited followed by $Hg_{0.8}Cd_{0.2}Te$ growth. The CdTe buffer layers typically have room temperature mobilities of 100 - 120 cm^2/Volt-sec and carrier concentrations of 10^{15} cm^{-3}, thus the improvement in the film quality is not considered to be due to a contribution from the CdTe buffer layer.

Because all $Hg_{1-x}Cd_xTe$ films grown were n-type, attempts were made at doping the layers with tertiarybutylphosphine (TBP). Capper et.al have shown phosphorous to be a good p-type dopant for $Hg_{1-x}Cd_xTe$ [82]. TBP was known to be a good candidate for photon-assisted deposition from our previous work on photon-assisted

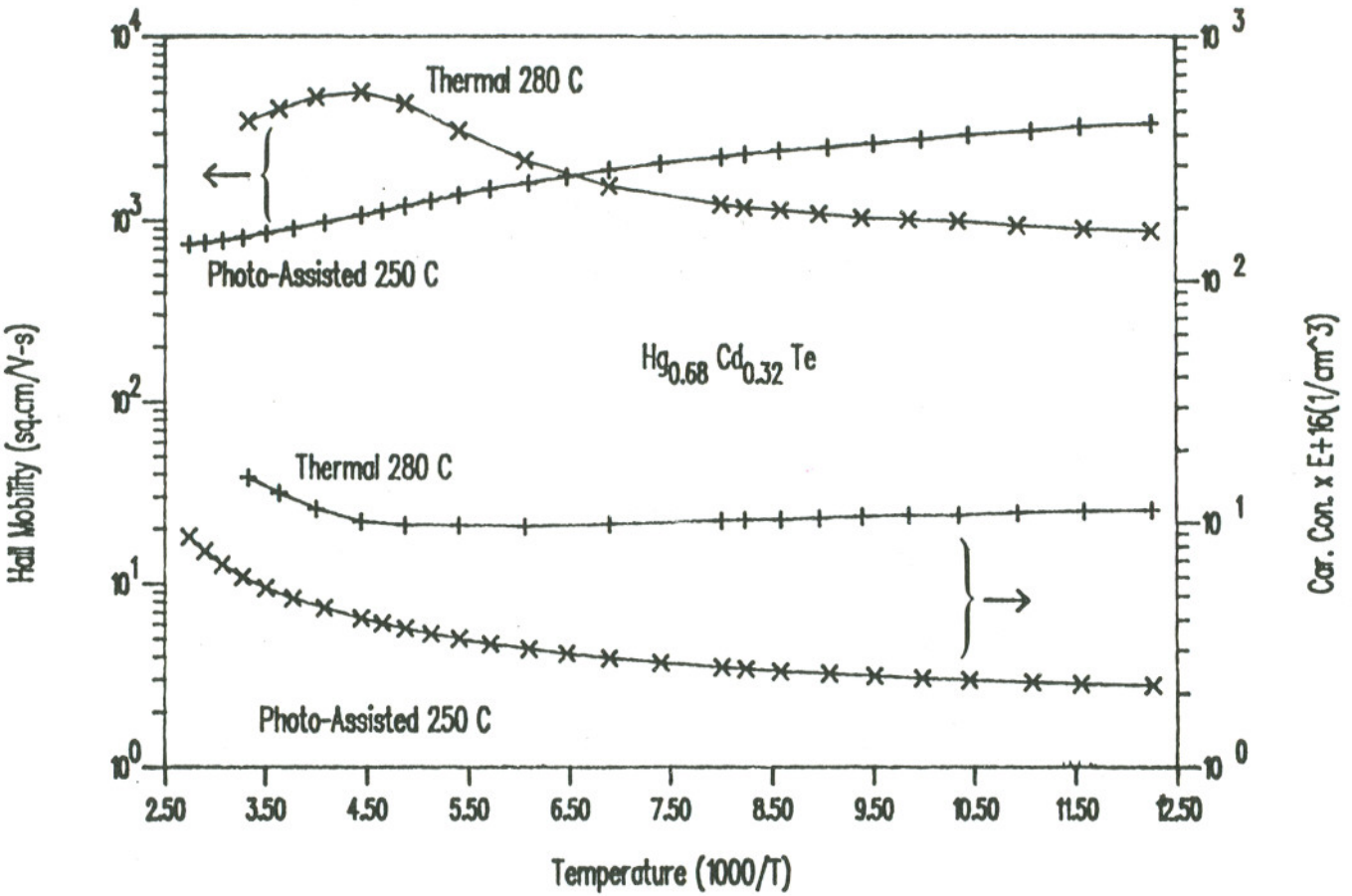

Figure 6.1 Hall mobiltiy and carrier concentration for thermally grown and photon-assisted $Hg_{0.68}Cd_{0.32}Te$ grown on CdTe.

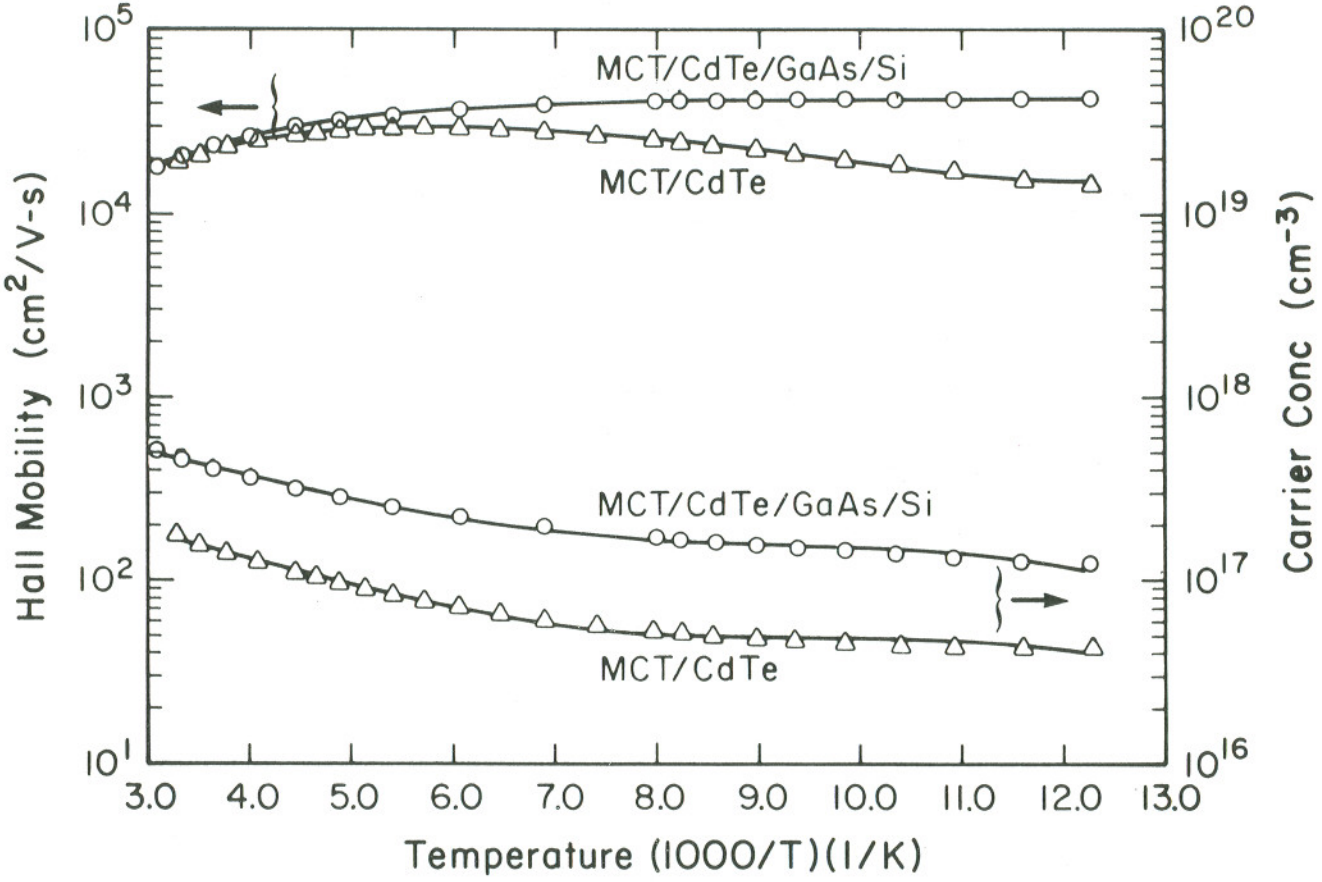

Figure 6.2 Comparison of Hall electron mobility and carrier concentration versus temperature of $Hg_{0.8}Cd_{0.2}Te$ on CdTe/GaAs/Si and CdTe substrates.

epitaxy of GaP [83]. However all growths conducted using TBP as a dopant source resulted in a large amount of gas phase nucleation giving rise to a degraded surface which tended toward polycrystalline.

Finally, GaAs/$Hg_{1-x}Cd_xTe$ heterostructure diodes were fabricated where $Hg_{0.8}Cd_{0.2}Te$ was grown on p-type GaAs using the photo-assisted process. The GaAs substrates were Zn doped (3.0×10^{19} cm^{-3}) on which n-type $Hg_{0.8}Cd_{0.2}Te$ epilayers of thickness 3 to 4μm were grown. Prior to growth contacts to the GaAs substrates were made by evaporation of Au:Zn (3% Zn) on the backside followed by a rapid thermal anneal at 400°C for 30sec. After growth, the backside was lightly etched with 5% Br in MeOH to remove any possible backside contamination. The diode area was defined by scribing the GaAs substrates thus forming "mesa type" devices. Samples were mounted on a copper block using Ag epoxy and contacts to the $Hg_{0.8}Cd_{0.2}Te$ layer were made using In solder dots.

Heterojunction diode characteristics similar to those obtained have been observed in other semiconductor materials. Shown in Figure 6.3 are diode current vs. voltage (I-V) curves from n-$In_{1-x}Ga_xAs$/p-$GaSb_{1-y}As_y$ heterojunctions showing variations from strong rectifying to ohmic type of characteristics [84]. These types of characteristics were found to be dependant on the band structures at the interface and controllable by varying the molar ratios of the heterostructure. Similar types of behavior were found to be present in the $Hg_{0.8}Cd_{0.2}Te$/GaAs heterostructures. From I-V and capacitance vs. voltage (C-V) measurements following charge profiles of the heterojunctions are proposed.

Most of the diodes showed a good exponential turn-on for forward bias but had soft breakdown characteristics in the reverse direction. Because the diodes do not saturate in the reverse direction, it is assumed that they are generation-recombination (g-r) limited. The standard g-r formulas used for homojunction semiconductors are still used but with some modifications. These modifications are needed because of the energy band-bending associated with the heterojunction interface. In addition, since the ratio of the bandgaps between GaAs:$Hg_{0.8}Cd_{0.2}Te$ is

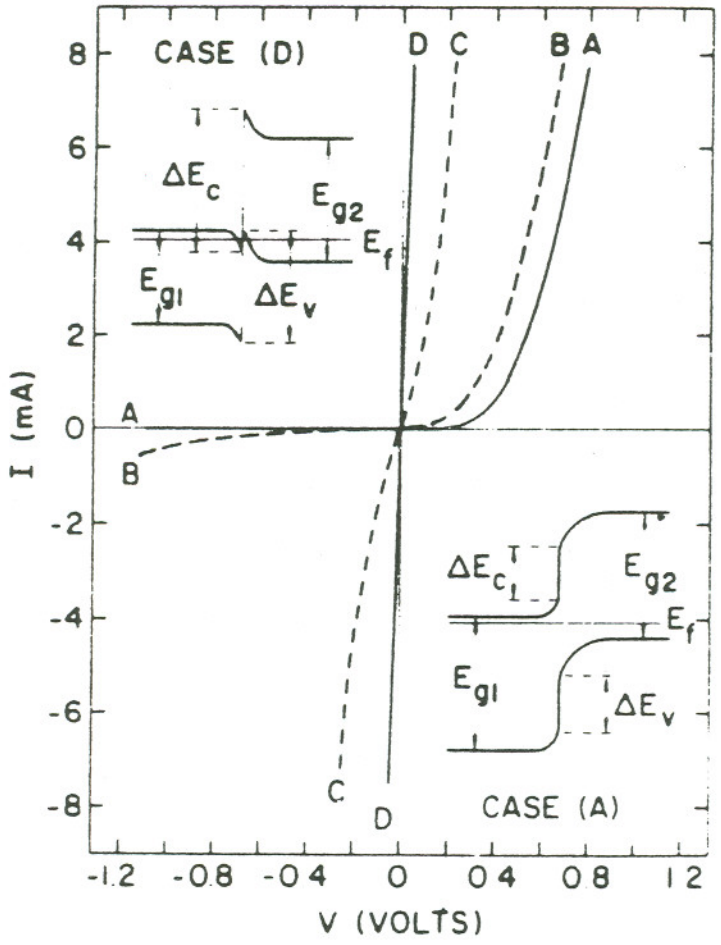

Figure 6.3 I-V characteristics of n-$In_{1-x}Ga_xAs$ - p-$GaSb_{1-y}As_y$ heterojunctions. (From Sakaki [84]).

over ten, it can be assumed that the g-r components from the $Hg_{0.8}Cd_{0.2}Te$ dominate with the GaAs contribution being minimal.

The simple models of g-r current across p-n junctions require I-V characteristics of the form [85];

A. Near zero or small forward-bias:

$$I = I_o(\exp\frac{qV}{nkT} - 1)$$

Where n=2, q is electron charge, k is Boltzman constant, and T is temperature.

B. Reverse-bias:

I-V roll-off as

$$-V^{\frac{1}{2}} \quad \textit{for abrupt junctions}$$

$$-V^{\frac{1}{3}} \quad \textit{for linearly graded junctions}$$

The standard data reduction technique for g-r limited diodes is to plot log(I) vs V for small forward bias to obtain a straight line of slope q/(nkT). In doing this procedure for the heterojunction diodes, values of n ranging from 7 to 24 were obtained. Shown in Figure 6.4 are two curves with corresponding n values of 24 and 17. This type of behavior in the standard g-r model would imply:

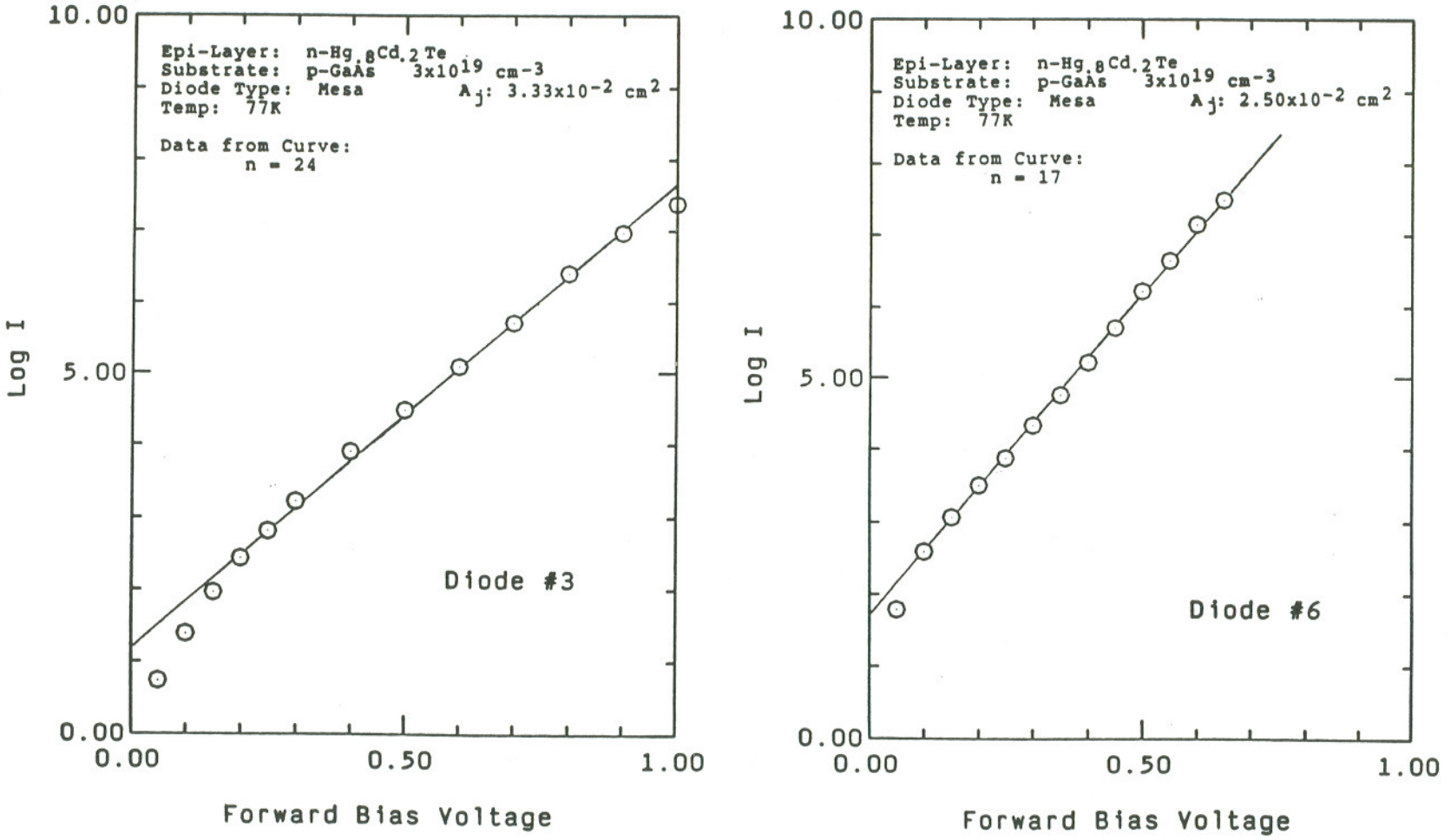

Figure 6.4 I-V data at 77°K obtained for heterojunction diodes.

$$I \propto \exp\frac{qV}{nkT} \propto n_i^{\frac{1}{n/2}}$$

where n_i is the intrinsic carrier concentration in $Hg_{1-x}Cd_xTe$

For the diodes studied this would imply that the current is dependant on the fourth to twelfth root of n_i. This type of behavior seems impractical. However, what seems more plausible is to let n have a value of two and adjust the voltage across the n-$Hg_{0.8}Cd_{0.2}Te$ side of the junction accordingly. With this approach the voltage applied to the n-$Hg_{0.8}Cd_{0.2}Te$ would be given by

$$V_{n\text{-}side} = \frac{2}{n} V_{applied}$$

This approach forces the I-V characteristics to fit the g-r model with the only variation being the applied voltage is not symmetrically distributed across the junction.

The C-V data collected on diodes does not follow either an abrupt or linearly graded type of behavior, i.e. C^{-2} or C^{-3} dependance versus reverse voltage. Instead what was observed is a $C^{-(m+2)}$ versus voltage with m varying from 2 to nearly -2. Shown in Figures 6.5 are C-V data for diodes having values of m equal to 2 and -0.09. These values of m would be indicative of a quadratically graded junction (m=2) and a near abrupt junction (m=-0.09). However shown in Figure 6.6 are data from two other diodes which indicate charge profiles of the form of a hyper-abrupt type of charge profile. Graphical interpretations of these type of profiles are given in Figure 6.7. In terms of an energy band diagram, the quadratically graded junction

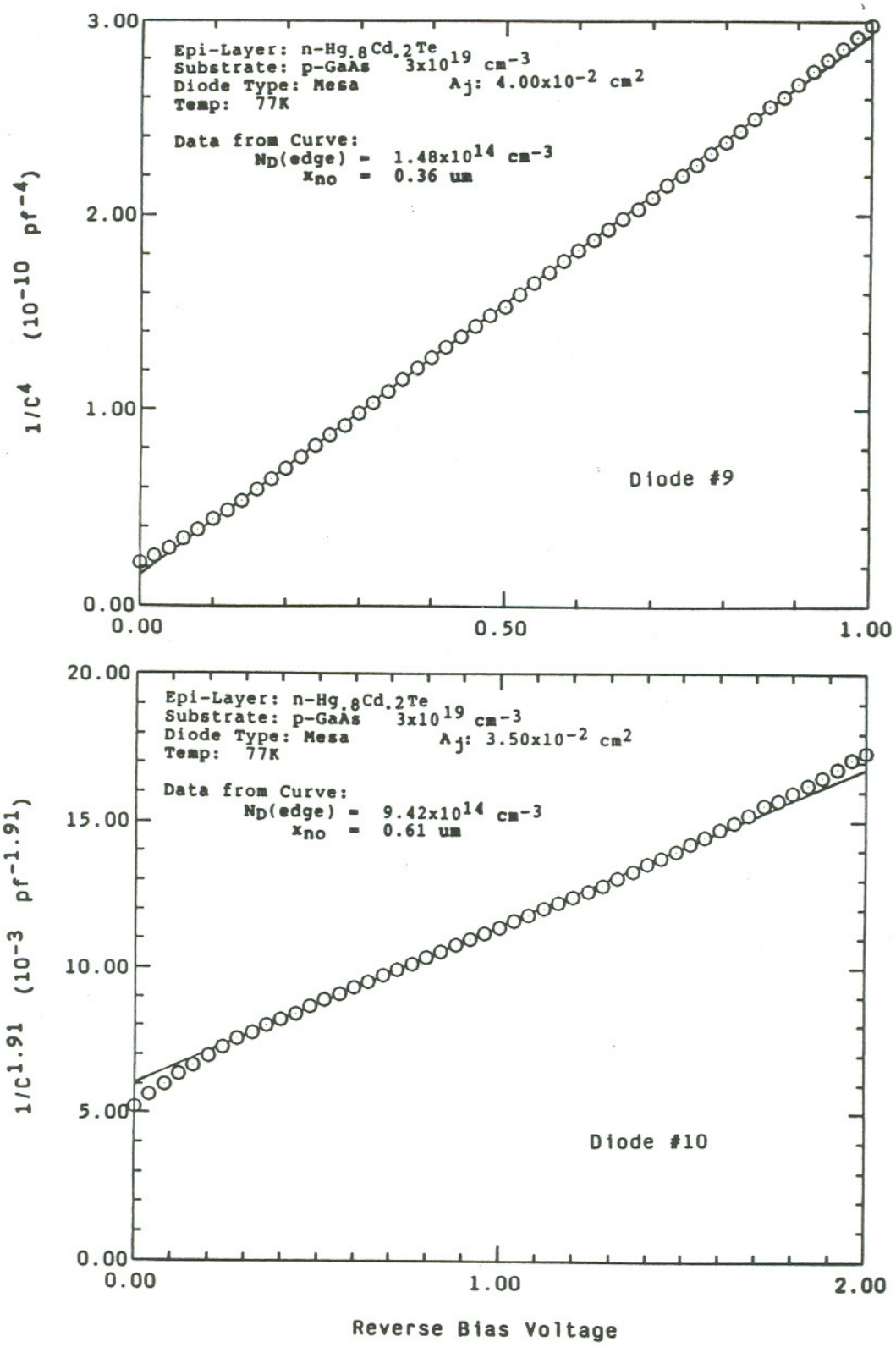

Figure 6.5 C-V data at 77°K for values of m=2 and m=-0.09.

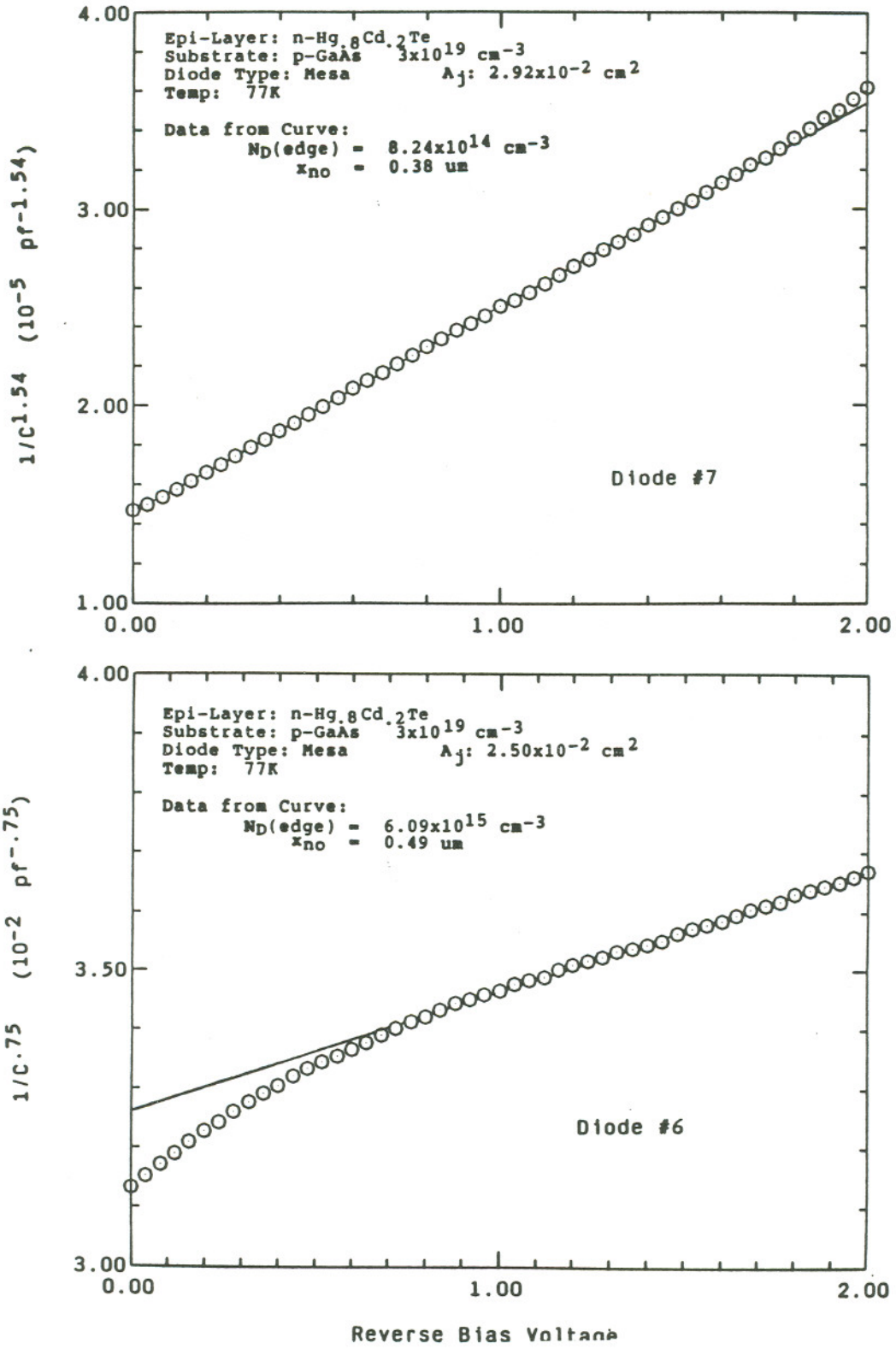

Figure 6.6 C-V data at 77°K for hyper-abrupt junctions.

Quadratically
Graded
Junctions
(Example: Diode #9)

Abrupt
Junction
(Example: Diode #8)

"Hyper-Abrupt"
Junction
(Example: Diode #6)

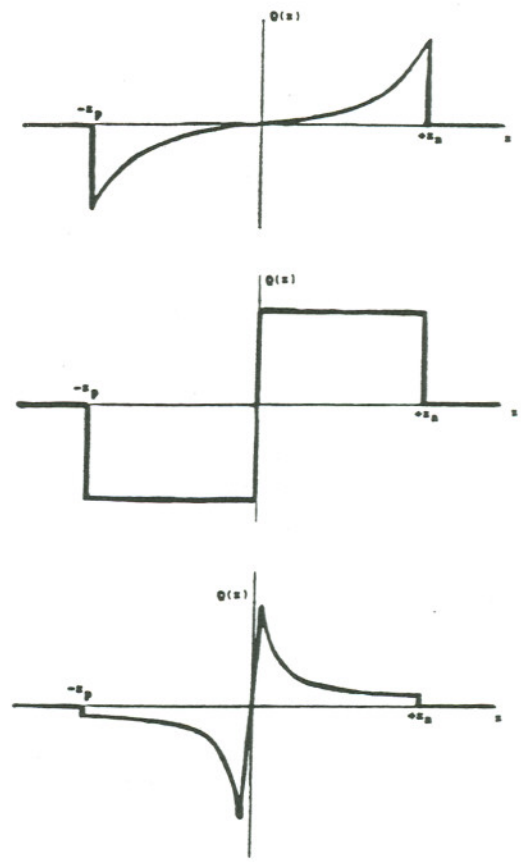

Figure 6.7 Non-linear charge profiles across the p-n junction as inferred from the C-V data.

would correspond to the bands bending downward at the interface giving rise to charge neutralization. However, for the hyper-abrupt junction the bands would bend upward which leads to charge accumulation at the interface.

The simplest charge profile, Q(x), which satisfies the experimental results is given by:

$$Q(x) = \begin{cases} 0 & for\ x < -x_{po} \\ -a_p|x|^m & for\ -x_{po} < x < 0 \\ a_n|x|^m & for\ 0 < x < +x_{no} \\ 0 & for\ x > x_{no} \end{cases}$$

where $a_p \neq a_n$ and $W = x_{po} + x_{no}$

The additional requirements needed to solve for a_p, a_n, x_{po}, and x_{no} for this charge profile are from the following

For Non-Linear Charge Profile

$$\frac{1}{C^{m+2}} \alpha\ V + V_{bi}$$

(m and V_{bi}, obtained from C-V data)

For Asymmetric Voltage Division Across the Junction

$$\frac{V_{p\text{-}side}}{V_{n\text{-}side}} = \frac{1 - \frac{2}{n}}{\frac{2}{n}} = R$$

(n obtained from I-V data)

$$\epsilon_n a_n^{\frac{1}{m+1}} = R\epsilon_p a_p^{\frac{1}{m+1}}$$

For Charge Neutrality

$$a_p (x_{po})^{m+1} = a_n (x_{no})^{m+1}$$

and Continuous V(x)

$$\frac{a_p (x_{po})^{m+2}}{\epsilon_p (m+2)} + \frac{a_n (x_{no})^{m+2}}{\epsilon_n (m+2)} = V_{bi}$$

Using the generalized charge profile with the additional constraints, charge profile parameters for the heterojunction diodes have been calculated. Given in Table 6.1 are the results from four diodes which range from extreme upward to downward band-bending as indicated by the "m" parameter. The value of "n" gives the amount of asymmetry associated with the applied voltage. Because the charge profile and the asymmetric applied voltage have such dramatic effects on the device performance it is difficult to determine any obvious trends. In addition, since the diodes were grown under similar conditions it would be expected that diode performances would be similar. However, it can be speculated that the differences observed are related to the initial growth of the $Hg_{0.8}Cd_{0.2}Te$ where the heterojunction interface is formed. We expect some variation in the x-value from the center of deposit to its outer perimeter and also a variation in defect density due to lattice mismatch, which has not been taken into consideration.

Table 6.1 Charge profile parameters as determined from C-V and I-V data on selected heterojunction diodes.

Diode #	m	n	x_{no}	N_D (edge) (cm^{-3})
9	2.0	22.1	0.357μm	$1.48x10^{14}$
10	-0.09	11.1	0.613μm	$9.42x10^{14}$
7	-0.46	19.6	0.381μm	$8.24x10^{14}$
6	-1.25	17.3	0.486μm	$6.02x10^{15}$

7.CONCLUSION

Low temperature epitaxy of $Hg_{1-x}Cd_xTe$ has been investigated using photo-assisted MOVPE. This process has been proven to give the advantage of a reduced substrate temperature compared to a purely thermal process while maintaining good growth rates. The limiting factor of this, or any other photo-assisted process, is the ability to keep the input window free of deposition. Although this problem was solved in the system used, the solution resulted in a substrate size limitation of 15 x 15mm. This size limitation may be resolved with a step and repeat type of process thus allowing for large areas to be processed.

For growth of CdTe, using the photo-assisted process, DETe is a very good tellurium precursor. However there does tend to be a growth rate threshold at which the epilayers quality deteriorates rapidly. Below this threshold films of good quality can be grown both homoepitaxially as well as on GaAs. For the growth of CdTe/GaAs the lattice mismatch tends to be accommodated within the first 0.5μm of the epilayer yielding a smooth surface morphology. These heteroepitaxial layers have also shown to give better quality $Hg_{1-x}Cd_xTe$ than directly on CdTe substrates. This capability eliminates the starting substrate size restrictions associated with CdTe substrates and gives the additional advantage of signal processing in Si via GaAs/Si substrates.

The tellurium precursor DIPTe, does not seem to be good for the deposition of $Hg_{1-x}Cd_xTe$ epilayers using the lamp system investigated. However this does not rule out that DIPTe would not be a suitable choice for a different optical output spectrum. Because DIPTe does readily dissociate, a slightly different spectrum may allow epitaxial layers to be grown without gas-phase nucleation.

The growth of $Hg_{1-x}Cd_xTe$ using MATe can be accomplished at 250°C using either a purely thermal or a photo-assisted approach. However the photo-assisted

approach allows for epitaxial growth at a substrate temperature of 230°C with a growth rate $\approx 4\ \mu$m/hr. In addition, at elevated temperatures there is a reduction in growth rate using a thermal process indicating that an intermediate product is possibly being formed. This decrease is not observed with the photo-assisted growth. Another difference between the two growth methods was observed in the electrical characterization. It is speculated that the differences are due to source impurities in the MATe. This type of a problem is typical of new metal organic sources but should be alleviated with time.

8. BIBLIOGRAPHY

1. A.M.Glass, Science, 235, 1003 (1987).
2. R.K.Willardson and A.C.Beer, Semiconductors and Semimetals, Vol.11, Academic Press, New York, (1975).
3. Kenneth Zanio, Semiconductors and Semimetals, Cadmium Telluride, Vol. 13, Academic Press, New York, (1978).
4. R.K.Willardson and A.C.Beer, Semiconductors and Semimetals, Mercury Cadmium Telluride, Vol. 18, Acedemic Press, New York, (1981).
5. J.T.Longo, D.T. Cheung, A.M.Andrews, C.C.Wang, and J.M.Tracy, IEEE Transactions on Electronic Devices, Ed-25, 213 (1978).
6. M.A.Herman and M.Pessa, J. Appl. Phys. 57, 2671 (1985).
7. W.F.Lawson, S.Nielson, E.H.Putly, And A.S.Young, J. Phys. Chem. Solids, 9, 325 (1959).
8. R.Dornhaus, G.Nimtz, and W.Richer, Springer Tracts in Modern Physics, Vol. 78, Springer-Verlag, New York, (1976).
9. R.K.Willardson and A.C.Beer, Semiconductors and Semimeteals, Infrared Detectors, Vol.5, Academic Press, New York, (1970).
10. D.E.Charlton, J.Crys. Growth, 59, 98 (1982).
11. R.C.Weast, CRC Handbook of Chemistry and Physics, Edition 68, CRC Press, (1987).
12. J.Brice and P.Capper, Properties of Mercury Cadmium Telluride, EMIS Datareviews Series 3,Inspec, New York, (1987).
13. G.L.Hansen, J.L.Schmit, J. Appl. Phys. 53, 7099 (1982).
14. J.Chu, S.Xu, and D.Tang, Appl. Phys. Lett., 43, 1064 (1983).
15. E.Finkman and Y.Nemirovsky, J. Appl. Phys., 50, 4356 (1979).
16. L.F.Lou and W.H.Frye, J. Appl. Phys., 56, 2253 (1984).

17. M.C.Chen, J. Appl. Phys., 65, 1571 (1989).
18. W.M.Higgins, G.N.Pultz, R.G.Roy, and R.A.Lancaster, J.Vac.Sci.Tech., A7, 271 (1989).
19. W.Scott, J. Appl. Phys., 43, 1055 (1972).
20. G.L.Hansen and J.L.Schmit, J. Appl. Phys., 54, 1639 (1983).
21. M.Astles, N.Gordon, D.Bradley, P.J.Dean, D.R.Wright, and G.Blackmore, J. Electron. Mater. 13, 167 (1984).
22. H.Kuwamoto, J.Crystal Growth, 73, 204 (1984).
24. K.Mochizuki, J.Crystal Growth, 73, 510 (1985).
25. T.H.Myers, Y.Lo, J.F.Schtzina, and S.R.Jost, J.Appl. Phys., 53, 9232 (1988).
26. K.Nishitani, R.Ohkata, and T.Murotani, J. Electron. Mater. 12, 619 (1983).
27. J.B.Mullin, S.J.C.Irvine, and D.J.Ashen, J.Crystal Growth, 55, 92 (1981).
28. W.E.Hoke, P.J.Lemonias, and R.Traczewski, Appl. Phys. Lett., 44, 1046 (1981).
29. S.K.Ghandi and I.Bhat, Appl.Phys. Lett., 45, 678, (1984); 50, 900 (1987).
30. J.E.Bowers, J.L.Schmit, C.J.Speerschneider, and R.B.Maciolek, IEEE Trans. Electron Devices, ED-27, 24 (1980).
31. J.R.Meyer,C.A.Hoffman,F.J.Bartoli, and J.N.Schulman, J.Vac.Sci.Techno., A7, 404 (1989).
32. J.P.Faurie,M.Boukerche,S.Sivananthan,J.Reno, and C.Hsu, Superlatt. Microstruct. 1, 237 (1985).
33. K.A.Harris, T.H.Myers, R.W.Yanka, L.M.Mohuhern, R.W.Green, and N.Otsaka, J.Vac.Sci.Technol. A8, 1013 (1990).
34. M.D.Lange,S.Sivananthan,X.Chu, and J.P.Faurie, Appl. Phys. Lett., 52, 978 (1988).
35. P.D.Brown, J.E.Hails, G.J.Russel, and J.Woods, Appl. Phys. Lett. 50, 1144 (1987).
36. R.D.Feldman,S.Nakahara,R.F..Austin,T.Boone,R.L.Opila, and A.S.Wynn, Appl. Phys. Lett., 51, 1239 (1987).
37. A.Million, L.DiCioccio, J.P.Gailliard, and J.Piaguet, J.Vac.Sci. Technol., A6, 2813 (1988).

38. R.J.Koestner, and H.F.Schaake, J.Vac.Sci.Technol., A6, 2834 (1988).
39. S.J.C.Irvine and J.B.Mullin, J. Crystal Growth, 55, 107 (1981).
40. T.C.Harman, J.Electron. Mater., 9, 954 (1980).
41. S.J.C.Irvine, J.B.Mullin, and A.Royal, J.Crystal Growth, 57, 15 (1985).
42. M.R.Czerniak and B.C.Easton, J.Crystal Growth, 68, 128 (1984).
43. J.B.Mullin, S.J.C.Irvine, J.Giess, and A.Royle, J.Crystal Growth, 72, 1 (1985).
44. I.B.Bhat, N.R.Tasker, and S.K.Ghandhi, J.Electrochem. Soc. 134, 195 (1987).
45. B.Liu, A.H.McDaniel, and R.F.Hicks, J. Crystal Growth, 112, 192, (1991).
46. J.B.Mullin and S.J.C.Irvine, J.Vac. Sci. Technol., 21, 178 (1982).
47. J.Tunnicliffe, S.J.C.Irvine, O.D.Dosser, and J.B.Mullin, J. Crystal Growth, 68, 245 (1984).
48. W.E.Hoke and P.J.Lemonias, Appl. Phys. Lett., 46, 398 (1985).
49. W.E.Hoke and P.J.Lemonias, Appl. Phys. Lett., 48, 1669 (1986).
50. W.E.Hoke, Mater. Res. Soc. Symp. Proc., 90, 379 (1987).
51. R.Korenstein, W.E.Hoke, P.J.Lemonias, K.T.Higa, and D.C.Harris, J.Appl. Phys., 62, 4929 (1987).
52. W.E.Hoke, P.J.Lemonias, and R.Korenstien, J. Mater. Res., 3, 329 (1988).
53. D.W.Kisker, M.L.Steigerwald, T.Y.Kometani, and K.S.Jeffers, Appl. Phys. Lett., 50, 1681 (1987).
54. S.J.C.Irvine, J.B.Mullin, and J.Tunnicliffe, J. Cryst. Growth, 68, 188 (1984).
55. S.J.C.Irvine, J.Giess, J.B.Mullin, G.W.Blackmore, and O.D.Dosser, J.Vac.Sci.Technol. B3, 1450 (1985).
56. S.J.C.Irvine, J.Giess, J.B.Mullin, G.W.Blackmore, and O.D.Dosser, Materials Letters, 3, 290 (1985).
57. S.J.C.Irvine, J.B.Mullin, D.J.Robbins, and J.L.Glasper, J.Electrochem. Soc., 132, 968 (1985).
58. C.Jonah, P.Chandra, and R.Bersohn, J. Chem. Phys., 55, 1903 (1971).
59. C.J.Chen and R.M.Osgood, J. Chem. Phys., 81, 327 (1984).
60. C.F.Yu, F.Youngs, K.Tsukiyama, and R.Bersohn, J.Chem. Phys., 85, 1382 (1986).

61. D.J.Ehrlich, R.M.Osgood, and T.F.Deutsch, J. Vac. Sci. Techhnol. 21, 23 (1982).

62. J.E.Jensen, P.D.Brewer, G.L.Olson, L.W.Tutt, and J.J.Zink, J. Vac. Sci. Technol., A6, 2808 (1988).

63. C.D.Stinesping and A.Freedman, Chemical Phys. Lett., 143, 584 (1988).

64. J.B.Mullin and S.J.C.Irvine, J.Vac.Sci.Technol., A4, 700 (1986).

65. S.J.C.Irvine, J.B.Muliin, H.Hill, G.T.Brown, and S.J.Barnett, J. Crystal Growth, 86, 188 (1988).

66. D.W.Kisker and R.D.Feldman, J. Crystal Growth, 72, 102 (1985).

67. J.J.Zink, P.D.Brewer, J.E.Jensen, G.L.Olson, and L.W.Tult, Appl. Phys. Lett. 52, 1434 (1988).

68. R.F.C.Farrow, G.R.Jones, G.M.Williams, and I.M.Young, Appl. Phys. Lett., 39, 954, (1981).

69. H.S.Cole, H.H.Woodbury, and J.F.Schetzina, J. Appl. Phys., 55, 3166 (1984).

70. H.A.Mar, K.T.Chee, and N.Salanski, Appl. Phys. Lett., 44, 237 (1984).

71. N.Otsuka, L.A.Kolodziejski, R.C.Gunshor, S.Dutta, R.N.Bicknell, and J.F.Schertzina, Appl. Phys. Lett., 46, 860 (1985).

72. F.A.Ponce, G.B.Anderson, and J.M.Ballingall, Surf. Sci., 168, 564 (1986).

73. P.Y.Lu, L.M.Williams, and S.N.G.Chu, J.Vac. Sci. Technol., A4, 2137 (1986).

74. J.Petruzzello, D.Olego, S.K.Ghandi, N.R.Taskor, and I.Bhat, Appl. Phys. Lett. 50, 1423 (1987).

75. J.D.Parsons and L.S.Lichtmann, J.Cryst. Growth, 86, 222 (1988).

76. S.K.Ghandhi, I.B.Bhat, H.Ehsani, D.Nucciarone, and G.Miller, Appl. Phys. Lett., 55, 137 (1989).

77. G.B.Stringfellow, Organometallic Vapor-Phase Epitaxy, Acedemic Press Inc., London, (1989).

78. J.Van de Ven,J.L.Weyher, H.Ikink, and L.Giling, J.Electrochem. Soc., 134, 989 (1987).

79. A.Rudra, J.C.Grenet, and P.Gibart, J.Cryst. Growth, 87, 535 (1988).

80. P.Capper, C.D.Maxey, P.A.C.Whiffin, and B.C.Easton, J.Cryst. Growth, 96, 519 (1989).

81. D.W.Snyder, S.Mahajan, E.I.Ko, and P.J.Sides, Appl. Phys. Lett., 58, 848 (1991).

82. P.Capper, B.C.Easton, P.A.C.Whiffin, and C.D.Maxey, J. Cryst. Growth, 79, 508 (1986).

83. U.Sudarsan, N.Cody, T.Doslogu, and R.Solanki, Appl. Phys. Lett., 55, 783 (1989).

84. H.Sakaki, L.L.Chang, R.Ludeke, C.Chang, G.A.Sai-Halasz, and L,Esaki, Appl. Phys. Lett., 31, 211 (1977).

85. S.M.Sze, Physics of Semiconductor Devices, John Wiley and Sons Inc., New York (1981).

9. Vita

The author was born March 3, 1960 in Denver Colorado. He received a Bachelor of Science degree in Electrical Engineering from Colorado State University in 1985. While working as an undergraduate student the author became interested in the processing of semiconductor thin films. In 1986 he accepted a graduate research position at the Oregon Graduate Institute to pursue work in metal organic vapor phase epitaxy of semiconductors. During the course of studies he has contributed the following publications.

1. N.Cody, U.Sudarsan, and R.Solanki "Low temperature epitaxial growth of HgCdTe using methylallyltelluride" (To be published)
2. U.Sudarsan, N.Cody, T.Doslogu, and R.Solanki "Excimer laser induced selective epitaxy of GaP" Appl. Phys. Lett., 50, 325 (1990).
3. U.Sudarsan, N.Cody, T.Doslogu, and R.Solanki "Ultraviolet laser induced low temperature epitaxy of GaP" Appl. Phys. Lett., 55, 783 (1989).
4. N.Cody, U.Sudarsan, and R.Solanki "Ultraviolet photon-assisted heteroepitaxy of CdTe and HgCdTe on GaAs/Si substrates" J. Appl. Phys. 66, (1) 449 (1989).
5. N.Cody, U.Sudarsan, and R.Solanki "Low temperature cadmium telluride homoepitaxy at high growth rates" J. Appl. Phys. 65, (5) 1932 (1989).
6. U.Sudarsan, T.Dosloglu, N.Cody, and R.Solanki "Selective heteroepitaxy of GaP on silicon" J. Crys. Growth 94, 978 (1989).
7. U.Sudarsan, N.Cody, and R.Solanki "Laser-induced selective etching of YBaCuO Films" J. Mat. Sci. Lett. 8, 501 (1989).
8. N.Cody, U.Sudarsan, and R.Solanki "Low temperature epitaxy of HgCdTe" Proc. MRS Vol. 129 (Fall 1988).

9. U.Sudarsan, N.Cody, And R.Solanki "Ar ion and Excimer laser induced epitaxy of GaP" Proc MRS Vol. 129 (Fall 1988).
10. N.Cody, U.Sudarsan, and R.Solanki "Ultraviolet photon-induced heteroepitaxy of CdTe on GaAs" J. Mat. Res. 3, 1144 (1988).
11. U.Sudarsan, N.Cody, and R.Solanki "Excimer laser induced sputtering of YBaCuO" J. Mat. Res. 3, 825 (1988).
12. N.Cody, U.Sudarsan, and R.Solanki "Rapid thermal anneal of sprayed YBaCuO slurry" Appl. Phys. Lett., 52, 1531 (1988).
13. H.Zarnani,J.J.Rocca,D.Bishop,N.W.Cody,G.J.Collins "Chemical vapor deposition of silicon insulating films induced with a perpendicular electron beam" Proc. MRS 38, 357 (1985).